MMP-dependent collagenolysis in vivo. Adipose tissues were fixed with 4% formaldehyde and frozen sections prepared for analysis. MMP-dependent collagen degradation products were detected with C1-2C antibody (IBEX) (12). Fibrillar collagens were stained with Sirius red and quantified with ImageJ (NIH) (7). Student's *t* test (unpaired and two tailed) was used for statistical analysis.

Collagenolysis in vitro. Primary preadipocytes were isolated from the inguinal fat pads of 3- to 4-week-old male wild-type and haploinsufficient (*MMP14*$^{+/-}$) mice (7). Type I collagen was extracted from rat tails and conjugated with Oregon Green 488 (Molecular Probe) (13). Preadipocytes were cultured atop fluoresceinated type I collagen polymers with or without an adipogenic mix (0.2 μmol/l insulin, 0.5 mmol/l 3-isobutyl-1-methylxanthine, and 0.25 μmol/l dexamethsone) (7). Nuclei were stained with DAPI and zones of collagenolysis identified with a fluorescent microscope (model no. IX71; Olympus) using an objective lens 40×/NA 0.65 (Olympus) at 25°C.

GeneChip microarray analysis. Total RNA was isolated from adipose tissues with RNeasy (Qiagen). Gene expression data were obtained by hybridizing labeled cRNA to Affymetrix Mouse Genome 430 2.0 Array. For analysis, data were standardized using the robust multiarray average expression measure (14). The paired *t* test was two tailed, and $P < 0.01$ was considered statistically significant. Replicated, minimum twofold differences were adopted as the threshold of differential expression. Gene ontology analysis was performed using GOstats packages (BioConductor).

Scanning electron microscopy. Scanning electron microscopy was used to examine the architecture of fat pad–associated collagen. Inguinal fat pads were fixed with 2% glutaraldehyde/1.5% paraformaldehyde in 0.1 mol/l Na cacodylate buffer and postfixed in 1% osmium tetroxide. Samples were immersed in liquid N_2, fractured to expose the inner mass of adipose tissues, and imaged with an AMRAY 1910 field emission scanning electron microscope.

Human subjects. Japanese healthy individuals with no obvious medical conditions (n = 3,653) were recruited through random sampling (15). All subjects gave written informed consent prior to the study, and the study design (Millennium Genome Project) was approved by the institutional review board and the ethics committee of the National Cardiovascular Center, Osaka, Japan.

***MMP14* gene SNP study.** Genomic DNA samples were collected from peripheral leukocytes. *MMP14* gene variations were detected by TaqMan PCR (ABI PRISM 7900HT) and verified in a subset of samples by direct sequencing (ABI 3700). Haplotype distribution was estimated with an EM algorithm (16). The association of *MMP14* gene haplotypes with age- and sex-adjusted quantitative traits was tested with the QTLHAPLO program (17) using logistic regression analysis (18). The genotype-phenotype association with rs2236302 was performed with one-way ANCOVA adjusted for age, history of smoking, drinking, diabetes, hypertension, and hyperlipidemia.

RESULTS

High-fat diet triggers acute collagenolytic activity in adipose tissue. To characterize the impact of nutritionally induced obesity on the remodeling of the extracellular matrix (ECM) in adipose tissues, 3-month-old C57BL/6 mice were placed on either a low-fat (control) or high-fat diet for 1 week. Subsequently, inguinal fat pads were isolated and type I collagen architecture was assessed by Sirius red staining. As expected, adipose tissues recovered from mice placed on a control diet displayed a web-like network of interlocking collagen fibrils (Fig. 1*A*). In marked contrast, a high-fat diet induced significant decreases in Sirius red staining consistent with an unexpectedly rapid activation of collagenolytic activity (Fig. 1*A* and *B*). Given the dominant role assigned to matrix metalloproteinases in type I collagen turnover in vivo (7,9), adipose tissues prepared from control or high-fat diet–challenged mice were probed for the generation of collagen cleavage products with a polyclonal antibody that recognizes type I collagen neoepitopes exposed following MMP-specific hydrolysis (12). While control fat pads contained only small amounts of immunoreactive material, collagen cleavage products increased more than threefold in the high-fat diet–challenged group (Fig. 1*A* and *C*). Consistent with these results, scanning electron microscopy confirmed that the high-fat diet challenge induces a marked loss in the adipocyte-associated meshwork of fibrillar collagen (Fig. 1*A*).

To assess the impact of high-fat diet–initiated ECM remodeling on the adipose tissue transcriptome, mRNA was isolated from inguinal fat pads of control or high-fat diet–challenged mice and analyzed with cDNA microarrays. Following 1 week's feeding of a high-fat diet, a subset of 113 transcripts was upregulated by twofold or greater with 34 transcripts suppressed (Fig. 1*D*). Uniquely up- and downregulated genes in the inguinal fat pads of wild-type mice can be found in supplemental Table 1 (available in an online appendix [http://diabetes.diabetesjournals.org/cgi/content/full/db10-0073/DC1]). Gene ontology analysis of upregulated transcripts revealed the enrichment for biologic processes related to collagen catabolism (P = 0.004), collagen fibril organization (P = 0.003), and integrin-mediated signaling (P = 0.002), a major transduction pathway for adipocyte-type I collagen interactions (19,20). Interestingly, gene programs consistent with acute changes in lipid biosynthesis (P = 0.001), steroid metabolism (P = 0.003), and biosynthesis (P = 0.003) were also upregulated in tandem with the recruitment of ECM-remodeling transcripts (Fig. 1*E*). Taken together, these data support a model wherein high-fat diet–induced changes in ECM remodeling are closely linked to the early transcriptional programs responsible for regulating lipid and cholesterol biosynthesis—a conclusion corroborated by recent studies linking a collagen subfamily member to the regulation of adipose tissue mass (21).

***MMP14* mediates high-fat diet–induced collagenolysis in adipose tissues.** While a number of secreted MMPs express type I collagenolytic activity (22), *MMP-13*, *MMP-8*, and *MMP-2* expression were not altered following challenge with a high-fat diet. By contrast, expression levels of the membrane-anchored collagenase, *MMP14*, were increased twofold during the 1-week-long high-fat diet challenge as assessed by quantitative PCR (relative mRNA levels: high-fat diet 7.2 ± 0.95 vs. control 3.4 ± 0.10; n = 4). MMP14 is a membrane-tethered matrix metalloproteinase that has been identified as the dominant pericellular collagenase used by mesenchymal cells (7,13,23). As the collagenolytic activity of isolated mouse preadipocytes is enhanced in the presence of an adipogenic cocktail (7), the impact of *MMP14* dosage on collagenolytic activity was first assessed in vitro. Under resting conditions, *MMP14*$^{+/+}$ or *MMP14*$^{+/-}$ preadipocytes cultured atop a three-dimensional bed of type I collagen fibrils degraded the underlying substrate comparably (Fig. 2*A* and *B*). When stimulated with an adipogenic mix, however, *MMP14*$^{+/+}$ cells displayed a two-fold increase in collagenolysis while *MMP14*$^{+/-}$ cells were unable to upregulate their collagen degrading activity (Fig. 2*A* and *B*). Loss of adipogenic collagenolysis in the haploinsufficient state is consistent with a quantitative requirement for the full complement of MMP14 protein on the cell surface (24).

Given these in vitro findings, the role of *MMP14* in regulating collagen turnover in adipose tissues in situ was assessed in haploinsufficient mice because *MMP14*-null mice fail to thrive from birth and exhibit a marked decrease in life span (9). *MMP14* haploinsufficient mice were indistinguishable from wild-type littermates, and no significant differences in adipose tissue size or morphology could be detected between *MMP14*$^{+/-}$ and *MMP14*$^{+/+}$ mice (supplemental Fig. 1). Furthermore, gene expression patterns of key adipogenic factors including peroxisome

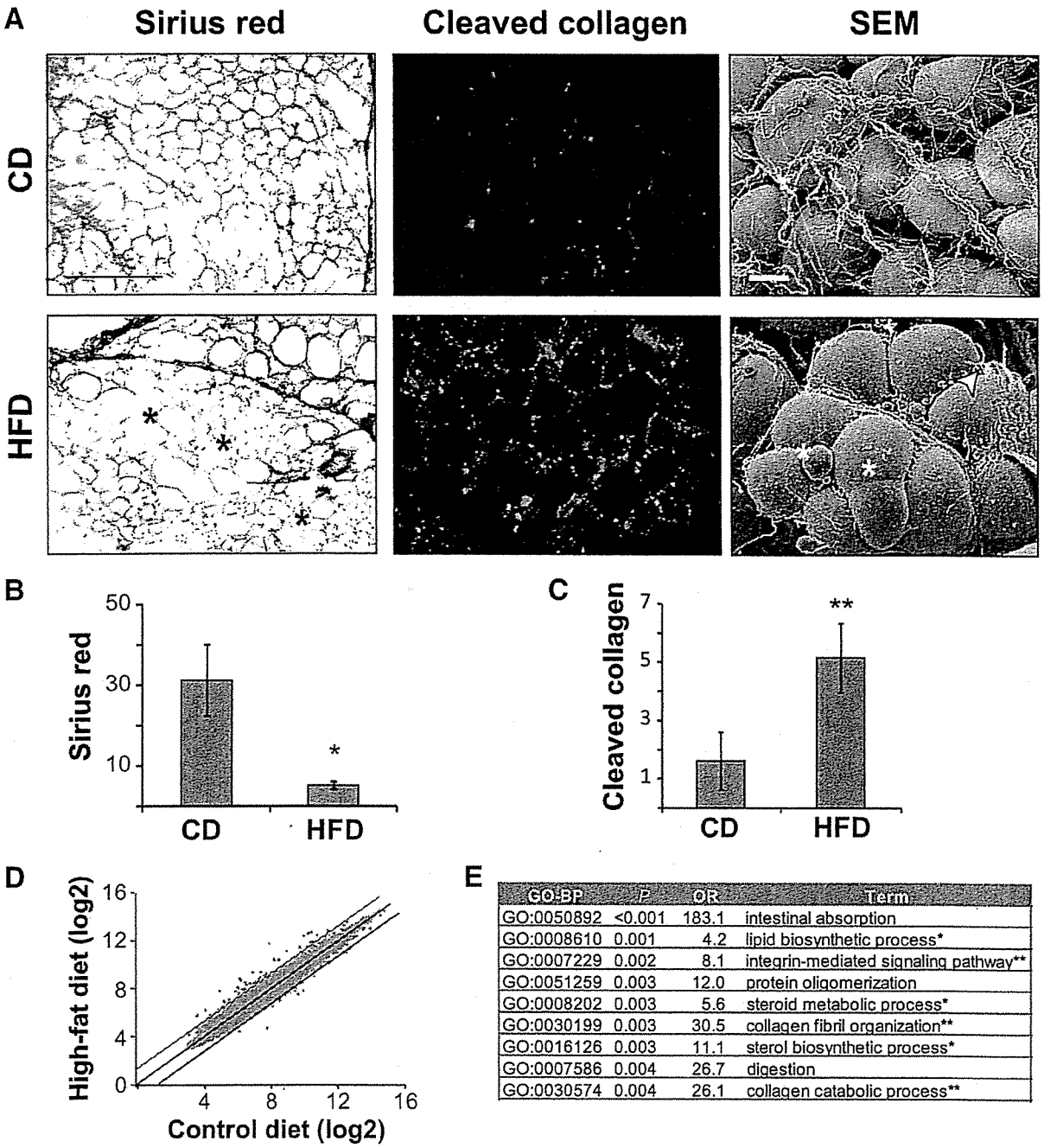

E

GO:BP	*P*	OR	Term
GO:0050892	<0.001	183.1	intestinal absorption
GO:0008610	0.001	4.2	lipid biosynthetic process*
GO:0007229	0.002	8.1	integrin-mediated signaling pathway**
GO:0051259	0.003	12.0	protein oligomerization
GO:0008202	0.003	5.6	steroid metabolic process*
GO:0030199	0.003	30.5	collagen fibril organization**
GO:0016126	0.003	11.1	sterol biosynthetic process*
GO:0007586	0.004	26.7	digestion
GO:0030574	0.004	26.1	collagen catabolic process**

FIG. 1. Type I collagen degradation induced by high-fat feeding. *A*: Type I collagen cleavage induced by a 1-week regimen of high-fat diet feeding. Fibrillar collagen is detected with Sirius red staining in inguinal fat pads of 3-month-old C57BL/6 mice under a control diet (CD) (*top row*) or high-fat diet (HFD) (*bottom row*) feeding. Type I collagen cleavage products are detected with C1, 2C antibody (cleaved collagen, red). Nuclei are stained with Hoechst dye (blue). The fibrillar status of type I collagen fibrils encircling adipocyte clusters is disrupted when mice are placed on an HFD (scanning electron microscopy [SEM]). Disrupted collagen fibers (*arrowhead*) are found in association with variably sized adipocytes (*asterisks*). Bar = 10 μm. *B* and *C*: Quantification of Sirius red–positive staining and cleaved collagen in the inguinal fat pads of mice after 1 week of control diet or high-fat feedings. For each group, images were collected from more than six randomly selected fields. $^*P < 0.01$; $^{**}P < 0.01$. *D*: Genome-wide transcriptome change induced by a 1-week high-fat diet challenge. While more than 99% of transcripts did not display significant changes (*x*-axis, control diet; *y*-axis, high-fat diet), a specific subset of genes display a significant increase in expression. Replicated dataset from two independent experiments. Slopes with *y*-intercepts 0, 1, and −1 (log 2 scale) are shown. *E*: Overrepresented gene ontology (GO) pathways. High-fat diet–dependent transcriptome changes after a 1-week high-fat diet challenge are categorized following validation in two or more independent experiments. Bar = 100 μm. *Lipid/cholesterol biosynthesis pathways; **ECM remodeling pathways. (A high-quality digital representation of this figure is available in the online issue.)

proliferator–activated receptor γ, insulin receptor, Glut4, and lipoprotein lipase (25) were similar between the two groups (supplemental Fig. 1). When, however, *MMP14*$^{+/-}$ mice were placed on a high-fat diet, only small decreases in fibrillar collagen content were detected relative to littermate controls (Fig. 2*C* and *D*). Furthermore, signifi-

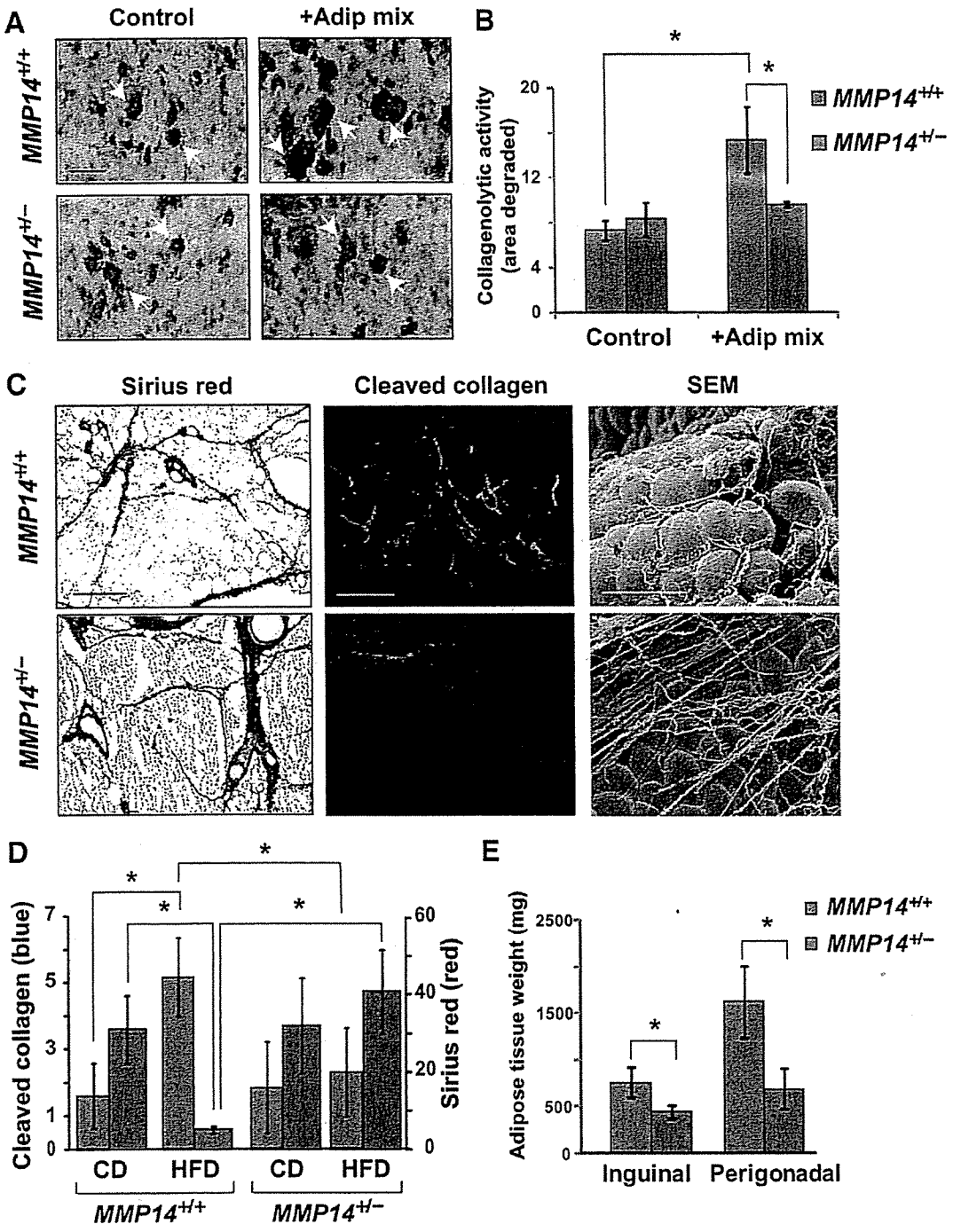

FIG. 2. *MMP14* gene dosage determines adipogenic collagenolysis in vitro and in vivo. *A* and *B*: Collagenolytic potential of $MMP14^{+/+}$ vs. $MMP14^{+/-}$ preadipocytes. Preadipocytes isolated from the inguinal fat pads of wild-type ($MMP14^{+/+}$) and haploinsufficient ($MMP14^{+/-}$) mice were cultured atop a bed of fluorescent type I collagen (green), and subjacent degradation was monitored by the disappearance of fluorescent signal after a 3-day culture period in the absence or presence of an adipogenic cocktail. Representative zones of degradation are indicated by arrows. Nuclei stained with DAPI (blue). Bar = 100 μm. Collagenolytic activity was quantified by scanning the total area of degraded collagen. Cells were isolated from a cohort of three mice for each group ($n = 3$). *$P < 0.05$. *C*: *MMP14* gene dosage modulates collagenolysis in vivo. High-fat diet–induced collagenolysis is almost completely blocked by *MMP14* haploinsufficiency (fibrillar collagen detected with Sirius red staining and cleaved collagen by immunofluorescence) (red). Bar = 100 μm. Scanning electron microscopy revealed intact collagen fibers enwrapping adipocytes in $MMP14^{+/-}$, but not $MMP14^{+/+}$, inguinal fat pads. Bar = 100 μm. *D*: Cleaved collagen and fibrillar collagen contents in inguinal fat pads of $MMP14^{+/+}$ and $MMP14^{+/-}$ mice following a 1-week control diet or high-fat diet challenge. Results are expressed as means ± 1 SD ($n = 6$). *$P < 0.01$. *E*: Following a 2-week high-fat diet, the inguinal and perigonadal fat pads were isolated from $MMP14^{+/+}$ or $MMP14^{+/-}$ mice and tissue weights determined. Results are expressed as means ± 1 SD ($n = 6$). *$P < 0.01$. (A high-quality digital representation of this figure is available in the online issue.)

cant increases in collagen cleavage products following high-fat challenge were not observed in *MMP14*$^{+/-}$ mice, while the fibrillar collagen architecture (as determined by scanning electron microscopy) remained unchanged (Fig. 2*C*). In concert with the diminished ability of *MMP14* haploinsufficient mice to remodel fat pad collagen architecture during high-fat feeding, the *MMP14*$^{+/-}$ mice were also unable to expand their adipose mass comparably with control (Fig. 2*E*). Whereas the weight of inguinal or perigonadal adipose tissue of *MMP14*$^{+/+}$ mice increased two- to threefold during the 1-week high-fat diet challenge, the haploinsufficient mice failed to mount a similar increase in adipose tissue mass (Fig. 2*E*).

Dysregulated transcriptome coordination in *MMP14* haploinsufficient mice. To probe the functional impact of *MMP14* in regulating the acute phase gene response to a high-fat diet, we examined the transcriptome profile of inguinal fat pads of *MMP14* haploinsufficient mice placed on a high-fat diet for 1 week. In contrast with *MMP14*-sufficient mice, the haploinsufficient animals failed to induce the gene sets enriched for ECM remodeling or lipid biosynthesis (Fig. 3*A* and *B*). Further, as opposed to wild-type mice, 42 genes were uniquely upregulated and 91 genes downregulated in the heterozygote animals (Fig. 3*A*, supplemental Fig. 2, and supplemental Table 2). In these mice, the high-fat diet challenge led to a paradoxical deregulation in the gene expression profile of transcripts involved in a wide range of biological processes, including glycerol-3-phosphate metabolism, acetyl-CoA biosynthesis, and both humoral immune and acute phase responses (Fig. 3*B*). These results indicate that a reduction in *MMP14* gene dosage leads to a disruption in the transcriptional link existing between ECM remodeling and lipid biosynthesis that coordinates the expansion of adipose tissue.

To next assess the long-term consequences of *MMP14* haploinsufficiency on high-fat diet–induced obesity, wild-type and haploinsufficient mice were placed on a high-fat diet for 3–6 months. The average percentage of fat mass of *MMP14* haploinsufficient and wild-type mice placed under a control diet was comparable (mean ± SD 5.29 ± 0.58 vs. 5.07 ± 0.7%; $n = 6$). On the high-fat diet, however, whereas wild-type mice displayed an approximate 20 and 60% weight gain after 3 and 6 months, respectively, *MMP14*$^{+/-}$ mice increased in total weight by less than one-half of that observed in the control (Fig. 3*C*). As expected, the dramatic changes in weight gain that occured in the long-term, high-fat feeding of *MMP14*$^{+/-}$ mice was also reflected in the attenuated expansion of tissue mass in isolated inguinal and perigonadal fat pads (Fig. 3*D*). Changes in *MMP14* expression did not, however, affect whole-body energy balance during high-fat feeding because the respiration rate, daily food intake, and locomotion of wild-type and heterozygous mice were not significantly different (Fig. 3*F*). These results stress the role of *MMP14* as a proteolytic modifier that acts locally within adipose tissues without overtly affecting the hypothalamic regulation of metabolism.

Human *MMP14* SNPs associate with obesity and diabetes traits. Obesity is driven by a complex process that is coordinated by a host of genetic, epigenetic, and environmental factors (26–28). To extend the findings of the genotype-phenotype link found in mice, the association of *MMP14* SNP genotypes with human obesity and diabetes traits was examined. The human *MMP14* gene is located at chromosome 14q11–12, comprising 10 exons and spanning a 10-kb region that contains 157 known SNPs (NCBI dbSNP). Using a preliminary group ($n = 48$) randomly sampled from a Japanese population (15), we assessed the minor allele frequencies of candidate *MMP14* SNPs (Fig. 4*A*). Initially, 16 SNPs spanning human *MMP14* gene (from rs17211964 at chr14:23,304,272 through rs2236307 at chr14: 23,312,554) were screened to determine their pairwise linkage disequilibrium coefficients (supplemental Tables 1 and 2). Three SNPs located in exon 5 (rs2236302; allele 2, C > allele 1, G), intron 5 (rs2236304; allele 2, C > allele 1, G), and exon 6 (rs2236307; allele 2, T > allele 1, C) were chosen based on their frequency (>10%), proximity to the catalytic domain of *MMP14*, and pairwise linkage disequilibrium that allow diverse haplotypes in combination. The minor allele (allele 1) frequency for the three SNPs among the study population was 11.0, 44.8, or 38.5%, respectively (Fig. 4*A*).

Using a study population that included 3,653 individuals consisting of 1,708 men and 1,945 women, we assessed *MMP14* haplotypes. The analysis of the pairwise linkage disequilibrium among the three SNPs suggested that they constitute a block of haplotypes (D′ >0.977). However, the estimated square of the correlation coefficient (r^2) among the studied SNPs were sufficiently low (Table 1) to allow for the assembly of at least four major haplotypes (Fig. 4*B*). The association of *MMP14* haplotypes with obesity and diabetes traits, i.e., BMI, waist-to-hip ratio, body fat, A1C, fasting blood glucose and insulin levels, homeostasis model assessment (HOMA) of insulin resistance and β-cell function, was examined in the dominant or recessive genetic model with multiple logistic regression analysis (17,18,28). Among the four major haplotypes of the *MMP14* gene (212, 221, 122, and 222), the haplotype 122 (GCT) was found to positively associate with BMI ($P = 0.0017$) (Fig. 4*C*) and waist-to-hip ratio ($P = 0.0079$) (Table 2). Because of the dominant role played by rs2236302 in defining the link between obesity traits and *MMP14* haplotypes, rs2236302 genotype was used to further delineate the link between *MMP14* genotype and quantitative obesity traits. The distribution of C/C, C/G, and G/G genotypes were 79.7% ($n = 2,908$), 19.1% ($n = 695$), and 1.2% ($n = 44$) among the study population. Due to the low frequency of the G/G genotype, the quantitative association study was performed by comparing between homozygote C/C and heterozygote C/G genotype groups. The association with obesity traits was then examined in a genotype or dominant model with ANCOVA. In the multivariate analyses of the total population, BMI and waist-to-hip ratio were associated with age ($P < 0.0001$), sex ($P < 0.0001$), history of smoking ($P = 0.0129$), hypertension ($P < 0.0001$), diabetes ($P = 0.0003$), and hyperlipidemia ($P < 0.0001$). When analyzed with adjustment for these variables, a highly significant correlation was observed between rs2236302 genotype and obesity traits (Fig. 4*D*) (mean ± SEM BMI, C/C 22.74 ± 0.06 vs. C/G 23.16 ± 0.11 kg/m^2; waist-to-hip ratio, C/C 0.901 ± 0.001 vs. C/G 0.906 ± 0.002). The increase of BMI caused by rs2236302 minor allele was 0.42 kg/m^2 (Cohen d = 0.13).

Of note, the positive effect of rs2236302 genotype on BMI and waist-to-hip ratio was preferentially observed in women (Fig. 4*D*), suggesting the existence of sexual dimorphism in the link between *MMP14* and obesity phenotype (women $P = 0.0004$, d = 0.199, vs. men $P = 0.5419$, d = 0.059). Finally, human *MMP14* SNPs were found to be weakly associated with A1C in men ($P =$

A

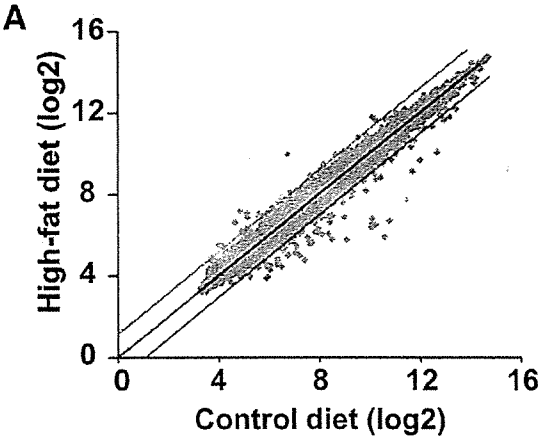

B

GO:BP	P	OR	Term
GO:0006941	<0.01	40.4	striated muscle contraction
GO:0003008	<0.01	6.5	system process
GO:0006936	<0.01	55.1	muscle contraction
GO:0006937	<0.01	27.9	regulation of muscle contraction
GO:0006085	<0.01	103.6	acetyl-CoA biosynthetic process*
GO:0045214	<0.01	103.6	sarcomere organization
GO:0007512	0.001	62.2	adult heart development
GO:0055002	0.001	62.2	striated muscle cell development
GO:0014706	0.003	7.4	striated muscle development
GO:0044262	0.004	5.2	carbohydrate metabolic process*

C

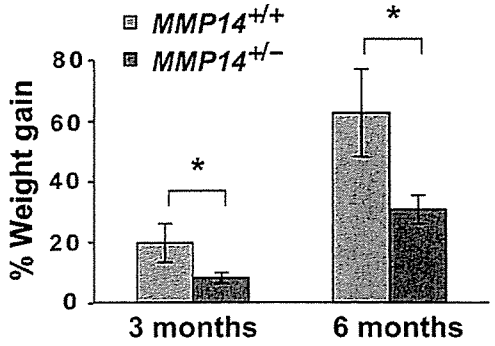

D

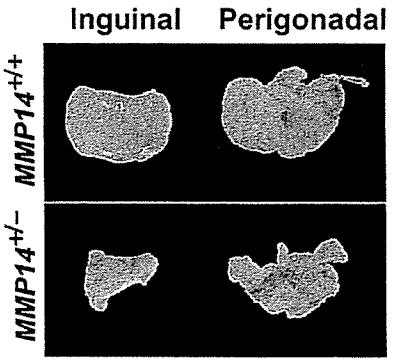

E

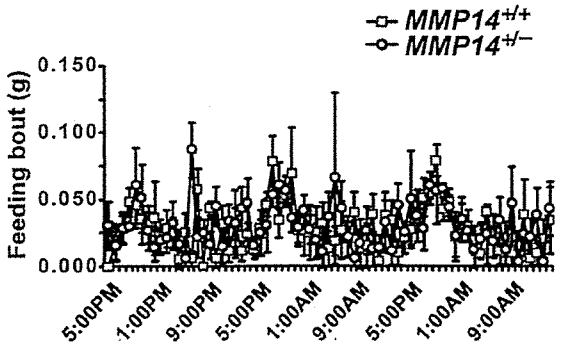

F

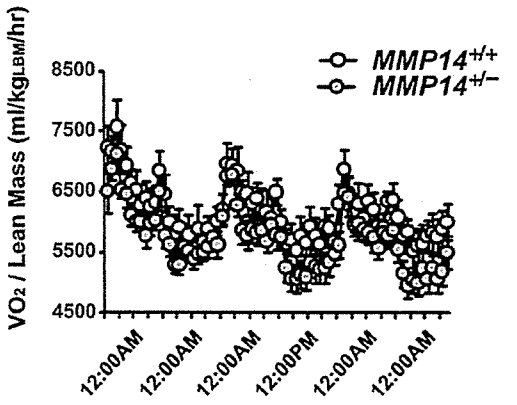

FIG. 3. *MMP14* gene dosage controls nutritional transcriptome response and obesity development. *A* and *B*: Disrupted high-fat diet–induced transcriptome changes in *MMP14* haploinsufficient mice. A scatter plot is shown of mRNA expression values (log2 scale) in inguinal fat pads isolated from *MMP14*$^{+/-}$ mice fed a control diet (*x*-axis) vs. high-fat diet (*y*-axis). In comparison with gene expression profiles obtained in wild-type mice (Fig. 1*B*), genes involved in a diverse set of metabolic pathways critical to adipose tissue function (*asterisks*) are misregulated in *MMP14*$^{+/-}$ mice. GO, gene ontology. *C* and *D*: *MMP14* haploinsufficiency protects mice from diet-induced increase of fat mass after 3 or 6 months of high-fat diet feeding (means ± SD; $n = 8$). Representative images of inguinal and perigonadal fat pads are shown following isolation from *MMP14*$^{+/+}$ and *MMP14* $^{+/-}$ mice that had been placed on high-fat feeding for 3 months. *E* and *F*: Feeding bouts (g/day) and metabolic rates adjusted for lean mass (Vo_2/kg lean mass) were determined in metabolic cages during high-fat diet feeding. (A high-quality digital representation of this figure is available in the online issue.)

0.0685) (Table 3), suggesting a paradoxical relationship of *MMP14* SNPs with diabetes predisposition in males. Consistently, *MMP14* haplotype (121) associated with increased fasting blood glucose ($P = 0.0069$) and HOMA of insulin resistance ($P = 0.0386$) (Table 3), supporting a potential link between *MMP14* and diabetes in men.

DISCUSSION

In this study, we have demonstrated that a high-fat diet acutely initiates the *MMP14*-dependent degradation of the type I collagen network found in adipose tissues and induces a selective set of transcripts that link ECM-related remodeling to lipid/cholesterol biosynthesis. While one

A

SNP	Position	Allele	Frequency	Residue
*rs2236302	exon 5	C>G	11.0%	P259
rs17881628	exon 5	G>A	2.1%	D273N
rs2236303	intron 5	C>T	47.8%	
*rs2236304	intron 5	C>G	44.8%	
rs2236305	intron 5	G>T	38.5%	
rs2236306	intron 5	G>C	38.5%	
*rs2236307	exon 6	T>C	38.5%	G285
rs17884719	exon 6	C>T	0.0%	R302W
rs17878814	intron 6	G>T	0.0%	

B

Haplotype	Frequency
2 1 2	48.0%
2 2 1	38.6%
1 2 2	10.6%
2 2 2	2.7%
1 1 2	0.1%
2 1 1	<0.1%
1 2 1	<0.1%

C

	Haplotype	Dominant	Recessive
All	1 * 2	0.0015	NS
	1 * *	0.0016	NS
	2 * *	NS	NS
	1 2 2	0.0016	NS
Women	122	0.0002	NS
	1**	0.0003	NS
	2**	NS	0.0003
	*22	0.0008	NS
	**2	NS	NS
	2**	NS	0.0003
Men	2*2	NS	0.0596
	1**	NS	NS
	2**	NS	NS
	1*2	NS	NS
	222	0.0882	NS

D

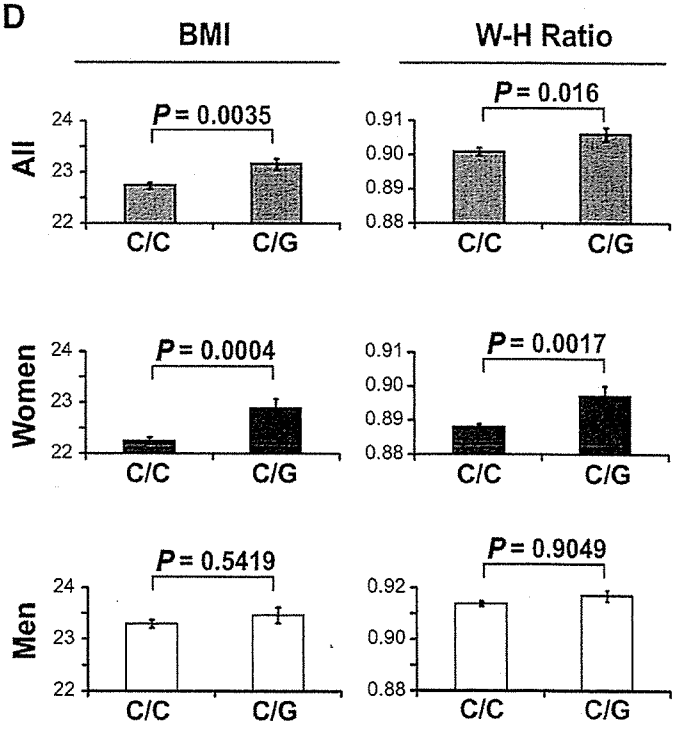

FIG. 4. Human *MMP14* SNP associations with obesity and diabetes traits in a Japanese cohort. *A*: Human *MMP14* SNPs located in the proximity of the region encoding MMP14 catalytic domain. Minor allele frequency for each SNP was determined. *SNPs used for haplotype analyses. *B*: *MMP14* haplotype determinations were based on the combination of rs2236302, rs2236304, and rs2236307. *C*: Association of human *MMP14* haplotypes with BMI. Haplotype associations with BMI of the total population (n = 3,531), women (n = 1,944), and men (n = 1,587) were assessed in both dominant and recessive inheritance models. The results of ANCOVA analyses are shown with P values. *Any genotype. NS, P value > 0.1. *D*: Association of rs2236302 genotype with BMI and waist-to-hip (W-H) ratio. Means ± SEM of BMI (*left panel*) and waist-to-hip ratio (*right panel*) are shown for the total population (n = 3,647), women (n = 1,944), and men (n = 1,703), respectively.

allele of *MMP14* is sufficient for postnatal adipose tissue development, our results highlight the quantitative requirement of this protease for diet-induced expansion of adipose tissues in vivo. *MMP14* gene expression, however, is not confined to preadipocyte/adipocyte cell population but can be found in vascular endothelial cells, pericytes, or fibroblasts (13,29,30). Consequently, *MMP14*-dependent remodeling of fat pad architecture may well involve the cooperative interplay of multiple cell populations. Never-

TABLE 1
Pairwise Linkage Disequilibrium

Pair of SNPs	D′	r^2
rs2236302 and rs2236304	0.977	0.107
rs2236302 and rs2236307	0.993	0.075
rs2236304 and rs2236307	0.995	0.580

D′, linkage disequilibrium measure.

TABLE 2
Association of *MMP14* haplotype with obesity/diabetes traits

	Dominant		Recessive	
	Haplotype	*P*	Haplotype	*P*
BMI	1*2	0.0016	2**	0.0016
	1**	0.0016		
	122	0.0017		
	12*	0.0017		
	*22	0.0211		
Waist-to-hip ratio	122	0.0079	2**	0.0086
	12*	0.0080		
	1*2	0.0084		
	1**	0.0086		
Leptin	NS		222	0.0394
A1C	NS		NS	
Fasting blood glucose	121	0.0113	NS	
	222	0.0460		
Fasting insulin	*2*	0.0158	*12	0.0125
	12*	0.0335	*1*	0.0158
	122	0.0404	212	0.0160
	*22	0.0419	21*	0.0200
	1**	0.0483	2**	0.0483
			2*2	0.0494
HOMA-IR	12*	0.0259	*12	0.0272
	122	0.0327	212	0.0322
	2	0.0343	*1*	0.0343
	1**	0.0358	2**	0.0358
	1*2	0.0445	2*	0.0404
	121	0.0496		
HOMA-β	*2*	0.0029	*12	0.0026
	*22	0.0604	*1*	0.0029
	22*	0.0725	212	0.0041
			21*	0.0045
			2*2	0.0236

NS, $P > 0.1$. *Any genotype. HOMA-β, HOMA of β-cell function; HOMA-IR, HOMA of insulin resistance.

theless, the direct physical association of the collagenous web with preadipocytes and adipocytes, coupled with the deposition of collagen degradation products in the peri-adipocyte space, supports a dominant role for these cells in diet-induced collagen remodeling. Further, our in vitro results also support the importance of adipogenic regulation on preadipocyte-mediated collagenolysis. Of note, human mesenchymal stem cells have recently been shown to mobilize MMP14 for trafficking and differentiation in three-dimensional collagen environments (31). Given that adipocyte progenitors can reside in perivascular stromal tissues (32,33), it is intriguing to speculate that MMP14 may likewise support the migration and differentiation of adipocyte progenitors within adipose tissues.

In addition to the ability of MMP14 to remodel collagen in a diet-dependent manner, the enzyme's role in regulating the high-fat diet–responsive early-onset transcriptome is notable. High-fat diet challenge rapidly—within a week—induces a selective set of genes enriched for ECM remodeling and lipid/cholesterol biosynthesis, including the previously described genes, *MEST* and *Npr3* (34). By contrast, the enrichment of genes associated with ECM remodeling and lipid/cholesterol biosynthesis is ablated in *MMP14* haploinsufficient mice, though induction of *MEST* and *Npr3* gene expression remains intact (supplemental Tables 1 and 2). The precise molecular mechanism by which *MMP14* gene selectively regulates the fat pad transcriptome is unknown; however, *MMP14*-dependent collagenolysis may regulate transcriptional programs by modulating cell shape and tension in collagen-rich microenvironments (7,20). Despite the marked changes in fat pad size and function observed in *MMP14* haploinsufficient mice, Vo_2 consumption, food intake, and physical activity in these mice appear to be comparable with controls. While white adipose tissues of high-fat diet–challenged *MMP14* haploinsufficient mice are small in size, the efficiency with which they oxidize fat versus carbohydrate may have undergone adaptive alterations in the in vivo setting. Indeed, respiratory ratio (VCo_2/Vo_2), was relatively lower in *MMP14* haploinsufficient mice, which is consistent with a preferred utilization of fat over carbohydrate. While severe lipodystrophy increases the risk of fatty liver (35), we were unable to detect increased triglyceride accumulation in the livers of *MMP14* haploinsuffi-

TABLE 3
Sexual dimorphism in the link between *MMP14* and obesity/diabetes traits

	Men				Women			
	Dominant		Recessive		Dominant		Recessive	
	Haplotype	*P*	Haplotype	*P*	Haplotype	*P*	Haplotype	*P*
BMI	NS		NS		122	0.0002	2**	0.0004
					1**	0.0004		
					*22	0.0008		
Waist-to-hip ratio	NS		2*2	0.0417	122	0.0009	2**	0.0015
					1**	0.0015		
					*22	0.0037		
Leptin	222	0.0369	222	0.0157	*22	0.0630	NS	
			2*2	0.0365	112	0.0944		
A1C	22*	0.0685	NS		NS		NS	
Fasting blood glucose	121	0.0069	NS		NS		NS	
	222	0.094						
Fasting insulin	NS		NS		*22	0.0361	NS	
HOMA-IR	121	0.0386	NS		*22	0.0379	NS	
HOMA-β	*2*	0.0075	*12	0.0065	222	0.0253	NS	
			1	0.0075				
			212	0.0090				

*Any genotype. HOMA-β, HOMA of β-cell function; HOMA-IR, HOMA of insulin resistance; NS, $P > 0.1$.

cient mice (total glycerol 14.4 ± 2.7 vs. 11.8 ± 1.7% in wild-type and *MMP14*$^{+/-}$ mice, respectively; n = 6).

In parallel with our findings in a mouse model of diet-induced obesity, human *MMP14* SNPs were found to be associated with quantitative traits of obesity and diabetes in a Japanese population. The link between *MMP14* SNPs and obesity or diabetes traits found in this study may well be due to altered *MMP14* gene expression, catalytic activity, exocytosis (36), or unknown effects on neighboring genes that are in linkage disequilibrium. Interestingly, however, a rare nonsynonymous polymorphism identified in exon 5 of *MMP14* appears to alter collagenolytic activity and adipogenic potential in vitro (T.-H.C., unpublished observations), supporting its potential link with MMP14 catalytic activity. A sib-pair linkage analysis of black and Caucasian nuclear family volunteers (364 sib pairs) has pointed to chromosome 14q11, where *MMP14* resides, as one of three candidate loci linked with BMI and fat mass (37). While genetic risks for obesity have recently been highlighted by the identification of *FTO* (38) and *MC4R* (39) gene variants by genome-wide association studies (GWAS), candidate-gene approaches are still needed to bridge the gaps that remain unfilled by GWAS analysis alone (40–42). Our study of a Japanese cohort is of moderate size (n = 3,653) but demonstrates a significant increase of BMI with rs2236302 heterozygosity. The effect size of this risk allele is modest (ΔBMI 0.42 kg/m^2), which may not allow for its detection by GWAS. Though multiple genes affect obesity traits in mice without relevant findings in humans, *MMP14* gene dose or polymorphism may define a genetic susceptibility for obesity traits that spans the gulf between mice and humans.

In humans, obesity and diabetes phenotypes of *MMP14* gene variants display a sexual dimorphism. The stronger association of *MMP14* genotype/haplotypes with obesity traits in women may relate their higher subcutaneous fat volume (43). Because subcutaneous fat depots contain higher concentrations of collagen fibers relative to other tissues, *MMP14*-dependent collagenolysis may contribute more to the size regulation of subcutaneous fat pads in women. Female mice in the C57BL/6 background, whether *MMP14* wild-type or haploinsufficient, did not significantly change their fat mass in response to diet. However, unlike male mice, *MMP14* haploinsufficient female mice displayed a ~30% reduction of fat mass even under the conditions of a control diet (mean ± SD 13.3 ± 1.9 vs. 9.5 ± 0.9% for *MMP14*$^{+/+}$ and *MMP14*$^{+/-}$ mice, respectively; n = 6). Of note, basal fat mass of female mice is more than two times higher than that of male mice. As such, *MMP14* might be fully engaged in maintaining adipose tissue mass in female mice—and perhaps in women as well. Under these conditions, *MMP14* gene variants may be expected to demonstrate an increased linkage with obesity traits. Additionally, the association of rs2236302 with BMI found in women was reproduced in postmenopausal women (n = 1,503, P = 0.0008), suggesting that constitutional but not hormonal differences contribute to the sexual dimorphism. Conversely, in men, *MMP14* gene variants are associated with diabetes but not obesity traits (Table 3). The genetic or epigenetic predisposition that determines obesity or diabetes phenotypes in men, therefore, may differentially interact with *MMP14* gene variants.

Given the diverse biological functions of MMP family members interacting with an array of substrates (44), it is often difficult to pin down the causal relationship between a specific MMP and a selective substrate. For example, *MMP3* gene expression and variations are associated with body fat in Pima Indian population (45). While *MMP3* gene expression decreases in obesity, *MMP3* has been shown to be necessary for adipocyte differentiation in a manner independent of ECM context (46). Indeed, *MMP3* is not required for type I collagen hydrolysis (47), and the substrate targets for MMP3 that regulates adiposity are unknown. By contrast, *MMP14*-dependent regulation of adipocyte differentiation is restricted to collagenous microenvironments (7), suggesting that the *MMP14*–type I collagen axis is the dominant pathway operative in adipocytes in vitro as well as in mouse and human adipose tissues. However, additional interactions with other *MMP14* substrates, or the involvement of additional MMP family members in this process, cannot be ruled out. Indeed, *MMP13* and *MMP2*, whose latent forms can be activated by MMP14 (10,48), may play cooperative roles in regulating adipocyte function. Additional studies will be required to identify other pathogenic links that may exist between *MMP* family members and their respective substrates during obesity progression. Along these lines, the metabolic impact of undigested collagen in *MMP14* wild-type and haploinsufficient male mice also bears consideration. For example, the transgenic expression of hypoxia-inducible factor-1α leads to increased fibrosis, inflammatory response, and insulin resistance (49). Hence, while targeting *MMP14* in adipose tissue may prevent diet-induced fat expansion, the overall impact of reduced collagen remodeling on inflammation and metabolism remains to be determined. Nonetheless, our data lend further support to a model wherein *MMP14* functions as a metabolic rheostat that controls the rate of collagen turnover in adipose tissues. Our in vitro and mouse studies, combined with SNP association analyses, point to a critical role for the *MMP14*/type I collagen axis in regulating adipose tissue mass in states of nutritional challenge.

ACKNOWLEDGMENTS

This research was supported by the Program for Improvement of Research Environment for Young Researchers (the Ministry of Education, Culture, Sports, Science and Technology, Tokyo, Japan), an American Heart Assocation Scientist Development grant, an ASCI Young Investigator's Award, grant K08DK078801 National Institute of Diabetes and Digestive and Kidney Diseases (to T.-H.C.), and National Institutes of Health grants CA088308 and CA071699 (to S.J.W.). This work used the Microarray and Animal Phenotyping Cores of the Michigan Diabetes Research and Training Center (supported by DK020572 from the National Institute of Diabetes and Digestive and Kidney Diseases).

No potential conflicts of interest relevant to this article were reported.

T.-H.C. analyzed data and wrote the manuscript, M.I. analyzed data, H.M. analyzed data, I.Y. analyzed data, Y.M. contributed to data and discussion, T.O. contributed to data and discussion, K.S.-K. analyzed data, and S.J.W. analyzed data and wrote the manuscript.

We thank Y. Yoshimasa, T. Morisaki, and Y. Kokubo of the National Cardiovascular Center (Osaka, Japan) for their discussion on the SNP association study; A.R. Saltiel at the University of Michigan; L.S.I. for his insightful advice on the project; Y. Ueno at the University of Tokyo and Y. Jiang at the University of Michigan for their

technical assistance; and J. Rohr at the University of Michigan for her assistance with the manuscript preparation. We thank N. Qi at the Animal Phenotyping Core and C. Johnson at the Microarray Core of the Michigan Diabetes Research and Training Center for advice and data analysis.

REFERENCES

1. Stewart ST, Cutler DM, Rosen AB. Forecasting the effects of obesity and smoking on U.S. life expectancy. N Engl J Med 2009;361:2252–2260
2. Saltiel AR, Kahn CR. Insulin signalling and the regulation of glucose and lipid metabolism. Nature 2001;414:799–806
3. Klein Woolthuis EP, de Grauw WJC, van Gerwen WHEM, van den Hoogen HJM, van de Lisdonk EH, Metsemakers JFM, van Weel C. Yield of opportunistic targeted screening for type 2 diabetes in primary care: the Diabscreen Study. Ann Fam Med 2009;7:422–430
4. Faust I, Johnson P, Stern J, Hirsch J. Diet-induced adipocyte number increase in adult rats: a new model of obesity. Am J Physiol Endocrinol Metab 1978;235:E279–E286
5. Klyde B, Hirsch J. Increased cellular proliferation in adipose tissue of adult rats fed a high-fat diet. J Lipid Res 1979;20:705–715
6. Napolitano L. The differentiation of white adipose cells: an electron microscopy study. J Cell Biol 1963;18:663–679
7. Chun TH, Hotary KB, Sabeh F, Saltiel AR, Allen ED, Weiss SJ. A pericellular collagenase directs the 3-dimensional development of white adipose tissue. Cell 2006;125:577–591
8. Prockop JD. Collagens: molecular biology, diseases, and potentials for therapy. Annu Rev Biochem 1995;64:403–434
9. Holmbeck K, Bianco P, Caterina J, Yamada S, Kromer M, Kuznetsov SA, Mankani M, Robey PG, Poole AR, Pidoux I, Ward JM, Birkedal-Hansen H. MT1-MMP-deficient mice develop dwarfism, osteopenia, arthritis, and connective tissue disease due to inadequate collagen turnover. Cell 1999;99:81–92
10. Sato H, Takino T, Okada Y, Cao J, Shinagawa A, Yamamoto E, Seiki M. A matrix metalloproteinase expressed on the surface of invasive tumour cells. Nature 1994;370:61–65
11. Yana I, Sagara H, Takaki S, Takatsu K, Nakamura K, Nakao K, Katsuki M, Taniguchi S, Aoki T, Sato H, Weiss SJ, Seiki M. Crosstalk between neovessels and mural cells directs the site-specific expression of MT1-MMP to endothelial tip cells. J Cell Sci 2007;120:1607–1614
12. Poole AR, Ionescu M, Fitzcharles MA, Billinghurst RC. The assessment of cartilage degradation in vivo: development of an immunoassay for the measurement in body fluids of type II collagen cleaved by collagenases. J Immunol Methods 2004;294:145–153
13. Chun TH, Sabeh F, Ota I, Murphy H, McDonagh KT, Holmbeck K, Birkedal-Hansen H, Allen ED, Weiss SJ. MT1-MMP-dependent neovessel formation within the confines of the three-dimensional extracellular matrix. J Cell Biol 2004;167:757–767
14. Irizarry RA, Hobbs B, Collin F, Beazer-Barclay YD, Antonellis KJ, Scherf U, Speed TP. Exploration, normalization, and summaries of high density oligonucleotide array probe level data. Biostatistics 2003;4:249–264
15. Mannami T, Baba S, Ogata J. Strong and significant relationships between aggregation of major coronary risk factors and the acceleration of carotid atherosclerosis in the general population of a Japanese city: the Suita Study. Arch Intern Med 2000;160:2297–2303
16. Kitamura Y, Moriguchi M, Kaneko H, Morisaki H, Morisaki T, Toyama K, Kamatani N. Determination of probability distribution of diplotype configuration (diplotype distribution) for each subject from genotypic data using the EM algorithm. Ann Intern Med 2002;66:183–193
17. Shibata K, Ito T, Kitamura Y, Iwasaki N, Tanaka H, Kamatani N. Simultaneous estimation of haplotype frequencies and quantitative trait parameters: applications to the test of association between phenotype and diplotype configuration. Genetics 2004;168:525–539
18. Chiano MN, Clayton DG. Fine genetic mapping using haplotype analysis and the missing data problem. Ann Intern Med 1998;62:55–60
19. Hynes RO. Integrins: bidirectional, allosteric signaling machines. Cell 2002;110:673–687
20. Wang N, Tytell JD, Ingber DE. Mechanotransduction at a distance: mechanically coupling the extracellular matrix with the nucleus. Nat Rev Mol Cell Biol 2009;10:75–82
21. Khan T, Muise ES, Iyengar P, Wang ZV, Chandalia M, Abate N, Zhang BB, Bonaldo P, Chua S, Scherer PE. Metabolic dysregulation and adipose tissue fibrosis: role of collagen VI. Mol Cell Biol 2009;29:1575–1591
22. Sabeh F, Shimizu-Hirota R, Weiss SJ. Protease-dependent versus -independent cancer cell invasion programs: three-dimensional amoeboid movement revisited. J Cell Biol 2009;185:11–19
23. Filippov S, Koenig GC, Chun T-H, Hotary KB, Ota I, Bugge TH, Roberts JD, Fay WP, Birkedal-Hansen H, Holmbeck K, Sabeh F, Allen ED, Weiss SJ. MT1-matrix metalloproteinase directs arterial wall invasion and neointima formation by vascular smooth muscle cells. J Exp Med 2005;202:663–671
24. Itoh Y, Ito N, Nagase H, Seiki M. The second dimer interface of MT1-MMP, the transmembrane domain, is essential for ProMMP-2 activation on the cell surface. J Biol Chem 2008;283:13053–13062
25. Rosen ED, MacDougald OA. Adipocyte differentiation from the inside out. Nat Rev Mol Cell Biol 2006;7:885–896
26. Yang X, Deignan JL, Qi H, Zhu J, Qian S, Zhong J, Torosyan G, Majid S, Falkard B, Kleinhanz RR, Karlsson J, Castellani LW, Mumick S, Wang K, Xie T, Coon M, Zhang C, Estrada-Smith D, Farber CR, Wang SS, van Nas A, Ghazalpour A, Zhang B, MacNeil DJ, Lamb JR, Dipple KM, Reitman ML, Mehrabian M, Lum PY, Schadt EE, Lusis AJ, Drake TA. Validation of candidate causal genes for obesity that affect shared metabolic pathways and networks. Nat Genet 2009;41:415–423
27. Gesta S, Tseng Y-H, Kahn CR. Developmental origin of fat: tracking obesity to its source. Cell 2007;131:242–256
28. Mizuta E, Kokubo Y, Yamanaka I, Miyamoto Y, Okayama A, Yoshimasa Y, Tomoike H, Morisaki H, Morisaki T. Leptin gene and leptin receptor gene polymorphisms are associated with sweet preference and obesity. Hypertens Res 2008;31:1069–1077
29. Lehti K, Allen E, Birkedal-Hansen H, Holmbeck K, Miyake Y, Chun T-H, Weiss SJ. An MT1-MMP-PDGF receptor-beta axis regulates mural cell investment of the microvasculature. Genes Dev 2005;19:979–991
30. Sabeh F, Li XY, Saunders TL, Rowe RG, Weiss SJ. Secreted versus membrane-anchored collagenases: relative roles in fibroblast-dependent collagenolysis and invasion. J Biol Chem 2009;284:23001–23011
31. Lu C, Li X-Y, Hu Y, Rowe RG, Weiss SJ. MT1-MMP controls human mesenchymal stem cell trafficking and differentiation. Blood 2010;115:221–229
32. Tang W, Zeve D, Suh JM, Bosnakovski D, Kyba M, Hammer RE, Tallquist MD, Graff JM. White fat progenitor cells reside in the adipose vasculature. Science 2008;322:583–586
33. Rodeheffer MS, Birsoy K, Friedman JM. Identification of white adipocyte progenitor cells in vivo. Cell 2008;135:240–249
34. Koza RA, Nikonova L, Hogan J, Rim J-S, Mendoza T, Faulk C, Skaf J, Kozak LP. Changes in gene expression foreshadow diet-induced obesity in genetically identical mice. PLoS Genet 2006;2:e81
35. Garg A. Acquired and inherited lipodystrophies. N Engl J Med 2004;350:1220–1234
36. Sakurai-Yageta M, Recchi C, Le Dez G, Sibarita J-B, Daviet L, Camonis J, D'Souza-Schorey C, Chavrier P. The interaction of IQGAP1 with the exocyst complex is required for tumor cell invasion downstream of Cdc42 and RhoA. J Cell Biol 2008;181:985–998
37. Chagnon YC, Rice T, Perusse L, Borecki IB, Ho-Kim M-A, Lacaille M, Pare C, Bouchard L, Gagnon J, Leon AS, Skinner JS, Wilmore JH, Rao DC, Bouchard C. Genomic scan for genes affecting body composition before and after training in Caucasians from HERITAGE. J Appl Physiol 2001;90:1777–1787
38. Frayling TM, Timpson NJ, Weedon MN, Zeggini E, Freathy RM, Lindgren CM, Perry JRB, Elliott KS, Lango H, Rayner NW, Shields B, Harries LW, Barrett JC, Ellard S, Groves CJ, Knight B, Patch A-M, Ness AR, Ebrahim S, Lawlor DA, Ring SM, Ben-Shlomo Y, Jarvelin M-R, Sovio U, Bennett AJ, Melzer D, Ferrucci L, Loos RJF, Barroso I, Wareham NJ, Karpe F, Owen KR, Cardon LR, Walker M, Hitman GA, Palmer CNA, Doney ASF, Morris AD, Smith GD, the Wellcome Trust Case Control Consortium, Hattersley AT, McCarthy MI. A common variant in the FTO gene is associated with body mass index and predisposes to childhood and adult obesity. Science 2007;316:889–894
39. Loos RJF, Lindgren CM, Li S, Wheeler E, Zhao JH, Prokopenko I, Inouye M, Freathy RM, Attwood AP, Beckmann JS, Berndt SI, Bergmann S, Bennett AJ, Bingham SA, Bochud M, Brown M, Cauchi S, Connell JM, Cooper C, Smith GD, Day I, Dina C, De S, Dermitzakis ET, Doney ASF, Elliott KS, Elliott P, Evans DM, Sadaf Farooqi I, Froguel P, Ghori J, Groves CJ, Gwilliam R, Hadley D, Hall AS, Hattersley AT, Hebebrand J, Heid IM, Herrera B, Hinney A, Hunt SE, Jarvelin M-R, Johnson T, Jolley JDM, Karpe F, Keniry A, Khaw K-T, Luben RN, Mangino M, Marchini J, McArdle WL, McGinnis R, Meyre D, Munroe PB, Morris AD, Ness AR, Neville MJ, Nica AC, Ong KK, O'Rahilly S, Owen KR, Palmer CNA, Papadakis K, Potter S, Pouta A, Qi L, Randall JC, Rayner NW, Ring SM, Sandhu MS, Scherag A, Sims MA, Song K, Soranzo N, Speliotes EK, Syddall HE, Teichmann SA, Timpson NJ, Tobias JH, Uda M, Ganz Vogel CI, Wallace C, Waterworth DM, Weedon MN, Willer CJ, Wraight VL, Yuan X, Zeggini E, Hirschhorn JN, Strachan DP, Ouwehand WH, Caulfield MJ, Samani NJ, Frayling TM,

Vollenweider P, Waeber G, Mooser V, Deloukas P, McCarthy MI, Wareham NJ, Barroso I. Common variants near MC4R are associated with fat mass, weight and risk of obesity. Nat Genet 2008;40:768–775
40. Loos RJF. Recent progress in the genetics of common obesity. Br J Clin Pharmacol 2009;68:811–829
41. Frazer KA, Murray SS, Schork NJ, Topol EJ. Human genetic variation and its contribution to complex traits. Nat Rev Genet 2009;10:241–251
42. Bogardus C. Missing heritability and GWAS utility. Obesity 2009;17:209–210
43. Pou KM, Massaro JM, Hoffmann U, Lieb K, Vasan RS, O'Donnell CJ, Fox CS. Patterns of abdominal fat distribution. Diabetes Care 2009;32:481–485
44. Page-McCaw A, Ewald AJ, Werb Z. Matrix metalloproteinases and the regulation of tissue remodelling. Nat Rev Mol Cell Biol 2007;8:221–233
45. Traurig MT, Permana PA, Nair S, Kobes S, Bogardus C, Baier LJ. Differential expression of matrix metalloproteinase 3 (MMP3) in preadipocytes/stromal vascular cells from nonobese nondiabetic versus obese nondiabetic Pima Indians. Diabetes 2006;55:3160–3165
46. Unoki H, Bujo H, Shibasaki M, Saito Y. Increased matrix metalloproteinase-3 mRNA expression in visceral fat in mice implanted with cultured preadipocytes. Biochem Biophys Res Comm 2006;350:392–398
47. Hotary K, Allen E, Punturieri A, Yana I, Weiss SJ. Regulation of cell invasion and morphogenesis in a three-dimensional type I collagen matrix by membrane-type matrix metalloproteinases 1, 2, and 3. J Cell Biol 2000;149:1309–1323
48. Knäuper V, Will H, López-Otin C, Smith B, Atkinson SJ, Stanton H, Hembry RM, Murphy G. Cellular mechanisms for human procollagenase-3 (MMP-13) activation. J Biol Chem 1996;271:17124–17131
49. Halberg N, Khan T, Trujillo ME, Wernstedt-Asterholm I, Attie AD, Sherwani S, Wang ZV, Landskroner-Eiger S, Dineen S, Magalang UJ, Brekken RA, Scherer PE. Hypoxia-inducible factor 1alpha induces fibrosis and insulin resistance in white adipose tissue. Mol Cell Biol 2009;29:4467–4483

Pretreatment ASPECTS on DWI predicts 3-month outcome following rt-PA

SAMURAI rt-PA Registry

T. Nezu, MD
M. Koga, MD
K. Kimura, MD
Y. Shiokawa, MD
J. Nakagawara, MD
E. Furui, MD
H. Yamagami, MD
Y. Okada, MD
Y. Hasegawa, MD
K. Kario, MD
S. Okuda, MD
K. Nishiyama, MD
M. Naganuma, MD
K. Minematsu, MD
K. Toyoda, MD

Address correspondence and reprint requests to Dr. Kazunori Toyoda, Department of Cerebrovascular Medicine, National Cerebral and Cardiovascular Center, 5-7-1 Fujishiro-dai, Suita, Osaka 565-8565, Japan
toyoda@hsp.ncvc.go.jp

ABSTRACT

Objective: To evaluate whether the pretreatment Alberta Stroke Programme Early CT Score (ASPECTS) assessed using diffusion-weighted imaging (DWI) predicts stroke outcomes at 3 months following IV recombinant tissue-type plasminogen activator (rt-PA) therapy.

Methods: Stroke patients treated with rt-PA (0.6 mg/kg alteplase) in 10 stroke centers in Japan were retrospectively studied. ASPECTS was assessed on DWI just prior to rt-PA injection. The primary outcome was a modified Rankin Scale (mRS) score of 0-2 at 3 months. Secondary outcomes included death at 3 months and symptomatic intracerebral hemorrhage (sICH) within 36 hours.

Results: For the 477 patients (316 men, 71 ± 11 years old) enrolled, the median NIH Stroke Scale score was 13 (interquartile range 7-18.5), the median ASPECTS on DWI was 8 (7-10), and sICH was identified in 15 patients (3.1%). At 3 months, 245 (51.4%) had an mRS score of 0-2, and 29 (6.1%) had died. Patients with an mRS score of 0-2 had higher median ASPECTS (9; interquartile range 8-10) than other patients (8; 6-9, $p < 0.001$). Using receiver operating characteristic curves, the optimal cutoff ASPECTS to predict an mRS score of 0-2 was ≥7. On multivariate regression analysis, ASPECTS ≥7 was related to an mRS score of 0-2 (odds ratio 1.85; 95% confidence interval 1.07-3.24), ASPECTS ≤4 was related to death (3.61; 1.23-9.91), and ASPECTS ≤5 was related to sICH (4.74; 1.54-13.64).

Conclusion: ASPECTS on DWI was independently predictive of functional and vital outcomes at 3 months, as well as sICH within 36 hours, following rt-PA therapy for stroke patients. *Neurology*® 2010;75:555-561

GLOSSARY

ASPECTS = Alberta Stroke Programme Early CT Score; **CI** = confidence interval; **DWI** = diffusion-weighted imaging; **EIC** = early ischemic change; **ICH** = intracerebral hemorrhage; **IQR** = interquartile range; **MRA** = magnetic resonance angiography; **mRS** = modified Rankin Scale; **NIHSS** = NIH Stroke Scale; **NINDS** = National Institute of Neurological Disorders and Stroke; **OR** = odds ratio; **PWI** = perfusion-weighted imaging; **ROC** = receiver operating characteristic; **rt-PA** = recombinant tissue-type plasminogen activator; **sICH** = symptomatic intracerebral hemorrhage; **SAMURAI** = Stroke Acute Management with Urgent Risk-factor Assessment and Improvement.

Early ischemic change (EIC) allows the prediction of subsequent infarct locations, and large EIC often results in clinically significant intracerebral hemorrhage (ICH) following thrombolysis.[1-4] Thus, for patients with large EIC on the initial CT, as assessed, for example, using the one-third-of cerebral hemisphere rule, IV recombinant tissue-type plasminogen activator (rt-PA) is contraindicated according to several guidelines from the United States, Canada, Europe, and Japan.[5-8] However, visual assessment of the EIC volume depends on the reader's experience and skill, and the intrarater and interrater reliabilities in detecting EIC are not

From the Department of Cerebrovascular Medicine (T.N., M.K., M.N., K.M., K.T.), National Cerebral and Cardiovascular Center, Suita; Department of Stroke Medicine (K. Kimura), Kawasaki Medical School, Kurashiki; Departments of Neurosurgery (Y.S.) and Neurology (K.N.) and Stroke Center (Y.S., K.N.), Kyorin University School of Medicine, Mitaka; Department of Neurosurgery and Stroke Center (J.N.), Nakamura Memorial Hospital, Sapporo; Department of Stroke Neurology (E.F.), Kohnan Hospital, Sendai; Stroke Center (H.Y.), Kobe City Medical Center General Hospital, Kobe; Department of Cerebrovascular Disease (Y.O.), National Hospital Organization Kyushu Medical Center, Fukuoka; Department of Neurology (Y.H.), St Marianna University School of Medicine, Kawasaki; Division of Cardiovascular Medicine (K. Kario), Department of Medicine, Jichi Medical University School of Medicine, Shimotsuke; and Department of Neurology (S.O.), National Hospital Organization Nagoya Medical Center, Nagoya, Japan.

Study funding: Supported in part by Grants-in-Aid (H20-Junkanki-Ippan-019 [K.T.]) from the Ministry of Health, Labour and Welfare, Japan.
Disclosure: Author disclosures are provided at the end of the article.

sufficiently high.[9] In addition, strict evaluation of the volume by computerized planimetry takes time to analyze. An alternative approach for grading EIC on CT is a quantitative topographic score, the Alberta Stroke Programme Early CT Score (ASPECTS).[10] For this score, the territory of the MCA is allotted 10 points, and 1 point is subtracted for each area of EIC for each of the defined regions.

Diffusion-weighted MRI (DWI) can quickly detect hyperacute ischemic brain tissue. The contrast between ischemic tissue and normal tissue can be clearer on DWI than on conventional MRI and CT. The scoring of ASPECTS using DWI (DWI-ASPECTS) has been reported to be similar to that using CT.[11] DWI-ASPECTS predicts the risk of symptomatic ICH (sICH) after thrombolysis.[12] However, the evidence for the association between DWI-ASPECTS and chronic outcome after rt-PA therapy has been inconclusive. The aim of the present study was to evaluate whether pretreatment DWI-ASPECTS predicts functional and vital outcomes 3 months after rt-PA therapy.

Table 1 Baseline characteristics[a]

	Total (n = 477)	mRS 0–2 (n = 245)	mRS 3–6 (n = 232)
Age, y	71 ± 11	69.0 ± 11.8[b]	73.9 ± 9.5
Male	316 (66.2)	180 (73.5)[b]	136 (58.6)
Hypertension	301 (63.5)	143 (58.6)[c]	158 (68.7)
Diabetes mellitus	89 (18.7)	46 (18.9)	43 (18.5)
Dyslipidemia	102 (21.5)	55 (22.5)	47 (20.4)
Congestive heart failure	30 (6.5)	8 (3.4)[b]	22 (9.8)
Stroke subtype[c]			
Cardioembolism	293 (61.4)	146 (59.6)	147 (63.4)
Atherothrombotic stroke	77 (16.2)	31 (12.8)	46 (19.8)
Lacunar stroke	22 (4.6)	15 (6.9)	7 (3.0)
Other	85 (17.8)	53 (21.7)	32 (13.8)
Arterial occlusion site (n = 457)[b]			
Internal carotid artery	73 (16.0)	8 (3.2)	65 (28.0)
Middle cerebral artery trunk (M1)	135 (29.5)	67 (27.3)	68 (29.3)
Middle cerebral artery branch (M2)	93 (20.4)	55 (22.4)	38 (16.4)
Anterior cerebral artery	7 (1.5)	2 (0.8)	5 (2.2)
Posterior cerebral artery	16 (3.5)	9 (3.7)	7 (3.0)
Vertebrobasilar arteries	21 (4.6)	11 (4.5)	10 (4.3)
Not occluded	99 (21.7)	71 (29.0)	28 (12.1)
Onset to treatment time, min	141 ± 28	140.0 ± 26.9	141.9 ± 29.4
Pretreatment systolic blood pressure, mm Hg	151 ± 20	151.6 ± 18.2	150.1 ± 21.4
Pretreatment diastolic blood pressure, mm Hg	82 ± 15	82.9 ± 13.5	81.7 ± 16.5
Baseline NIH Stroke Scale score	13 (7–18.5)	9 (6–14)[b]	17 (11–20.75)
DWI-ASPECTS	8 (7–10)	9 (8–10)[b]	8 (6–9)

Abbreviations: ASPECTS = Alberta Stroke Programme Early CT Score; DWI = diffusion-weighted imaging; mRS = modified Rankin Scale.
[a] Data are mean ± SD for age, onset to treatment time, and blood pressure, median (interquartile range) for baseline NIH Stroke Scale score and DWI-ASPECTS, and number of patients (%) for others.
[b] $p < 0.01$ vs mRS 3–6 by t test, χ^2 test, or Mann-Whitney U test.
[c] $p < 0.05$.

METHODS Patients were derived from the Stroke Acute Management with Urgent Risk-factor Assessment and Improvement (SAMURAI) rt-PA Registry. The details of this study have been described previously.[13] In brief, this was a retrospective, observational study involving consecutive stroke patients treated with IV rt-PA from October 2005 through July 2008 in 10 stroke centers in Japan. Patient eligibility for alteplase therapy was determined based on the Japanese guideline for IV rt-PA therapy,[5] which followed the inclusion and exclusion criteria used in the National Institute of Neurological Disorders and Stroke (NINDS) study and the Japan Alteplase Clinical Trial.[14,15] According to the Japanese guideline, patients with CT-documented extensive EIC (size is not defined) were not eligible for the treatment. Since the guideline does not refer to EIC on DWI, the eligibility of patients having large EIC on DWI depended on each physician's decision. Each local ethics committee approved the retrospective collection of clinical data from the database and submission of the data to our central office. Each patient received a single alteplase dose of 0.6 mg/kg (the recommended dose in Japanese guidelines and the approved labeling) IV, with 10% given as a bolus within 3 hours of stroke onset, followed by a continuous IV infusion of the remainder over 1 hour.

Baseline data, including sex, age, comorbidities (hypertension, diabetes, hyperlipidemia, and congestive heart failure), blood pressure on admission, time from onset to treatment, neurologic deficits using the NIH Stroke Scale (NIHSS) score, and stroke subtype according to the TOAST categories,[16] were collected for all patients. Before rt-PA infusion, MRI studies, including DWI and magnetic resonance angiography (MRA), were performed on a 1.5-Tesla machine immediately before or after CT studies, principally within 10 minutes after CT. Administration of rt-PA was began around 10 minutes after CT and MRI. For the DWI sequence, high-b-value images corresponding to diffusion measurements in 3 gradient directions were acquired, in addition to a single, low-b-value image. The high b-value was 1,000 s/mm^2 and the low b-value was 0 s/mm^2 in all stroke centers. At least 2 experienced vascular neurologists in each stroke center evaluated the initial DWI and CT images to calculate quantitative EIC using ASPECTS later as a post hoc analysis. Arterial occlusion was assessed on the initial MRA. ICH was defined as CT evidence of new parenchymal hemorrhage type I or type II within the initial 36 hours[2]; it was also assessed by at least 2 experienced vascular neurologists of each stroke center. Symptomatic ICH was defined as a parenchymal ICH associated with neurologic deterioration corresponding to an increase of ≥4 points from the baseline NIHSS score.

The primary outcome was independence at 3 months, corresponding to a modified Rankin Scale (mRS) score of

0–2. Secondary outcomes were the mRS score of 0–1 at 3 months, death at 3 months, and sICH within the initial 36 hours.

Statistical analysis was performed using the JMP 7.0 statistical software (SAS Institute Inc., Cary, NC). Baseline characteristics were compared between patients with an mRS score of 0–2 and those with an mRS score of 3–6 using χ^2 tests, unpaired t tests, and the Mann-Whitney U test, as appropriate. To obtain the cutoff DWI-ASPECTS for discriminating between patients with and without each outcome, receiver operating characteristic (ROC) curves were constructed. Multivariate analyses were performed to identify predictors for primary and secondary outcomes. For each outcome, a backward selection procedure was performed using $p > 0.10$ of the likelihood ratio test as the exclusion criterion. These analyses were later repeated for patients who did not have culprit infarcts or culprit arterial occlusions in the vertebrobasilar arterial territory, the isolated anterior cerebral artery territory, or the isolated posterior cerebral artery territory. Statistical significance was established at $p < 0.05$.

RESULTS A total of 600 consecutive patients were enrolled from the SAMURAI register. Of these, 70 patients could not undergo MRI prior to rt-PA mainly due to contraindications, unsteadiness, or time limitation, and 14 patients had inferior quality DWI images that were unsuitable for evaluating EIC. Of the remaining 516 patients who received pretreatment DWI, 35 were excluded from the analysis because their premorbid mRS score was 3 or more, and 4 were excluded because their 3-month mRS scores were not available. Finally, 477 patients (316 men, 71 ± 11 years old) were studied. The baseline clinical characteristics of these patients are presented in table 1. The median NIHSS score was 13 (interquartile range [IQR] 7–18.5). The median initial DWI-ASPECTS was 8 (IQR 7–10). DWI-ASPECTS was 6 or less in 107 patients (22.4%); of these, 37 patients had ASPECTS on the initial CT of 6 or less. ASPECTS on CT for most of these 37 patients was judged to be 7 or more at the time of the treatment decision, and was revised to be lower on the later reassessment.

Of these 477 patients, 245 (51.4%) were independent (mRS 0–2), and 29 (6.1%) had died by 3 months (figure 1). Within the initial 36 hours, 40 (8.4%) had parenchymal ICH, including 15 (3.1%) with sICH.

Association of DWI-ASPECTS with functional outcome. In table 1, the baseline characteristics are compared between patients with mRS scores of 0–2 and those with mRS scores of 3–6. The median initial DWI-ASPECTS was 9 (IQR 8–10) in patients with mRS scores of 0–2 and 8 (IQR 6–9) in those with mRS scores of 3–6 ($p < 0.001$). Patients with mRS scores of 0–2 were more frequently male ($p < 0.001$), younger ($p < 0.001$), less hypertensive ($p = 0.028$), less commonly had congestive heart failure ($p = 0.007$), and had lower baseline NIHSS scores ($p < 0.001$) than those with mRS scores of 3–6. Stroke subtype ($p = 0.030$) and arterial occlusion site ($p < 0.001$) differed between the groups; the internal carotid artery was relatively often occluded in patients with mRS scores of 3–6. Figure 2A shows the 3-month mRS scores in patients with different DWI-ASPECTS. The percentage of patients with mRS scores of 0–2 was similar among those with DWI-ASPECTS ≥7 and gradually decreased with the reduction in the DWI-ASPECTS when the score was ≤6. The optimal cutoff DWI-ASPECTS to predict patients with mRS scores of 0–2 at 3 months was ≥7, with a sensitivity of 88%, specificity of 33%, and an area under the ROC curve of 0.623 (figure 3). Overall, 215 (58.1%) of 370 patients with DWI-ASPECTS ≥7 and 30 (28.0%) of 107 patients with DWI-ASPECTS ≤6 had mRS scores of 0–2 ($p < 0.001$, figure 1). On multivariate regression analysis using backward selection, DWI-ASPECTS ≥7 was an independent predictor of an mRS score of 0–2 (odds ratio [OR] 1.85, 95% confidence interval [CI] 1.07–3.24; $p = 0.029$), along with younger age, male sex, lower NIHSS score, and absence of internal carotid artery occlusion (table 2).

For the analysis of the secondary outcome on mRS scores of 0–1 at 3 months, 26 patients with the premorbid mRS score of 2 were excluded. For the remaining 451 patients (304 men, 71 ± 11 years old), the optimal cutoff DWI-ASPECTS to predict patients with mRS scores of 0–1 was ≥9, with a sensitivity of 62%, specificity of 56%, and an area under the ROC curve of 0.627. On multivariate

Figure 1 Modified Rankin Scale score at 3 months

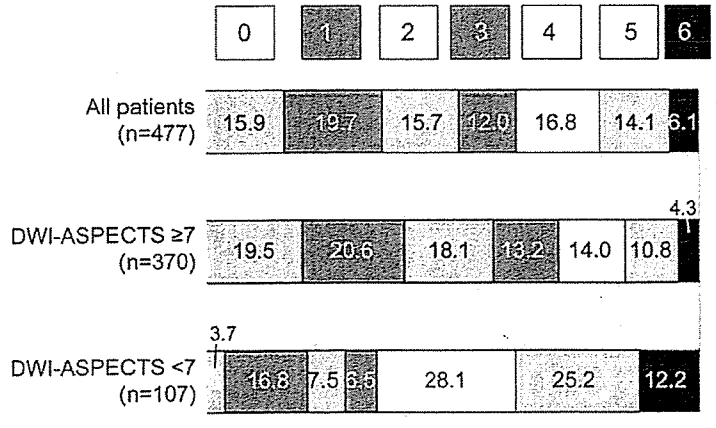

DWI-ASPECTS = scoring of Alberta Stroke Programme Early CT Score using diffusion-weighted imaging.

regression analysis, DWI-ASPECTS ≥9 was not an independent predictor of an mRS score of 0–1 (OR 1.40, 95% CI 0.87–2.24; $p = 0.160$).

Association of DWI-ASPECTS with mortality. DWI-ASPECTS was lower in patients who had died by 3 months (median 7, IQR 4–9.5) than in survivors (median 9, IQR 7–10; $p = 0.038$). Among patients with different DWI-ASPECTS, mortality was similar among patients with DWI-ASPECTS ≥7 and exceeded 20% when the score was ≤4 (figure 2A). The optimal cutoff DWI-ASPECTS to predict death at 3 months was ≤5, with a sensitivity of 38%, specificity of 88%, and an area under the ROC curve of 0.613. On multivariate regression analysis, DWI-ASPECTS ≤5 was not related to death at 3 months (OR 1.93, 95% CI 0.68–5.03; $p = 0.206$). When lowering the cutoff by 1 point, based on the findings in figure 2A, DWI-ASPECTS ≤4 was independently related to death (OR 3.61, 95% CI 1.23–9.91; $p = 0.021$) (table 2).

Association of DWI-ASPECTS with ICH. DWI-ASPECTS was lower in patients with sICH (median 7, IQR 5–9) than in those without (median 9, IQR 7–10; $p = 0.011$). The percentage of sICH was 4% or less among patients with DWI-ASPECTS ≥6, and exceeded 10% among patients with DWI-ASPECTS 4 and 5 (figure 2B). The optimal cutoff DWI-ASPECTS for predicting symptomatic ICH was ≤5, with a sensitivity of 40%, specificity of 87%, and an area under the ROC curve of 0.689. On multivariate regression analysis, DWI-ASPECTS ≤5 was an independent predictor of sICH (OR 4.74, 95% CI 1.54–13.64; $p = 0.008$) (table 2).

Analyses excluding patients with vertebrobasilar, anterior cerebral, and posterior cerebral arterial strokes. After excluding 44 patients with ischemia in the vertebrobasilar, anterior cerebral, and posterior cerebral artery systems, 433 patients (287 men, 71 ± 11 years old) were analyzed. The optimal cutoff DWI-ASPECTS to predict patients with mRS scores of 0–2 at 3 months was ≥7, with a sensitivity of 87%, specificity of 37%, and an area under the ROC curve of 0.637. On multivariate regression analysis, DWI-ASPECTS ≥7 was an independent predictor of an mRS score of 0–2 (OR 1.82, 95% CI 1.03–3.24; $p = 0.040$). Similarly, DWI-ASPECTS ≤4 was independently related to death (OR 3.96, 95% CI 1.31–11.19; $p = 0.016$), and DWI-ASPECTS ≤5 was an independent predictor of sICH (OR 4.76, 95% CI 1.52–14.20; $p = 0.009$).

Figure 2 Modified Rankin Scale score (mRS) at 3 months (A) and parenchymal intracranial hemorrhage (ICH) within the initial 36 hours (B) in patients with each DWI-ASPECTS score

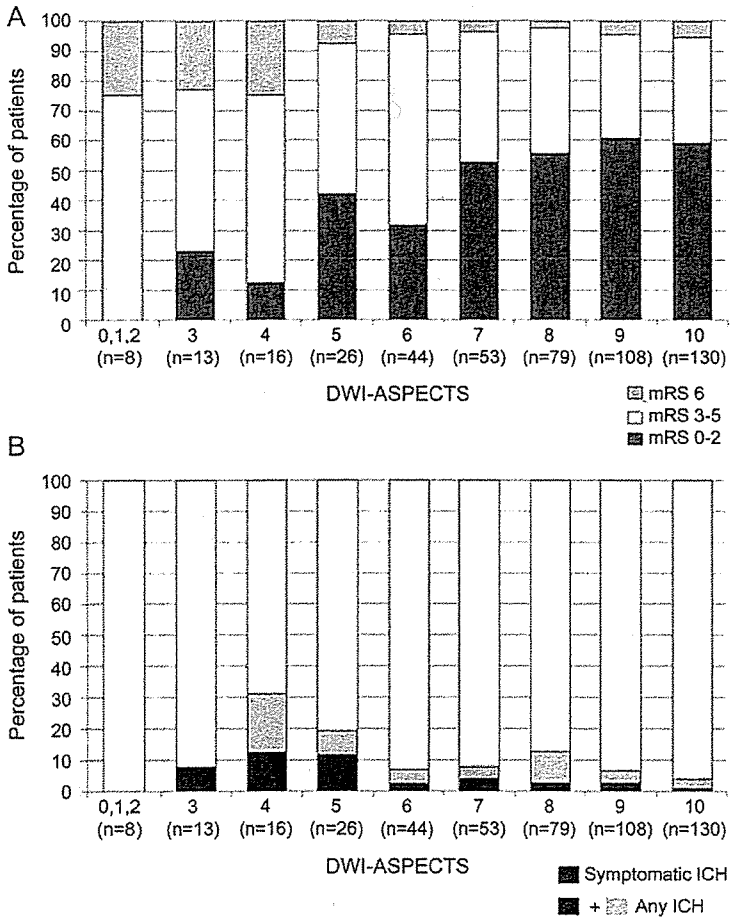

DWI-ASPECTS = scoring of Alberta Stroke Programme Early CT Score using diffusion-weighted imaging.

DISCUSSION In this study, the associations between DWI-ASPECTS and clinical outcomes at 3 months after IV rt-PA therapy were assessed. The major new finding of this study was that pretreatment DWI-ASPECTS was associated with functional and vital outcomes at 3 months; DWI-ASPECTS ≥7 was predictive of an mRS score of 0–2, and DWI-ASPECTS ≤4 was predictive of death.

Extensive EIC over one-third of the MCA territory on CT has been reported to be predictive of poor functional outcome and symptomatic ICH after thrombolytic therapy.[1-3] ASPECTS ≥8 could exclude most patients with EIC over one-third of the MCA territory on CT,[17] and it had a prognostic value for favorable outcome among acute stroke patients treated with IV rt-PA.[10,18] In contrast, EIC on DWI is the earliest indicator of brain ischemic changes, and it is more sensitive and clearer to delineate the extension of brain ischemia than EIC on CT.[19] A coauthor of this study previously reported

that initial DWI-ASPECTS ≤5 was independently associated with NIHSS score ≥20 at 7 days after rt-PA therapy.[20] In our single-center study, initial DWI-ASPECTS ≥7 was independently associated with an mRS score of 0–1 at 3 months after rt-PA.[21] In this study, DWI-ASPECTS ≥7 was independently predictive of patients with a 3-month mRS score of 0–2.

Barber et al.[11] assessed ASPECTS for stroke patients within 6 hours of onset using both CT and DWI, and they found that DWI-ASPECTS was lower than ASPECTS on CT. The mean ASPECTS difference between the 2 modalities was 0.43. The superior ability of DWI over CT to detect the extension of EIC, as well as the time delay for DWI performance, appeared to cause the difference. Thus, the present cutoff of DWI-ASPECTS ≥7 to predict functional outcome appears to have a close relationship with the cutoff ASPECTS ≥8 on CT as a known prognostic variable for rt-PA-treated patients.[10,18]

In the NINDS rt-PA Stroke Study, IV rt-PA for patients with baseline ASPECTS on CT <3 increased mortality compared with placebo treatment; 2 of the 5 deaths in the rt-PA therapy group were associated with symptomatic ICH compared with none in the placebo group.[22] DWI-ASPECTS was reported to predict unfavorable short-term outcome (NIHSS score ≥20 at 7 days)[20]; however, to our knowledge, the score has not been previously reported to affect mortality after rt-PA. In figure 2A, the marked increase in mortality is shown below DWI-ASPECTS ≤4, indicating the association of low DWI-ASPECTS and higher mortality rates. However, precise cutpoints were difficult to define. Of the 9 deaths in patients with DWI-ASPECTS ≤4, 3 resulted from symptomatic ICH, 5 from cerebral herniation due to massive stroke, and 1 from severe cardiac failure (data not shown).

Pretreatment DWI volume has recently been recognized as an independent risk for sICH after thrombolysis.[4,23,24] Pretreatment DWI-ASPECTS ≤7 was advocated as a predictor of sICH after IV or intraarterial thrombolysis within 6 hours of onset.[12] In contrast, for our patients receiving IV thrombolysis within 3 hours, pretreatment DWI-ASPECTS ≤5 was an independent predictor of sICH.

MRI is currently not generally the primary imaging modality in acute stroke patients because of the possible time delay, its potentially inferior ability for detecting acute ICH, and its contraindications, which are mainly due to metal implants. Several studies have reported that MRI screening within 3 hours of onset did not delay IV rt-PA therapy or lead to worse outcomes relative to CT screening.[25,26] Regarding hyperacute ICH, MRI was reported to be as reliable as CT, because small amounts of deoxyhemoglobin are detectable within the first hours of ICH on T2*-weighted images.[27,28] Thus, MRI could be used as the modality for emergency imaging of acute stroke patients, whether ischemic or hemorrhagic.[29] In addition, MRI penumbral assessment with the mismatch between DWI and perfusion-weighted imaging (PWI) is promising to improve patient selection and outcome for IV rt-PA therapy.[30,31] Since planimetric PWI-DWI mismatch assessment is time-consuming, ASPECTS can be applied to assess PWI-DWI mismatch.[32]

This study has several limitations. First, DWI-ASPECTS is not useful for evaluating strength and size variations of high-intensity change within each allotted lesion on DWI. Because slight alterations in high intensity on DWI are believed to contain reversible ischemic tissues, DWI-ASPECTS may overestimate the extension of EIC.[33] Second, this was an observational study and patient eligibility for rt-PA was determined according to each patient's situation, though the determination was principally based on the Japanese guidelines.[8] In particular, eligibility of patients having large EIC on DWI depended on each physician's decision, and we did not assess how many patients with low DWI-ASPECTS and relatively high ASPECTS on CT were excluded from the

Figure 3 **Receiver operating characteristic curves of scoring of Alberta Stroke Programme Early CT Score using diffusion-weighted imaging for predicting modified Rankin Scale scores of 0–2**

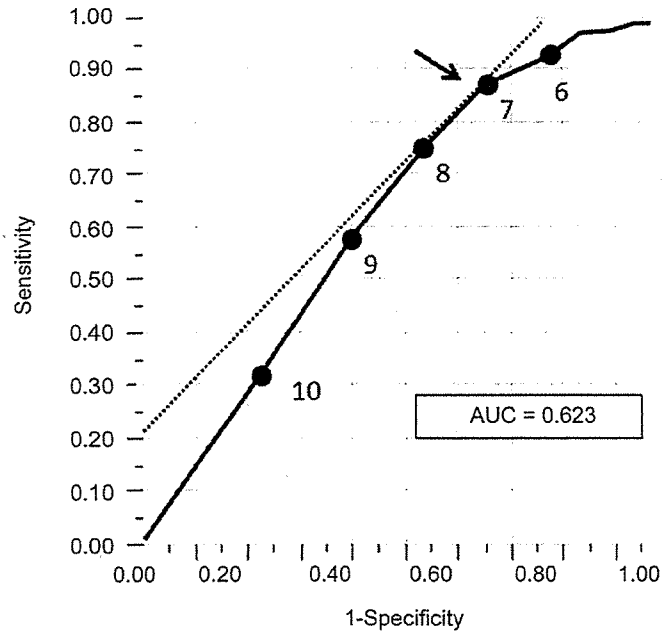

The arrow indicates the optimal cutoff point. AUC = area under the receiver operating characteristic curve.

Table 2 Characteristics associated with a modified Rankin Scale score of 0–2 and death at 3 months, and symptomatic intracerebral hemorrhage[a]

	OR	95% CI	p
mRS 0–2			
Age, per 1-year increase	0.97	0.95–0.99	<0.001
Female	0.59	0.37–0.95	0.031
Hypertension	0.67	0.42–1.05	0.083
Baseline NIHSS, per 1-point increase	0.92	0.89–0.96	<0.001
DWI-ASPECTS ≥7	1.85	1.07–3.24	0.029
ICA occlusion	0.13	0.06–0.28	<0.001
Death			
Congestive heart failure	7.61	2.46–22.35	<0.001
DWI-ASPECTS ≤4	3.61	1.23–9.91	0.021
ICA occlusion	4.45	1.69–11.64	0.003
Symptomatic ICH			
DWI-ASPECTS ≤5	4.74	1.54–13.64	0.008

Abbreviations: ASPECTS = Alberta Stroke Programme Early CT Score; CI = confidence interval; DWI = diffusion-weighted imaging; ICA = internal carotid artery; ICH = intracerebral hemorrhage; mRS = modified Rankin Scale; NIHSS = NIH Stroke Scale; OR = odds ratio.
[a] Adjusted by characteristics selected by a backward selection procedure.

study. Third, 84 patients lacked MRI information, which may have caused selection bias. Fourth, all of the patients received 0.6 mg/kg alteplase, which is the recommended dose in Japan. Thus, the clinical value of DWI-ASPECTS in patients treated with the generally accepted standard dose of alteplase (0.9 mg/kg) outside of Japan was not ascertained. Fifth, we did not collect data for stroke patients who did not receive thrombolysis. Thus, we could not compare the present results with stroke outcome of patients who were excluded from the therapy because of extensive EIC. Finally, since DWI-ASPECTS for most of the patients was high (the lower 25% value was 7), the median DWI-ASPECTS did not differ much between patients with good outcomes and those without.

Pretreatment MRI with DWI provides valuable information for predicting clinical outcome after IV rt-PA therapy. Although clinical use of rt-PA should not be chosen solely using DWI-ASPECTS because it requires consideration of various underlying conditions, patients with DWI-ASPECTS of 4 or less do not seem to be good candidates for IV rt-PA since most patients with these scores have fatal or dependent outcomes. DWI-ASPECTS of 5 may be another warning sign for choosing rt-PA since more than 10% of patients with this score developed sICH. A confirmation of the present findings using patients treated with the regular dose of alteplase is needed.

DISCLOSURE

Dr. Nezu, Dr. Koga, Dr. Kimura, Dr. Shiokawa, Dr. Nakagawara, Dr. Furui, Dr. Yamagami, Dr. Okada, Dr. Hasegawa, Dr. Kario, Dr. Okuda, Dr. Nishiyama, and Dr. Naganuma report no disclosures. Dr. Minematsu serves on the editorial boards of *Cerebrovascular Diseases*, the *International Journal of Stroke*, and the *Journal of Stroke and Cerebrovascular Diseases* and receives research support from Asteras Pharma Inc., Takeda Pharmaceutical Company Limited, Sanofi-Aventis, Lundbeck Inc., Mitsubishi Tanabe Pharma Corporation, Kyowa Hakko Kirin Pharma, Inc., Hitachi Medical Corporation, MHLM, Japan, Research Grants for Cardiovascular Diseases, Grant-in-Aid, and the Foundation for Biomedical Research and Innovation. Dr. Toyoda receives research support from Grants-in-Aid from the Ministry of Health, Labour and Welfare, Japan.

Received December 3, 2009. Accepted in final form April 28, 2010.

REFERENCES

1. Moulin T, Cattin F, Crepin-Leblond T, et al. Early CT signs in acute middle cerebral artery infarction: predictive value for subsequent infarct locations and outcome. Neurology 1996;47:366–375.
2. Hacke W, Kaste M, Fieschi C, et al. Intravenous thrombolysis with recombinant tissue plasminogen activator for acute hemispheric stroke: The European Cooperative Acute Stroke Study (ECASS). JAMA 1995;274:1017–1025.
3. Silver B, Demaerschalk B, Merino JG, et al. Improved outcomes in stroke thrombolysis with pre-specified imaging criteria. Can J Neurol Sci 2001;28:113–119.
4. Butcher K, Christensen S, Parsons M, et al. Post-thrombolysis blood pressure elevation is associated with hemorrhagic transformation. Stroke 2010;41:72–77.
5. Adams HP Jr, del Zoppo G, Alberts MJ, et al. Guidelines for the early management of adults with ischemic stroke: a guideline from the American Heart Association/American Stroke Association Stroke Council, Clinical Cardiology Council, Cardiovascular Radiology and Intervention Council, and the Atherosclerotic Peripheral Vascular Disease and Quality of Care Outcomes in Research Interdisciplinary Working Groups: the American Academy of Neurology affirms the value of this guideline as an educational tool for neurologists. Stroke 2007;38:1655–1711.
6. Norris JW, Buchan A, Cote R, et al. Canadian guidelines for intravenous thrombolytic treatment in acute stroke: a consensus statement of the Canadian Stroke Consortium. Can J Neurol Sci 1998;25:257–259.
7. The European Stroke Organisation Executive Committee. Guidelines for management of ischaemic stroke and transient ischaemic attack 2008. Cerebrovasc Dis 2008;25:457–507.
8. Shinohara Y, Yamaguchi T. Outline of the Japanese Guidelines for the Management of Stroke 2004 and subsequent revision. Int J Stroke 2008;3:55–62.
9. Wardlaw JM, Mielke O. Early signs of brain infarction at CT: observer reliability and outcome after thrombolytic treatment–systematic review. Radiology 2005;235:444–453.
10. Barber PA, Demchuk AM, Zhang J, Buchan AM. Validity and reliability of a quantitative computed tomography score in predicting outcome of hyperacute stroke before thrombolytic therapy: ASPECTS Study Group Alberta

Stroke Programme Early CT Score. Lancet 2000;355:1670–1674.
11. Barber PA, Hill MD, Eliasziw M, et al. Imaging of the brain in acute ischaemic stroke: comparison of computed tomography and magnetic resonance diffusion-weighted imaging. J Neurol Neurosurg Psychiatry 2005;76:1528–1533.
12. Singer OC, Kurre W, Humpich MC, et al. Risk assessment of symptomatic intracerebral hemorrhage after thrombolysis using DWI-ASPECTS. Stroke 2009;40:2743–2748.
13. Toyoda K, Koga M, Naganuma M, et al. Routine use of intravenous low-dose recombinant tissue plasminogen activator in Japanese patients: general outcomes and prognostic factors from the SAMURAI register. Stroke 2009;40:3591–3595.
14. The National Institute of Neurological Disorders and Stroke rt-PA Stroke Study Group. Tissue plasminogen activator for acute ischemic stroke. N Engl J Med 1995;333:1581–1587.
15. Yamaguchi T, Mori E, Minematsu K, et al. Alteplase at 0.6 mg/kg for acute ischemic stroke within 3 hours of onset: Japan Alteplase Clinical Trial (J-ACT). Stroke 2006;37:1810–1815.
16. Adams HP Jr, Bendixen BH, Kappelle LJ, et al. Classification of subtype of acute ischemic stroke: definitions for use in a multicenter clinical trial TOAST Trial of Org 10172 in Acute Stroke Treatment. Stroke 1993;24:35–41.
17. Phan TG, Donnan GA, Koga M, et al. The ASPECTS template is weighted in favor of the striatocapsular region. Neuroimage 2006;31:477–481.
18. Dzialowski I, Hill MD, Coutts SB, et al. Extent of early ischemic changes on computed tomography (CT) before thrombolysis: prognostic value of the Alberta Stroke Program Early CT Score in ECASS II. Stroke 2006;37:973–978.
19. Barber PA, Darby DG, Desmond PM, et al. Identification of major ischemic change: diffusion-weighted imaging versus computed tomography. Stroke 1999;30:2059–2065.
20. Kimura K, Iguchi Y, Shibazaki K, et al. Large ischemic lesions on diffusion-weighted imaging done before intravenous tissue plasminogen activator thrombolysis predicts a poor outcome in patients with acute stroke. Stroke 2008;39:2388–2391.
21. Nakashima T, Toyoda K, Koga M, et al. Arterial occlusion sites on MRA influence the efficacy of intravenous low-dose (0.6 mg/kg) alteplase therapy for ischemic stroke. Int J Stroke 2009;4:425–431.
22. Demchuk AM, Hill MD, Barber PA, Silver B, Patel SC, Levine SR. Importance of early ischemic computed tomography changes using ASPECTS in NINDS rtPA Stroke Study. Stroke 2005;36:2110–2115.
23. Lansberg MG, Thijs VN, Bammer R, et al. Risk factors of symptomatic intracerebral hemorrhage after tPA therapy for acute stroke. Stroke 2007;38:2275–2278.
24. Singer OC, Humpich MC, Fiehler J, et al. Risk for symptomatic intracerebral hemorrhage after thrombolysis assessed by diffusion-weighted magnetic resonance imaging. Ann Neurol 2008;63:52–60.
25. Kang DW, Chalela JA, Dunn W, Warach S. MRI screening before standard tissue plasminogen activator therapy is feasible and safe. Stroke 2005;36:1939–1943.
26. Schellinger PD, Thomalla G, Fiehler J, et al. MRI-based and CT-based thrombolytic therapy in acute stroke within and beyond established time windows: an analysis of 1210 patients. Stroke 2007;38:2640–2645.
27. Linfante I, Llinas RH, Caplan LR, Warach S. MRI features of intracerebral hemorrhage within 2 hours from symptom onset. Stroke 1999;30:2263–2267.
28. Schellinger PD, Jansen O, Fiebach JB, Hacke W, Sartor K. A standardized MRI stroke protocol: comparison with CT in hyperacute intracerebral hemorrhage. Stroke 1999;30:765–768.
29. Chalela JA, Kidwell CS, Nentwich LM, et al. Magnetic resonance imaging and computed tomography in emergency assessment of patients with suspected acute stroke: a prospective comparison. Lancet 2007;369:293–298.
30. Hjort N, Butcher K, Davis SM, et al. Magnetic resonance imaging criteria for thrombolysis in acute cerebral infarct. Stroke 2005;36:388–397.
31. Donnan GA, Baron JC, Ma H, Davis SM. Penumbral selection of patients for trials of acute stroke therapy. Lancet Neurol 2009;8:261–269.
32. Butcher K, Parsons M, Allport L, et al. Rapid assessment of perfusion-diffusion mismatch. Stroke 2008;39:75–81.
33. Bykowski JL, Latour LL, Warach S. More accurate identification of reversible ischemic injury in human stroke by cerebrospinal fluid suppressed diffusion-weighted imaging. Stroke 2004;35:1100–1106.

Biomaterials 31 (2010) 4231–4237

Contents lists available at ScienceDirect

Biomaterials

journal homepage: www.elsevier.com/locate/biomaterials

Continuous separation of cells of high osteoblastic differentiation potential from mesenchymal stem cells on an antibody-immobilized column

Atsushi Mahara [1], Tetsuji Yamaoka*

Department of Biomedical Engineering, Advanced Medical Engineering Center, National Cardiovascular Center Research Institute, Suita, Japan

ARTICLE INFO

Article history:
Received 24 December 2009
Accepted 21 January 2010
Available online 24 February 2010

Keywords:
Mesenchymal stem cells
Selection
Interface
Osteoblast

ABSTRACT

Here, we report that two distinctive cell populations with osteoblastic differentiation ability were found in adherent cell populations from bone marrow. Mesenchymal stem cells (MSCs) were conventionally isolated by using adherent property of bone marrow cells onto a plastic culture dish. MSCs enriched on the basis of their adherent property were considered phenotypically and functionally heterogeneous. We developed a ligand-immobilized surface for separating subpopulation of adherent cells derived from bone marrow by the cell rolling process. We successfully isolate two cell populations with high differentiation ability for osteoblasts in adherent bone marrow cells by using the anti-CD34 antibody-immobilized column. The antibody was covalently conjugated with polyacrylic acid and introduced onto the inner surface of a silicone tube. When cell suspension of MSCs was injected into the antibody-immobilized column, different cell populations were isolated. After the cultivation of isolated cells in the osteoblastic differentiation medium for 1 week, few sub-populations were strongly induced to form osteoblastic cells. This study revealed that the ligand-immobilized surface can be used to continually separate cell populations under a labeling-free condition.

1. Introduction

It is widely known that adherent cells found in bone marrow have an ability to differentiate into osteoblasts, adipocytes and chondrocytes. That stem cell is generally named as marrow stromal cells or mesenchymal stem cells (MSCs). Cell differentiation property and its mechanisms have been widely studied in clinical and biological fields. In particular, the field of regenerative medicine focuses on tissue derived stem cells for autologous cell transplantation [1,2]. One important finding is that MSCs, which exist in not only bone marrow but also cord blood and adipose tissue, have therapeutic potential for heart, neural, and brain diseases [3–5]. A standard procedure for isolation of MSCs was reported by Pittenger et al. [6]. MSCs are easily separated by using the adherent property of bone marrow cells onto plastic culture dishes. Ficoll-Hypaque density gradient centrifugation is also used for separating mononuclear cells containing MSCs [7,8]. Other isolation methods based on selection of non-adherent cell population [9], STRO-1 antibody-recognized antigen level [10], and size-sieved cell population [11] have been reported. Isolation methods based on various combinations of cell surface markers have been reported by many groups [12–16].

Although the adherent property of MSCs has been widely used for their isolation, MSCs enriched on the basis of their adherent property are considered as phenotypically and functionally heterogeneous [17]. Surface marker characteristics such as marker density and its variation change with the differentiation process and development of MSCs. Surface marker profile of murine MSCs significantly differ with the passage levels [18,19]. CD34 expression of hematopoietic stem cells continuously decreases with the developmental stage [20]. Consequently, the development of a new approach to isolate MSCs population is important for homogeneous separation.

We have recently developed an antibody-immobilized column which can separate CD34-positive KG-1a cells from CD34 negative HL60 cell [21]. The separation mechanism seems to be based on dynamic interaction between cell surface marker (CD34) and immobilized antibody, known as the cell rolling. In nature, cell rolling is mainly observed in blood vessels as an inflammatory response of leukocytes [22], and its mechanism is derived from temporary interaction between cell surface and ligands. Rolling velocity is regulated by the ligand or cell surface receptor density [23–27]. Thus, cells with different rolling velocities are separated on the surface constantly modified with the ligand against a specific cell surface marker. This separation technique would

* Corresponding author. Tel.: +81 6 6833 5012x2637; fax: +81 6 6835 5476.
E-mail addresses: mahara@ri.ncvc.go.jp (A. Mahara), yamtet@ri.ncvc.go.jp (T. Yamaoka).
[1] Tel.: +81 6 6833 5012x2621; fax: +81 6 6835 5476.

0142-9612/$ – see front matter © 2010 Elsevier Ltd. All rights reserved.
doi:10.1016/j.biomaterials.2010.01.126

principally enable a labeling-free process, and the isolated cells are not contaminated with fluorescent or magnetic-labeled antibody. This procedure would be effective in separating sub-populations of MSCs with different density of surface marker.

In the present study, we applied the antibody-immobilized column to heterogeneous which acquired from murine bone marrow by conventional isolation procedures, and successfully found two different populations in the crude MSCs. The fractions of MSCs were cultured under an osteoblastic differentiation condition for 1 week, and gene expression of specific markers was analyzed by real-time polymerase chain reaction (PCR). To evaluate calcium deposition on the cells, staining with alizarine red S solution was carried out.

2. Materials and methods

2.1. Isolation and culture of mouse MSCs

MSCs were collected according to a protocol modified from Tropel et al. [16]. Mouse bone marrow cells (BMCs) were isolated by flushing the marrow cavities of 8–10-weeks-old C57Bl/6 mice (Japan SLC, Inc., Shizuoka, Japan). BMCs were cultured on a polystyrene cell culture dish (Iwaki Glass, Chiba, Japan) with alpha-MEM (Gibco-Invitrogen, Carlsbad, CA) containing 15% fetal bovine serum (FBS; MB Biomedicals, Inc., Eschwege, Germany), 25 U/ml penicillin, and 25 μg/ml streptomycin (Wako Pure Chemical Industries, Ltd., Osaka, Japan). Non-adherent cells were removed by replacing the culture medium after 3 days. The cells were grown to confluency, washed with the medium, and subcultured by using the Trypsin/EDTA kit (Lonza, Walkersville, MD). Confluent cells were plated at 1:2 to 1:3 dilutions. The adherent cells enriched into plastic culture dish with early passage (passage 3 or 4) were subjected to all experiment as crude MSCs.

2.2. Surface marker analysis and cell sorting by fluorescence activated cell sorting

To evaluate the expression of surface markers by fluorescence-activated cell sorting (FACS), cells were suspended in PBS buffer for 30 min at 4 °C with fluorescein- or phenylephrine-conjugated antibodies against the surface markers CD29, CD31, CD34, CD44, CD45, CD81, CD11b and Sca-1. Antibody labeling was performed using the standard protocol. CD29 and CD31 antibodies were purchased from AbD Serotec (Oxford, UK) and Immunotech (Marseille, France), respectively. CD34, CD11b and Sca-1 antibodies were purchased from eBiocience (San Diego, CA). CD44, CD45 and CD81 antibodies were purchased from Pharmingen (San Diego, CA). After labeling with antibodies, 10^4 cells were analyzed with a FACScalibur flow cytometer (BD Biosciences, San Jose, CA). Conventional sorting of cells with different CD34 expression levels was conducted by FACSAria (BD Biosciences), as control experiment.

2.3. Preparation of the anti-CD34 antibody-immobilized column

Silicone tubes with 0.5 mm inner diameter were used as a substrate for the antibody-immobilized column. Graft polymerization of acrylic acid onto the silicone tube surface was conducted as follows. The tube was treated with ozone gas (ON-3-2, Nippon Ozone Co., LTD., Tokyo, Japan) for 4 h, dipped in 10% acrylic acid/methanol solution, and incubated at 60 °C. After 4 h, the tube was washed with water [28,29]. Graft polymerization was confirmed by toluidine blue staining. To immobilize anti-CD34 antibody on the tube surface, the poly(-acrylic acid)-grafted tube was pre-activated with 1-ethyl-3-(3-dimethylaminopropyl) carbodiimide hydrochloride (WSC), filled with the anti-mouse CD34 rat IgG antibody (AbD Serotec) solution at concentration of 10 μg/ml, and incubated at 37 °C for 15 h. The tube was washed with PBS, treated with 1 mM 2-aminoethanol solution for 1 h, and preserved at 4 °C until experimental use. The column length was 10 cm, and the tilt angle was 20°.

2.4. Separation of crude MSCs on the antibody-immobilized column

A total of 2×10^4 cells of crude MSCs in 10 μL PBS were injected into the column. The column was flushed with PBS buffer at the flow rate of 50 μL/min until the flow

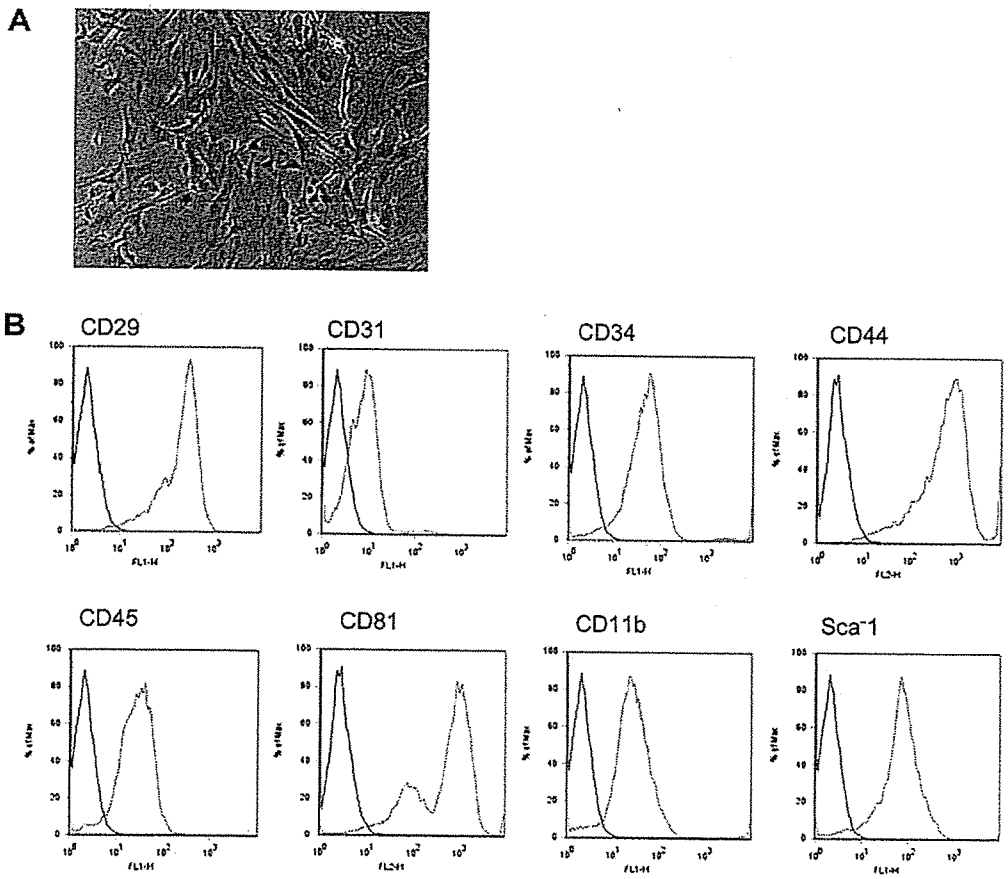

Fig. 1. (A) Morphology of murine MSCs culture. Cultured cells contained some type of cells like small round cells and fibroblast-like cells. (B) Surface marker expression of murine MSCs at passage 2. MSCs were stained with an FITC or PE-labeled antibody. Staining cells were shown in red histogram, and the black is unstained cells as control. These data were confirmed by 3 independent experiments.

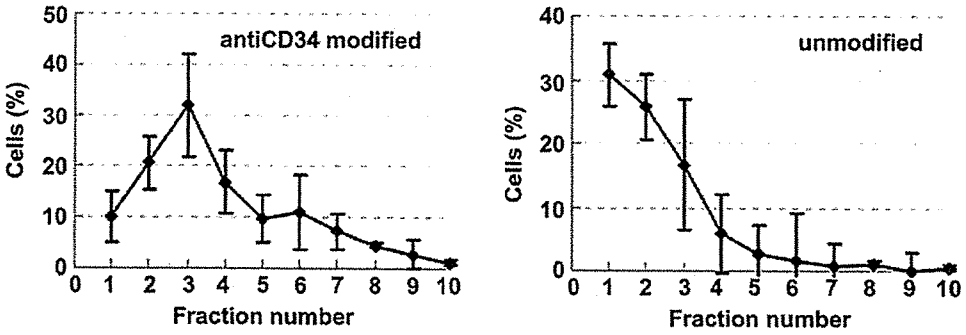

Fig. 2. Elution profiles of murine MSCs on the anti-CD34 antibody-immobilized column or unmodified column. Cell number ratio normalized by the total cell number was plotted against the fraction number. Each data point represents results from 3 independent experiment and the data are presented as mean ± standard error of the means.

volume of 250 μL, and at 600 μL/min thereafter. Eluted cell suspension was collected from top of the column, and cell suspensions were fractionated by elution volume (12.5 μL per fraction). Number and surface marker profile of cells in each fraction was analyzed by the FACS system.

2.5. Differentiation of isolated MSCs into osteoblasts

Purified MSC fractions were acquired from 2×10^4 crude MSCs. MSCs separated on the antibody-immobilized column were cultured on fibronectin-coated 24-well plates (FALCON, Oxnard, CA) with the osteoblastic differentiation medium containing 10^{-8} M dexamethasone, 10 mM β-glycerophosphate, and 0.3 mM ascorbic acid (all three reagents from Sigma–Aldrich, St. Louis, MO). The medium was changed 3 times per week. The cells were fixed with 10% formalin for 20 min at room temperature (RT) and stained with alizarin red S solution.

2.6. Gene expression analysis by real-time PCR

After culturing in differentiation medium for 1 week, total cellular RNA was isolated using Quickgene Mini80 with Quickgene RNA cultured cell kit S (FUJIFILM, Tokyo, Japan). Reverse transcription (ReverTra Ace, TOYOBO Co., LTD., Osaka, Japan) using oligo dT_{18} primer was performed on aliquots (200 ng) of total RNA as a template. The resultant cDNA was used for PCR amplification, and PCR analysis was

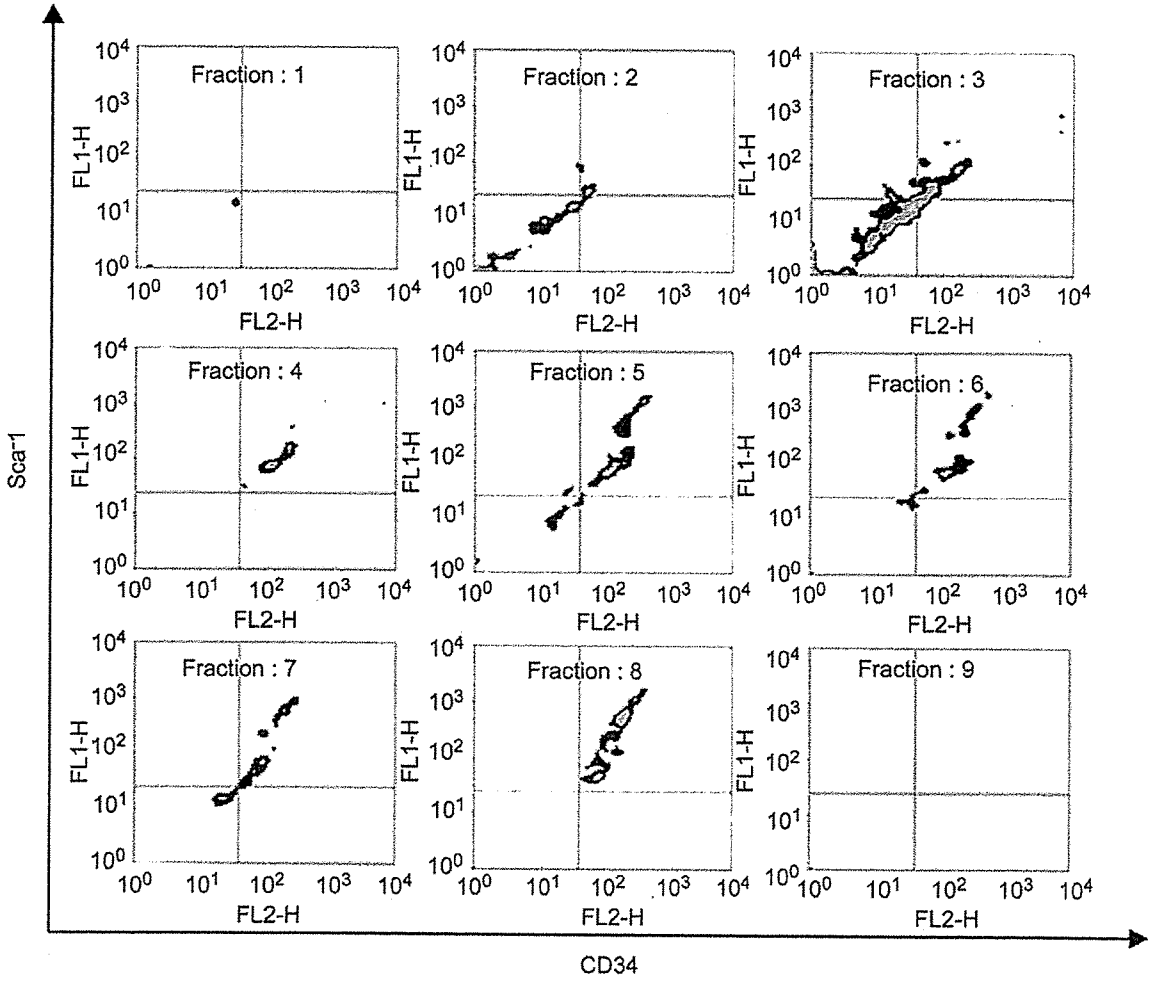

Fig. 3. Surface maker expression of isolated MSCs. Two-dimensional expression analysis of CD34 or Sca-1 was carried out in isolated cells fractions.

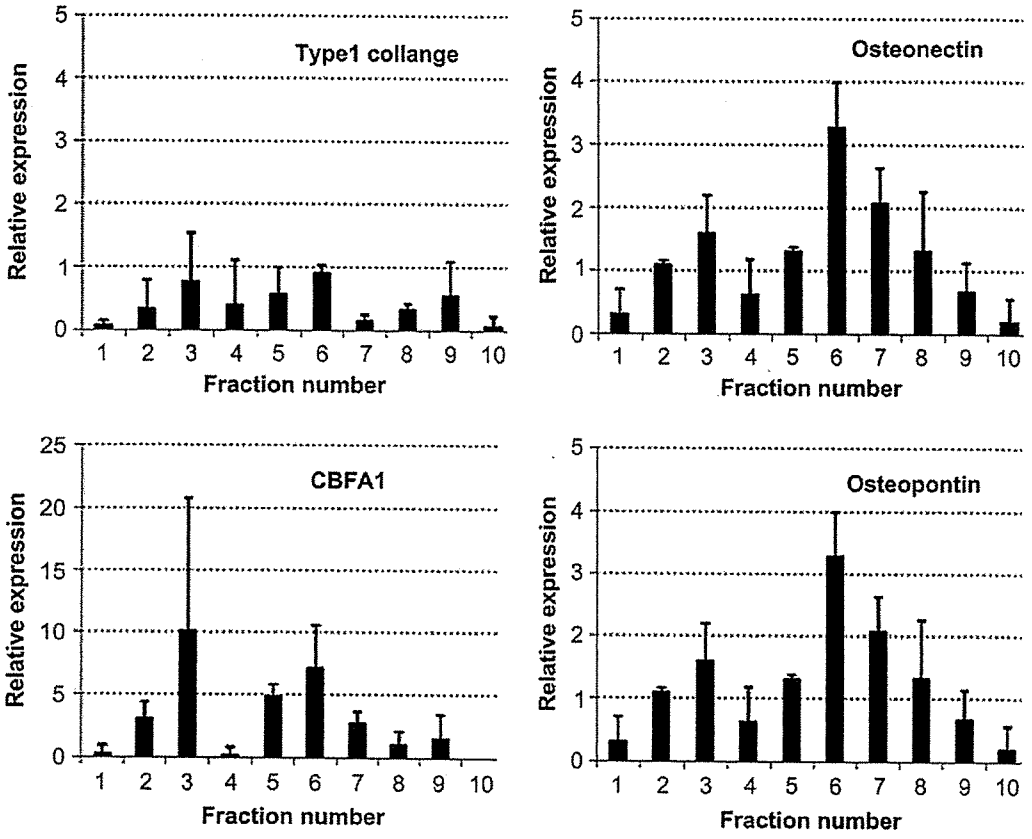

Fig. 4. Gene expression analyses of isolated MSCs on the anti-CD34 antibody-immobilized column for osteoblastic differentiation after 1 week. Relative expression is normalized by the expression of crude MSCs. GAPDH expression level was used as the internal standard control. Each data point represents results from 3 independent experiment and the data are presented as mean ± standard error of the means.

carried out by the GeneAmp 5700 Sequence Detection System (Applied Biosystems, Foster City, CA). PCR primers were designed by Primer Express software (Applied Biosystems). Type 1 collagen, CBFA1, osteopontin and osteonectin were selected as specific marker genes for differentiation. PCR reaction mixture contained 0.52 μL cDNA, 5 pmol of each primer, 25 μL SYBR Green Real-time PCR Master Mix (TOYOBO Co., LTD., Osaka, Japan). Amplification conditions were as follows: 40 cycles of 95 °C for 1 min; 60 °C for 15 s; 74 °C for 1 min. Primers used were (5′ to 3′) CBFA1: CCGCACGACAACCGCACCAT (forward), CGCTCCGGCCCACAAATCTC (reverse); Type 1 collagen: GAAGTCAGCTGCATACAC (forward), AGGAAGTCCAGGCTGTCC (reverse); Osteopontin: TCACCATTCGGATGAGTCTG (forward), ACTTGTGGCTCTGATGTTCC (reverse); Osteonectin: AGCGCCTGGAGGCTGGAGAC (forward), CTTGATGCCAAAG-CAGCCGG (reverse); GAPDH: CAAAATGGTGAAGGTCGGTGTG (forward), ATTT-GATGTTAGTGGGGTCTCG (reverse).

3. Results and discussion

3.1. Surface marker analysis of adherent cell population

MSCs are isolated by the bases of adherent property of bone marrow in some species, such as human [6] and rat [30]. However, it is difficult to isolate homogeneous MSCs by adhesion separation because of unwanted contamination. The crude MSCs displayed a fibroblast-like morphology shown in Fig. 1(A). To eliminate the monocytic cell fraction in adhesion cell population, magnetic beads conjugated with anti-CD11b or anti-CD45 antibodies were used for negative selection [14,16]. Although some surface markers for MSCs were reported in a recent study, homogeneous MSCs could not be identified by such kinds of markers [17,31]. Surface marker expression level of adherent population of murine MSCs are shown in Fig. 1(B). A strong expression of the surface markers CD29, CD44, CD81, and Sca-1, and a weak expression of the surface markers CD34, CD45, and CD11b were observed. No expression of CD31 was observed. Some studies have reported that murine MSCs were positive for the surface markers CD29, CD44 and Sca-1 [14,15,32], and this finding was confirmed in our experimental data. Sca-1 expression level changed with the culture period (data not shown). This phenomenon was already reported in other studies [32]. The MSCs showed a weak and broad expression of CD34, a hematopoietic lineage marker. Umezawa et al. reported that murine MSCs with a low expression of CD34 have a high potential for the regenerative effect in cardiopulmonary disease. CD34 is the progenitor or stem cell marker, and the expression continuously decreased with the culture period. That is, the CD34 expression would be closely related with the differentiation stage. Hence, we chose the anti-CD34 antibody as the immobilized ligand and evaluated the differentiation ability of MSCs isolated on the anti-CD34 antibody-immobilized column.

3.2. Separation profile of MSCs on the anti-CD34 antibody-immobilized column

We have developed a separation column in previous work [21]. Details about the separation column were shown in Materials and methods. The antibody-immobilized column was connected with an injection tube. The length of the column and injection tube was 100 mm. Medium flow into the column was accomplished with a syringe pump. Elution profile of crude MSCs on the anti-CD34 antibody-immobilized column was evaluated by counting the number of eluted cells in each fraction. When the crude MSCs were injected into an unmodified column, almost all the cells were eluted in early fractions. On the other hand, when the crude MSCs were injected into the anti-CD34 antibody-immobilized column,

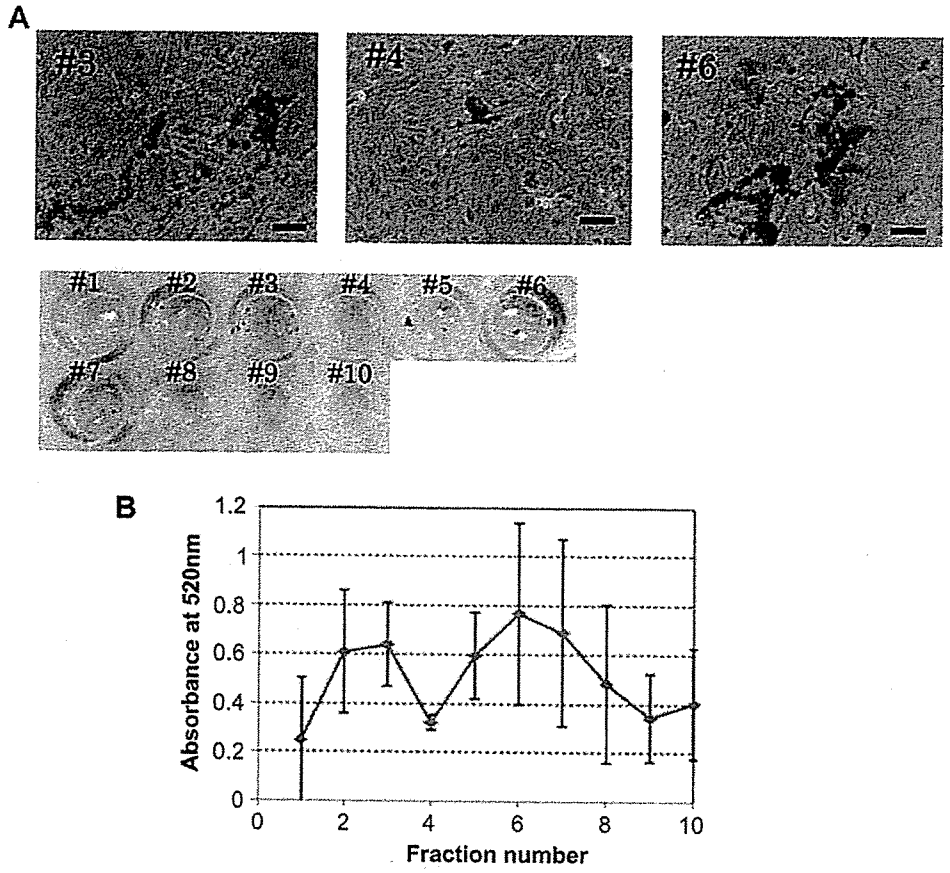

Fig. 5. (A) Photograph of alizarin red S staining MSCs after differentiation for 1 week. Cells were cultured on fibronectin-coated 24-well plate. (B) Quantification of alizarin red S staining in each fraction by absorbance spectrum. Absorption at 540 nm was plotted against the fraction number. Each data point represents results from 3 independent experiment and the data are presented as mean ± standard error of the means.

two peaks were observed (Fig. 2). That is, the delay of cell elution observed in the case of the anti-CD34 antibody-immobilized column probably resulted from the continuous interaction between the surface marker and the immobilized antibody. In our previous work, KG-1a (CD34+) and HL60 (CD34-) cells know as cell line were separated on antibody-immobilized column [21]. In the results, cells were separated by a marker specific manner, and the elution pattern was distinctly depended on the marker expression level. In the case of MSC separation, elution patterns were comparatively broad because of heterogeneity of crude MSCs. Then, surface marker expression of the isolated MSCs on the anti-CD34 antibody-immobilized column was evaluated by FACS. Two-dimensional FACS analysis of CD34 expression against Sca-1 expression is shown in Fig. 3. MSCs with a high expression of CD34 and Sca-1 were presented in later fractions, and a continuous change in the marker expression level was observed with increasing fraction number. These data indicated that the crude MSCs were separated on the column on the basis of the surface marker density. From the above results, we suggest that the antibody-immobilized column could be used to isolate murine MSCs on the basis of their surface marker density.

3.3. Differentiation of isolated MSCs on the anti-CD34 antibody-immobilized column

Osteoblastic differentiation was evaluated by gene expression analysis and alizarin red S staining. Type 1 collagen, osteonectin, CBFA1, and osteopontin were selected as specific markers for osteoblastic differentiation. The gene expression level was analyzed in separated MSCs obtained from the column. Type 1 collagen and osteonectin are constantly expressed during osteoblastic differentiation [33–35], while CBFA1 is expressed during the process of maturation. CBFA1 is a transcriptional factor, and the osteopontin expression was promoted by the CBFA1. Fig. 4 shows the expression levels of specific marker genes analyzed by real-time PCR. Type 1 collagen was expressed in almost all fractions, and the expression level was the same as that of crude MSCs. In the case of CBFA1, the expression level in fractions 3, 5, and 6 was higher than that in other fractions. This tendency was the same as that observed for the expression pattern of osteopontin.

CBFA1 is a key factor for mature osteoblastic differentiation. The suppression of CBFA1 expression by mutation of CBFA1 completely restricted bone formation of murine neonatal or newborn [33]. That is, the expression of CBFA1 is necessary for calcium deposition on the cells. The isolated MSCs after differentiation were stained with alizarin red S solution. Fig. 5 shows the picture of stained cells. Isolated MSCs in early fractions (fractions #2- and #3) or later fraction (fractions #5–7) were strongly positive. This staining pattern in terms of the fraction number was similar to that of CBFA1 expression pattern.

These results suggest that separated MSCs in early fraction or later fraction had a high potential for osteoblastic differentiation. It has been reported that osteoblastic progenitor cells were enriched in the CD34-positive population from bone marrow [36]. That is, the cells with high expression of CD34 in later fractions are mainly osteoblastic progenitor cells. It is difficult to determine the origin of these progenitor cells. However, there are two possibilities with

regard to their origin. First, the osteoblastic progenitor cells in bone marrow were contaminated in TCPS-adherent cells. Second, a fraction of MSCs differentiated into progenitor cells during cultivation. Stem cells are difficult to be cultured on a TCPS dish keeping with differentiation properties. Because the environment of MSCs on a culture dish is largely different from that *in vivo*, cultured MSCs have heterogeneous characteristics in terms of surface marker [17] and differentiation property. The purification process of stem cells is important for experimental or clinical use. From these results, we suggested that the ligand-immobilized column could be used to isolate MSCs from the heterogeneous cell populations consisting of progenitor or differentiated cells.

3.4. Differentiation of sorted MSCs by FACS

To verify the effect of surface marker density on the differentiation ability of MSCs, crude MSCs were sorted by FACS as a conventional method for cell separation. Four cell populations were sorted for the evaluation of osteoblastic differentiation (Fig. 6). The CD34 expression level in each population was different, and MSCs with a high density of CD34 were contained in $CD34^{High}FSC^{Low}$ population. In contrast, the low density of CD34 was collected in $CD34^{Low}FSC^{High}$ population. The surface marker density of the cells in $CD34^{High}FSC^{High}$ or $CD34^{Low}FSC^{Low}$ population was almost the same. Fig. 6(B) shows the relative expression of specific marker genes for osteoblastic differentiation. In case of MSCs sorted by FACS, cell population with high and low marker density of CD34 has shown high expression of differentiation markers. This tendency was the same as that observed for separated MSCs on the antibody-immobilized column. This result supported that the two cell populations with high ability for osteoblastic differentiation were present in crude MSCs, and the populations were separated using a CD34 antibody-immobilized column.

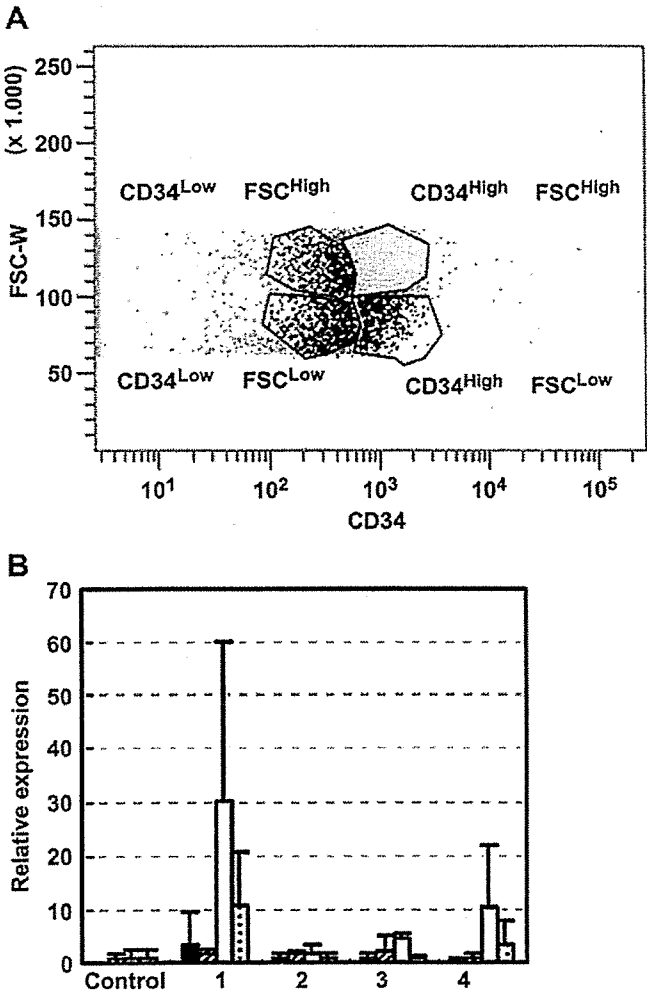

Fig. 6. (A) Sorting regions of isolated cell populations with distinct expression density. Crude MSC populations were divided into four cell populations. Cells with highest CD34 expression density were in the $CD34^{High}FSC^{Low}$ population. On the other hand, cells with lowest expression density were in the $CD34^{Low}FSC^{Hihg}$ population. (B) Gene expression analysis of sorted MSCs by FACS. Sorted MSCs were cultured in the osteoblastic differentiation medium for 8 days. Specific surface markers (bar with lines: type 1 collagen, bar with dots; osteonectin, closed bar; CBFA1, open bar; osteopontin) were analyzed by real-time PCR. Relative expression was normalized by GAPDH. Each data point represents results from 3 independent experiment and the data are presented as mean ± standard error of the means.

4. Conclusion

An anti-CD34 antibody-immobilized column was developed for separating MSCs based on their surface marker density. We selected the anti-CD34 antibody as the immobilized ligand, and crude MSCs were separated on this column. Two cell populations with a high ability for osteoblastic differentiation were purified on this column. MSCs express some surface markers, and their combinations have been explored in many groups in order to specify homogeneous MSCs population. In our approach, marker density is considered as the essential factor for the characterizing MSCs. Two different cell populations could be separated on this column based on their surface marker density. To characterize the cells with a high differentiation ability, it might be effective to use some kinds of ligand-immobilized columns. Further studies on the design of ligand-immobilized surface and construction of the column system are required for effective separation of MSCs.

Acknowledgment

This work was supported by the Research Grant for Cardiovascular Disease (18A-2) from the ministry of Health, Labour and Welfare & Grant-in-Aid for Scientific Research on Innovation Areas (20106014).

Appendix

Figures with essential colour discrimination. Most of the figures (Figs. 1, 3, 5 and 6) in this article have parts that may be difficult to interpret in black and white. The full colour images can be found in the on-line version, at doi:10.1016/j.biomaterials.2010.01.126.

References

[1] Langer R, Vacanti JP. Tissue engineering. Science 1993;260:920–6.
[2] Holden C, Vogel G. Plasticity: time for a reappraisal. Science 2002;296:2126–9.
[3] Kim SW, Han H, Chae GT, Lee SH, Bo S, Yoon JH, et al. Successful stem cell therapy using umbilical cord blood-derived multipotent stem cells for Buerger's disease and ischemic limb disease animal model. Stem Cells 2006;24:1620–6.
[4] Kim SS, Yoo SW, Park TS, Ahn SC, Jeong HS, Kim JW, et al. Neural induction with neurogenin1 increases the therapeutic effects of mesenchymal stem cells in the ischemic brain. Stem Cells 2008;26:2217–28.
[5] Fukuda K, Yuasa S. Stem cells as a source of regenerative cardiomyocytes. Circ Res 2006;98:1002–13.
[6] Pittenger MF, Mackay AM, Beck SC, Jaiswal RK, Douglas R, Mosca JD, et al. Multilineage potential of adult human mesenchymal stem cells. Science 1999;284:143–7.
[7] Yang IH, Kim SH, Kim YH, Sun HJ, Kim SJ, Lee JW. Comparison of phenotypic characterization between "alginate bead" and "pellet" culture systems as chondrogenic differentiation models for human mesenchymal stem cells. Yonsei Med J 2004;45:891–900.

[8] Lisignoli G, Cristino S, Piacentini A, Toneguzzi S, Grassi F, Cavallo C, et al. Cellular and molecular events during chondrogenesis of human mesenchymal stromal cells grown in a three-dimensional hyaluronan based scaffold. Biomaterials 2005;26:5677–86.
[9] Wan C, He Q, McCaigue M, Marsh D, Li G. Nonadherent cell population of human marrow culture is a complementary source of mesenchymal stem cells (MSCs). J Orthop Res 2006;24:21–8.
[10] Gronthos S, Zannettino AC, Hay SJ, Shi S, Graves SE, Kortesidis A, et al. Molecular and cellular characterisation of highly purified stromal stem cells derived from human bone marrow. J Cell Sci 2003;116:1827–35.
[11] Hung SC, Chen NJ, Hsieh SL, Li H, Ma HL, Lo WH. Isolation characterization of size-sieved stem cells from human bone marrow. Stem Cells 2002;20:249–58.
[12] Reyes M, Lund T, Lenvik T, Aguiar D, Koodie L, Verfaillie CM. Purification and ex vivo expansion of postnatal human marrow mesodermal progenitor cells. Blood 2001;98:2615–25.
[13] Jiang Y, Jahagirdar BN, Reinhardt RL, Schwartz RE, Keene CD, Ortiz-Gonzalez XR, et al. Pluripotency of mesenchymal stem cells derived from adult marrow. Nature 2002;418:41–9.
[14] Baddoo M, Hill K, Wilkinson R, Gaupp D, Hughes C, Kopen GC, et al. Characterization of mesenchymal stem cell isolated from murine bone marrow by negative selection. J Cell Biochem 2003;89:1235–49.
[15] Gojo S, Gojo N, Takeda Y, Mori T, Abe H, Kyo S, et al. In vivo cardiovasculogenesis by direct injection of isolated adult mesenchymal stem cells. Exp Cell Res 2003;288:51–9.
[16] Tropel P, Noël D, Platet N, Legrand P, Benabid AL, Berger F. Isolation and characterisation of mesenchymal stem cells from adult mouse bone marrow. Exp Cell Res 2004;295:395–406.
[17] Phinney DG, Hill K, Michelson C, DuTreil M, Hughes C, Humphries S, et al. Biological activities encoded by the murine mesenchymal stem cell transcriptome provide a basis for their developmental potential and broad therapeutic efficacy. Stem Cells 2006;24:186–98.
[18] Li Y, Zhang C, Xiong F, Yu MJ, Peng FL, Shang YC, et al. Comparative study of mesenchymal stem cells from C57BL/10 and mdx mice. BMC Cell Biol 2008;9:24.
[19] Wieczorek G, Steinhoff C, Schulz R, Scheller M, Vingron M, Ropers HH, et al. Gene expression profile of mouse bone marrow stromal cells determined by cDNA microarray analysis. Cell Tissue Res 2003;311:227–37.
[20] Matsuoka S, Ebihara Y, Xu M, Ishii T, Sugiyama D, Yoshino H, et al. CD34 expression on long-term repopulating hematopoietic stem cells changes during developmental stages. Blood 2001;97:419–25.
[21] Mahara A, Yamaoka T. Antibody-immobilized column for quick cell separation based on cell rolling. Biotechnol Prog, in press.
[22] von Andrian UH, Chambers JD, McEvoy LM, Bargatze RF, Arfors KE, Butcher EC. Two-step model of leukocyte-endothelial cell interaction in inflammation: distinct roles for LECAM-1 and the leukocyte beta 2 integrins in vivo. Proc Natl Acad Sci U S A 1991;88:7538–42.
[23] Eniola AO, Willcox PJ, Hammer DA. Interplay between rolling and firm adhesion elucidated with a cell-free system engineered with two distinct receptor-ligand pairs. Biophys J 2003;85:2720–31.
[24] Greenberg AW, Hammer DA. Cell separation mediated by differential rolling adhesion. Biotechnol Bioeng 2001;73:111–24.
[25] Greenberg AW, Brunk DK, Hammer DA. Cell-free rolling mediated by L-selectin and sialyl lewisx reveals the shear threshold effect. Biophys J 2000;79:2391–402.
[26] Hammer DA, Apte SM. Simulation of cell rolling and adhesion on surfaces in shear flow: general results and analysis of selectin-mediated neutrophil adhesion. Biophys J 1992;63:35–57.
[27] Hammer DA, Lauffenburger DA. A dynamical model for receptor-mediated cell adhesion of surfaces. Biophys J 1987;52:475–87.
[28] Fujimoto K, Takebayashi Y, Inoue H, Ikada Y. Ozone-induced graft polymerization onto polymer surface. J Polym Sci A Polym Chem 1993;31:1035–43.
[29] Yamauchi J, Yamaoka A, Ikemoto K, Matsui T. Graft copolymerization of methyl methacrylate onto polypropylene oxidized with ozone. J Polym Sci A Polym Chem 1991;43:1197–203.
[30] Wakitani S, Saito T, Caplan AI. Myogenic cells derived from rat bone marrow mesenchymal stem cells exposed to 5-azacytidine. Muscle Nerve 1995;18:1417–26.
[31] Pittenger MF. Mesenchymal stem cells from adult bone marrow. Methods Mol Biol 2008;449:27.
[32] Meirelles Lda S, Nardi NB. Murine marrow-derived mesenchymal stem cell: isolation, in vitro expansion, and characterization. Br J Haematol 2003;123:702–11.
[33] Komori T, Yagi H, Nomura S, Yamaguchi A, Sasaki K, Deguchi K, et al. Targeted disruption of Cbfa1 results in a complete lack of bone formation owing to maturational arrest of osteoblasts. Cell 1997;89:755–64.
[34] Ducy P, Zhang R, Geoffroy V, Ridall AL, Karsenty G. Osf2/Cbfa1: a transcriptional activator of osteoblast differentiation. Cell 1997;89:747–54.
[35] Otto F, Thornell AP, Crompton T, Denzel A, Gilmour KC, Rosewell IR, et al. Cbfa1, a candidate gene for Cleidocranial dysplasia syndrome, is essential for osteoblast differentiation and bone development. Cell 1987;89:765–71.
[36] Chen JL, Hunt P, McElvain M, Black T, Kaufman S, Choi ES. Osteoblast precursor cells are found in CD34+ cells from human bone marrow. Stem Cells 1987;15:368–77.

Biomaterials 31 (2010) 3590–3595

Contents lists available at ScienceDirect

Biomaterials

journal homepage: www.elsevier.com/locate/biomaterials

The use of high-hydrostatic pressure treatment to decellularize blood vessels

Seiichi Funamoto [a,b], Kwangwoo Nam [a,b], Tsuyoshi Kimura [a,b], Ayako Murakoshi [a], Yoshihide Hashimoto [a,c], Kazuo Niwaya [d], Soichiro Kitamura [d], Toshiya Fujisato [d,e,**], Akio Kishida [a,b,*]

[a] Division of Biofunctional Molecules, Institute of Biomaterials and Bioengineering, Tokyo Medical and Dental University, 2-3-10, Kanda-surugadai, Chiyoda-ku, Tokyo 101-0062, Japan
[b] Japan Science and Technology Agency CREST, Japan 4-1-8, Honmachi, Kawaguchi, Saitama 332-0012, Japan
[c] Japan Society for the Promotion of Science, 5-3-1, Kojimachi, Chiyoda-ku, Tokyo 102-8471, Japan
[d] National Cardiovascular Center, 5-7-1, Fujishirodai, Suita, Osaka 565-8565, Japan
[e] Department of Biomedical Engineering, Osaka Institute of Technology, 5-16-1, Omiya, Asahi-ku, Osaka 535-8585, Japan

ARTICLE INFO

Article history:
Received 16 December 2009
Accepted 13 January 2010
Available online 9 February 2010

Keywords:
Arterial tissue engineering
Vascular graft
Mechanical property
Transplantation

ABSTRACT

A decellularization method using high-hydrostatic pressure (HHP) technology (>600 MPa) is described. The HHP disrupts the cells inside the tissue. The cell debris can be eliminated with a simple washing process, producing clean, decellularized tissue. In this study, porcine aortic blood vessel was decellularized by HHP. The mechanical properties and in vivo performance of the decellularized tissue were evaluated. Mechanical properties of the decellularized tissue were not altered by the HHP treatment. Reduced inflammation of the decellularized tissue was confirmed by xenogenic transplant experimentation. An allogenic transplantation study showed that decellularized blood vessel endured the arterial blood pressure, and there was no clot formation on the luminal surface. In addition, cellular infiltration into the vessel wall was observed 4 weeks after implantation, suggesting that HHP treatments could be applied widely as a high-quality decellularization method.

1. Introduction

Tissue engineering is one of the key technologies for treatment of atherosclerotic vascular diseases, valvular heart disease, aneurysm, and varices [1–4]. Decellularized tissue is promising as an ideal scaffold for cardiovascular tissue engineering. Several technologies have been developed to fabricate artificial valves and some of them have already been used clinically [5–7]. Decellularization techniques are classified by the chemicals used, such as acid or alkaline treatment, detergent treatment, or enzymatic digestion, and the physical methods used, such as snap freezing and mechanical agitation [8–12]. Among these, detergent treatment is the most widely used. Decellularization of biological tissues by detergent treatment has the advantage of being easy to use, but its drawbacks include long treatment time, alteration of mechanical properties, and residual toxicity [13]. Researchers have developed specific treatment recipes to overcome each of these problems.

As another candidate for a new decellularization treatment, we have reported our work on the high-hydrostatic pressure (HHP) method [14,15]. The unique characteristics of the HHP method are the destruction of cell membranes, uniform treatment, and short treatment time. Subsequent washing of the treated tissue can produce a decellularized tissue that does not adopt any chemical agents.

Decellularizing corneal tissue with detergent treatment is difficult, whereas by using HHP treatment, almost complete decellularization of corneal tissue was accomplished [15]. Experiments with decellularized porcine corneal tissue implanted into rabbit eye showed superior functionality, i.e. transparency. However, there are still few reports on decellularization using, and there is no a specific study on the decellularization condition yet.

In this study, we attempted to use HHP to prepare decellularized cardiovascular tissues. Cardiovascular tissues, such as heart valve, aortic vessel, and small diameter blood vessel, should have superior properties to corneal tissue. For instance, they should be pressure resistant, anti-thrombogenic, and have anti-calcification ability. Porcine aortic blood vessel was decellularized by HHP treatment and the efficiency of decellularization, mechanical properties, immunogenicity, and in vivo performance were evaluated. This

* Corresponding author. Division of Biofunctional Molecules, Institute of Biomaterials and Bioengineering, Tokyo Medical and Dental University, 2-3-10, Kanda-surugadai, Chiyoda-ku, Tokyo 101-0062, Japan. Fax: +81 3 5280 8028.
** Corresponding author. National Cardiovascular Center, 5-7-1, Fujishirodai, Suita, Osaka 565-8565, Japan. Fax: +81 6 6954 4746.
E-mail addresses: fujisato@bme.oit.ac.jp (T. Fujisato), kishida.fm@tmd.ac.jp (A. Kishida).

0142-9612/$ – see front matter © 2010 Elsevier Ltd. All rights reserved.
doi:10.1016/j.biomaterials.2010.01.073

article focuses particularly on the preparative conditions for the decellularized blood vessel using the HHP technique. Determining the optimal conditions for obtaining biologic scaffold with undamaged extracellular matrices (ECM) and high decellularization was one of the goals of this study. For this purpose, the effect of water state (ice formation) during pressurization was investigated in detail.

2. Materials and methods

2.1. Materials

Fresh porcine hearts were obtained from a local slaughterhouse (Tokyo Shibaura Organ Co. Ltd, Japan). The aortic blood vessel next to the aortic valves was excised and cut into 1 × 0.2 cm pieces. Aortic tissue was cleaned to remove fat and stored immediately at 4 °C in phosphate buffer saline (PBS) without Ca^{2+} or Mg^{2+} for transport to the laboratory for further processing.

2.2. Decellularization by HHP

2.2.1. Pressurization profile

The decellularization protocol consisted of two steps: 1) HHP treatment and 2) washing. The blood vessel samples were pressurized using a cold isostatic pressurization machine (Dr. Chef; Kobelco, Japan). The detailed procedures were as follows. After packing each sample in a plastic bag filled with PBS, the bag was immersed into the transmission fluid in the sample chamber of the machine. Before compression, the onset temperature was set at 10 or 30 °C. Then, the atmosphere inside the sample chamber was pressurized at a predetermined rate (196.1 or 65.3 MPa/min) until the pressure reached 980 MPa. The pressure was maintained at 980 MPa for 10 min and then was decreased at a predetermined rate (196.1 or 65.3 MPa/min) until atmospheric pressure was reached.

2.2.2. Washing process

After the HHP process, samples were washed with PBS for 14 days. Then, the samples were immersed in new PBS containing antibiotics and stored at 4 °C.

2.3. Preparation of decellularized aortic scaffold by detergent treatment

Triton® X-100 treatment: The blood vessels were placed in a solution of 1% Triton® X-100 (Sigma–Aldrich, Japan) with 0.02% EDTA (Wako, Japan) in PBS for 24 h, together with RNase A (20 mg/mL) (Roche, USA), DNase I (0.2 mg/mL) (Roche, USA), and 1% penicillin and streptomycin (Gibco, Japan) [16]. The blood vessels were washed with PBS several times to remove residual substances.

SDS treatment: The blood vessels were placed in a solution of 0.1% SDS (sodium dodecyl sulfate, Wako, Japan), together with RNase A (20 mg/mL), DNase (0.2 mg/mL), and 1% penicillin and streptomycin for 1 h at room temperature [17]. Then, they were washed with PBS for 48 h to remove residual substances.

Trypsin treatment: The blood vessels were placed in a trypsin solution (0.05% trypsin (Biochrom KG, Germany) and 0.02% EDTA) for 48 h at 37 °C [18].

2.4. Evaluation of decellularized tissue

2.4.1. Observation of structure of the decellularized tissue

Decellularized blood vessels were fixed by immersion with 10% neutral buffered formalin solution. The specimens were dehydrated in graded alcohol, embedded in paraffin blocks, and sectioned. The sections were stained with 1% hematoxylin–eosin (H–E). The slides were observed by optical microscope (Coolscope, Nikon Co., Ltd. Japan). For transmission electron microscopy (TEM), the decellularized blood vessels were fixed with 2.5% glutaraldehide in PBS. The specimens were prepared and observed by standard procedures for TEM.

2.4.2. Mechanical properties

Mechanical strength testing of the non-treated and the decellularized blood vessels was performed longitudinally. The samples were cut into dumbbell-shaped pieces. The tested parts were 15–20 mm long and 2 mm wide. Wall thickness was measured by micrometer prior to mechanical testing. Stress–strain curves were obtained with a creep meter RE2-33005 B (Yamaden Co., Ltd. Japan). Each sample was strained at a rate of 10 mm/min. All testing was conducted in air at room temperature (25 °C).

The stress–strain curve for each individual specimen was analyzed with regard to four parameters: early phase modulus of elasticity, late phase modulus of elasticity, ultimate tensile strength (UTS), and failure strain [19]. These parameters are defined that illustrates the typical stress–strain curve of blood vessel tissue. The analysis parameters from each group were averaged over the number of specimens in each group ($n = 10$). Results were expressed as the mean ± standard deviation (SD). Additionally, the individual means from each treatment group were compared by Student's t-test.

2.4.3. Quantification of residual DNA

Twenty-five mg of samples were placed in 10% proteinase K (Quiagen, USA) in lysis buffer solution overnight. The DNA from each sample was purified using a DNeasy® assay kit (Quiagen, USA). The DNA amounts were measured by spectrophotometry ($\lambda = 280$ nm).

2.4.4. Xeno-transplantation (pig to rat)

The animal study was performed in accordance with the NIH guidelines for the care and use of laboratory animals (NIH Publication 85-23, revised 1985) and the institutional guidelines for the care and use of experimental animals of Tokyo Medical and Dental University. Porcine blood vessel samples were dissected to be 1 × 1 cm segments. Native aorta samples and samples decellularized by several pressurization programs (the two experimental conditions) were implanted in the subcutaneous mucosal position of Wister rats (250 g, 7 weeks old) ($n = 3$). The implantation periods were 1 and 4 weeks. At a predetermined time, all animals were terminated by elective euthanasia with anesthesia of ether. The explanted specimens were fixed, dissected, and stained by H–E.

2.4.5. Measurement of immune response in xeno-transplantation area

The measurement of immune response was done by calculation of the area that was had an inflammatory response. Image J (National Institute of Health, USA) was used to measure the immunologic site surrounding in the transplant tissue.

2.4.6. Allo-transplantation (pig to pig)

The decellularized blood vessel was implanted into abdominal porcine aorta. No anticoagulants were administered after surgery. The implantation periods were 4, 12, and 24 weeks. The explanted specimens were fixed, dissected and stained by H–E.

3. Results and discussion

3.1. Effect of ice formation during pressurization

The effect of high pressure on the extracellular matrix is largely still unknown. Denaturation of proteins at high pressure has been widely studied [20,21] while the research on collagen is quite limited. In our HHP treatment, collagen denaturation would have a great impact on the physical properties of the tissue. So, an important point in this study was to find out whether the extracellular matrix structure was maintained throughout the treatment.

First, the relationship between the pressure and the temperature of the treatment chamber was studied. Pressure–temperature curves for each pressurization condition were drawn in the phase diagram of water to see whether ice would form during the pressurization and depressurization processes. It is known that the lowest freezing point of water is −20 °C at about 200 MPa, and it increases to 30 °C at 980 MPa (The phase diagram of water is shown in Fig. 1, inset) [22,23]. The phase diagram of the pressure–temperature graph for water suggests that increased pressure would induce the water to freeze. This suggests that the high pressure treatment of native tissue may also cause the formation of ice during our process. It has been reported that the freezing process generally destroys the structure of biological tissues under normal pressure [24,25]. Therefore, temperature control during pressurization is necessary.

As shown in Fig. 1 (large image), under condition I (the starting temperature was 10 °C, pressurization and depressurization rates were 196.1 MPa/min), the samples passed the freezing zone from 937 to 980 MPa during the increasing pressure process. In our conditions, the highest pressure was maintained for 10 min before depressurization. From 980 to 759 MPa, the water would be in the freezing state and would return to the liquid state after further depressurization under 759 MPa. On the other hand, under condition II (the starting temperature was 30 °C, pressurization and depressurization rates were 65.3 MPa/min), the samples did not pass the freezing zone throughout the pressurizing process. This means that the destruction of tissue structure by the formation of ice would not occur when the starting temperature was 30 °C. It should be noted that the pressurization and depressurization rates should be controlled to maintain the starting temperature. Fast

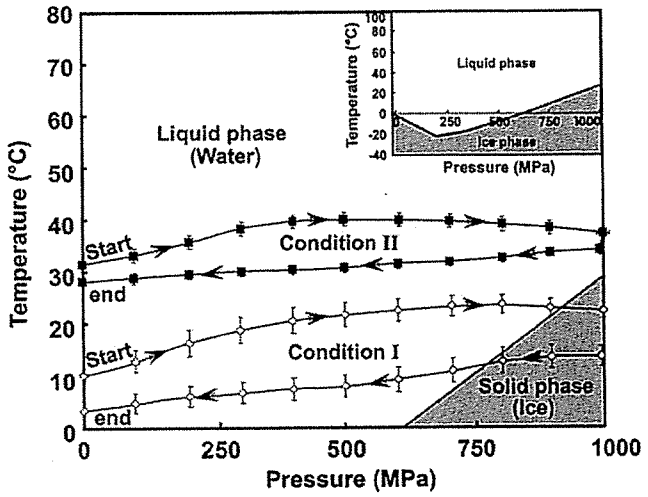

Fig. 1. Pressure–temperature phase diagram from 1 to 980 MPa. The small figure is the water phase diagram [19]. (■) Pressurization/depressurization rate: 65.3 MPa/min. Onset temperature: 30 °C (◇) Pressurization/depressurization rate: 196.1 MPa/min. Onset temperature: 10 °C.

pressurization and depressurization should be avoided because it induces drastic increases and decreases in the temperature.

The decellularized tissues treated under conditions I and II were evaluated by H–E stain and TEM (Fig. 2). As shown in Fig. 3 (b) and (c), the cell nuclei were removed in conditions I and II. This shows that passing the freezing point had little effect on decellularization efficiency. However, change of tissue structure was observed at high magnification [Fig. 2 (e) and (f)]. For condition I, the expansion of the space between collagen fiber filaments of the tissue was observed, while the samples in condition II showed relatively tighter arrays of collagen fiber filaments. When the structures of the samples were observed with TEM, collagen fibrils were observed in native tissue and in process condition II [Fig. 2 (g) and (i)], but no fibrils were observed for condition I [Fig. 2 (h)]. These results show that the extracellular matrix structure is maintained in condition II, and the collagen fibrils were destroyed in condition I. This is because of the ice formation during the pressurization and depressurization, as shown in Fig. 1. The tensile strength of the tissues was evaluated for the biomechanical characterization of the decellularized tissue. Ingham et al. have divided the section into the three phases: the early phase elasticity is dependent on the elastic modulus of the elastin in the tissue (elastin phase), the latter-phase elasticity is dependent on the elastic modulus of the collagen in the tissue (collagen phase), and the transition phase, where is located between the elastin and collagen phase [19]. In the elastin phase, the tissue offers little resistance to elongation because force transmission and load bearing are provided mainly by the elastin fiber. Following the elastin and transition phases, in the collagen phase, all the elastin fibers are uncoiled and the load is entirely supported by collagen. So, to evaluate the mechanical strength of the blood vessel, the elasticity in the elastin and collagen phases should be measured and calculated.

Table 1 shows the results of the tensile test in the longitudinal direction of the decellularized blood vessel. After decellularization under condition I, the elasticity in the elastin phase increased, while elasticity in the collagen phase decreased compared to that of native tissue. This shows that the pressurization effect damages both elastin and collagen and alters their physical properties. A

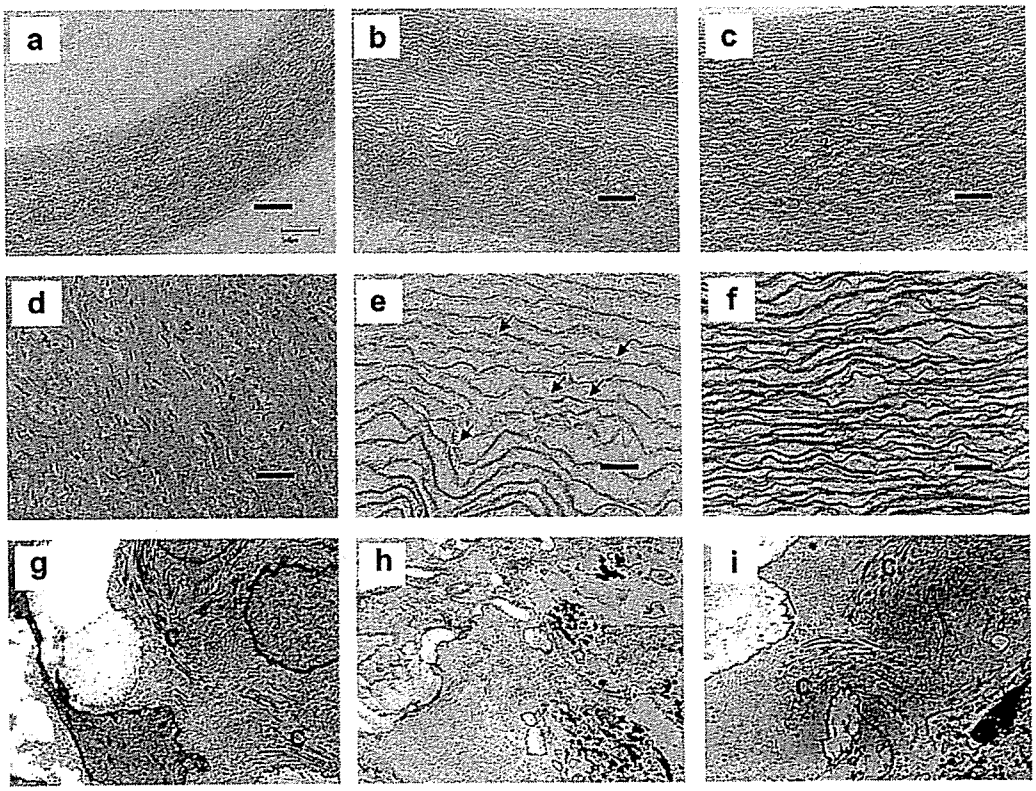

Fig. 2. Histological evaluation: (a)–(f) H–E staining, (g)–(l) TEM observation. (a),(d), (g) Non-treated. (b),(e), and (h) Ultra-high pressure (condition I) and 20-day wash. (c),(f), and (i) Ultra-high pressure (condition II) and 20-day wash. Scale bar: (a)–(c) 500 μm, (d)–(f) 50 μm. Magnification ratio: (g)–(i) × 10,000. Black arrows indicate the cleavage of collagen fibers. C: Collagen fibrils.

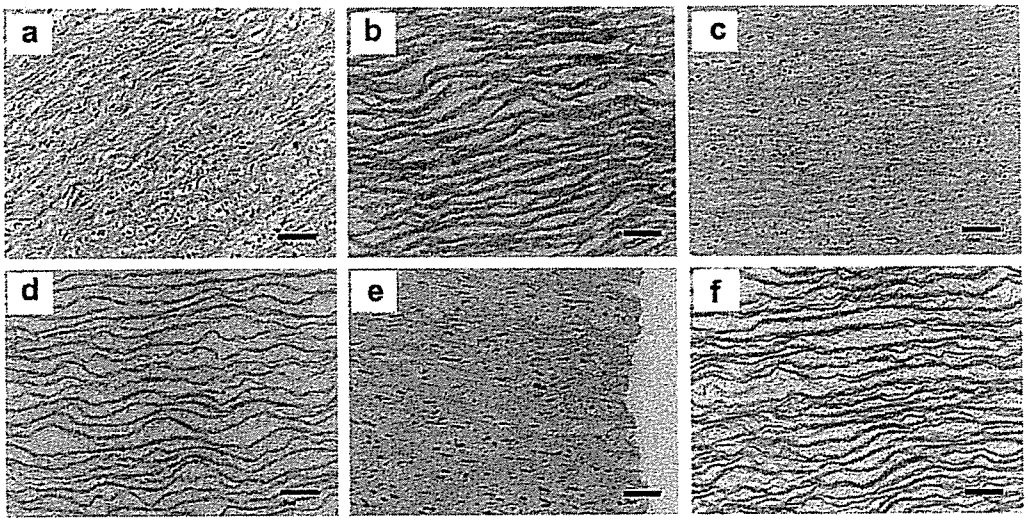

Fig. 3. H–E staining of the decellularized aorta samples by various washing methods. (a) Non-treated, (b) Trypsin, (c) Triton® X-100, (d) SDS, (e) SDC, and (f) UHP (Initial temperature 30 °C, Pressurization/depressurization rate: 65.3 MPa/min). Scale bar = 50 μm.

decrease of UTS in condition I was also observed, but there was no significant difference in failure strain. In Fig. 2 (e), cleavage of the collagen fibers is shown, which seems to be the cause of the decrease of the elasticity. In condition II, the four parameters were similar to those of native tissue. This shows that the structure of the decellularized blood vessel under condition I was well maintained. These results indicate that it is necessary to avoid the freezing phase when the HHP treatment is applied in order to maintain the native structure of the blood vessel.

3.2. Comparison and quantification of cell removal

The various decellularization methods are compared by H–E micrographs and DNA removal efficiency. Fig. 3 shows H–E micrographs of the blood vessels decellularized by various treatments. The HHP treatment shows almost the same or even better decellularization efficiency than the chemical treatments. For the SDS treatment and trypsin treatment, cells were not observed in the blood vessel. On the other hand, in the SDC treatment and Triton® X-100 treatment, the nuclei of the cells were still observed in the tissue. This means that decellularization with these two methods was imperfect. This was because of insufficient infiltration of the detergent into the inside of the tissue; the blood vessels used were too thick for the detergent to penetrate the entire tissue in 24 h. Another possible reason is that the decellularization conditions were set for SDS treatment. The concentration of the detergent and the washing time appropriate for SDS might have been inadequate for Triton® X-100 and SDC.

To quantify the amount of cells remaining inside the blood vessel, the amount of residual DNA in the tissue was measured (Fig. 4). For the chemical treatment methods, the amount of residual DNA varied from 0.3 to 1.3 μg/mg. Although Fig. 4 shows that the SDS and trypsin treatments showed no cells within the tissue, there was still a detectable amount of DNA. This means that residual DNA quantification is a more sensitive method for judging completeness of cells removal. For the HHP method, residual DNA was removed to the measurement limit level.

It was noteworthy that the washing process was important for HHP treatment. The detergent methods destroy and wash out the cells simultaneously, whereas in the HHP treatment, destruction and washing out were independent processes. The high pressure only destroys the cells within the native tissue, leaving DNA exposed to the environment. The washing process involves the degradation of the exposed DNA by DNaseI. By washing out the cell debris thoroughly, it is possible to obtain a decellularized blood vessel that contains no cell debris at all.

Table 1
Mechanical property change in longitudinal direction after UHP decellularization ($n = 3$).

Methods	Elastin region Elasticity ($10^5 \times$ Pa)	Collagen region Elasticity ($10^5 \times$ Pa)	Ultimate tensile Stress (UTS) ($10^5 \times$ Pa)	Ultimate failure Strain (%)
Non-treated	2.2 ± 1.5	26.7 ± 5.7	8.0 ± 0.4	67.7 ± 2.4
Condition I	8.2 ± 1.4**	9.6 ± 0.9	3.6 ± 0.4*	63.2 ± 38.8
Condition II	2.4 ± 0.7	16.7 ± 5.7	5.9 ± 0.1	60.5 ± 19.0

Non-treated *vs* *$p < 0.01$. Non-treated *vs* **$0.01 < p < 0.05$.

3.3. In vivo studies

The host reaction to tissue decellularized by HHP treatment (condition II) was evaluated by xenogenic transplantation. Fig. 5 (a)

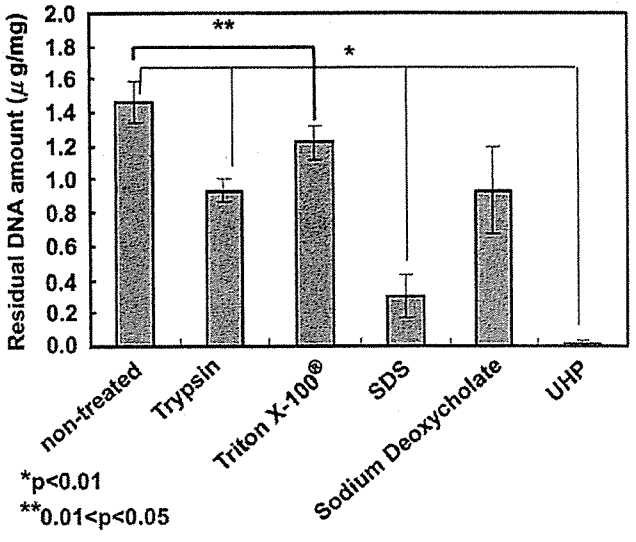

Fig. 4. Quantification of residual DNA in the aorta decellularized by various methods.

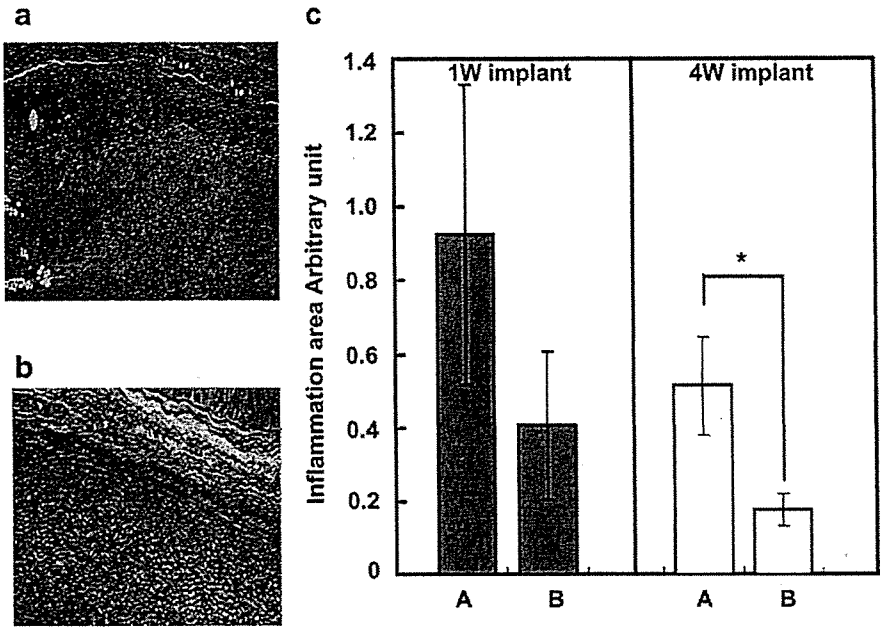

Fig. 5. Histological evaluation of xeno-transplantation study and immune response after xeno-transplantation. (a) Native aorta tissue ($n = 3$). (b) Aorta tissue decellularized by UHP process ($n = 3$). (c) Immune response for the implantation of decellularized aortic tissue. ($n = 3$, $^*p < 0.05$). Formula: Score = the area stained by hematoxylin dye/the total surface area of porcine aorta. A. Non-treated. B UHP treated by condition II.

and (b) show H–E microphotographs of the samples implanted subcutaneously in a rat after 4 weeks. As shown in Fig. 5 (a), severe inflammation was observed around the native porcine blood vessel. On the other hand, for the decellularized porcine blood vessel, the inflammation seemed to be suppressed (Fig. 5 (b)). The ratios of the area of inflammation were compared for each sample [Fig. 5 (c)]. There was a difference in the inflammatory response after 1 week of implantation. This continued for the 4 weeks of implantation. The inflammation area of native tissue was 2.5 times higher than that of decellularized blood vessel. It became clear that the HHP

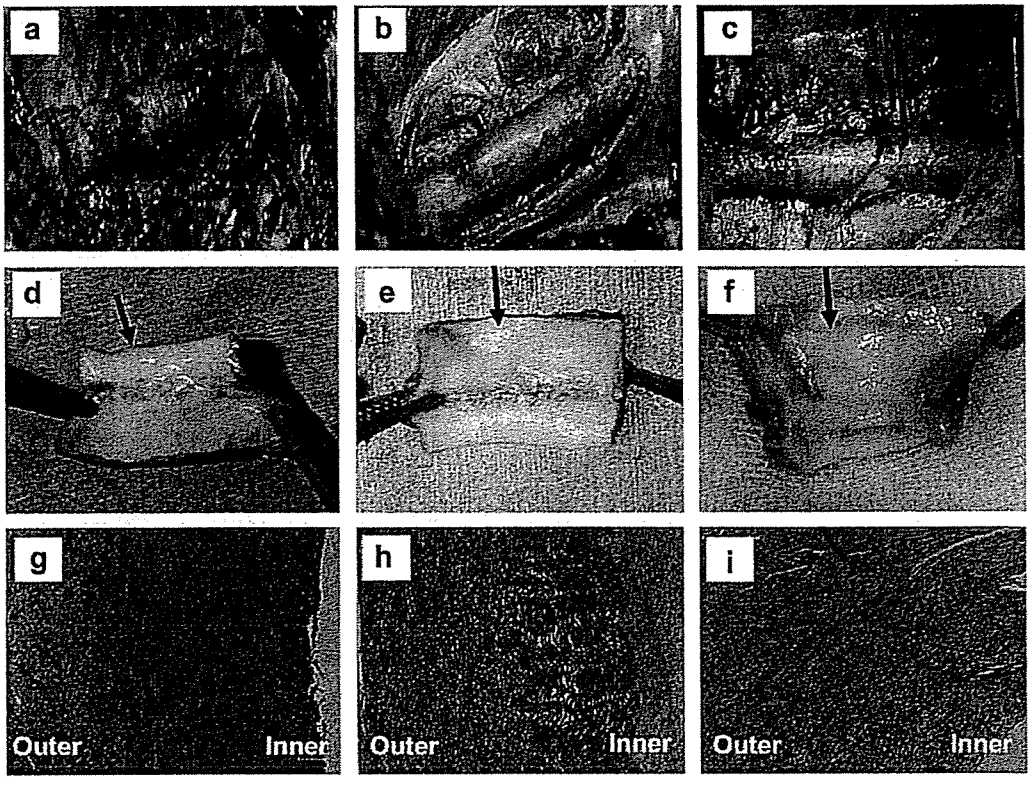

Fig. 6. Results of allo-transplantation study. (a),(d),(g) decellularized tissue (condition II) implantation after 4 weeks. (b),(e),(h) decellularized tissue implantation after 12 weeks. (c),(f),(i) decellularized tissue implantation after 24 weeks.

treatment could remove the cells that cause the xenogenic inflammation, and it can be concluded that the HHP treatment is an effective method for xenogenic tissue transplantation.

An allogenic transplant of the decellularized porcine blood vessel that was processed under condition II was performed to evaluate the in vivo performance of tissue decellularized by HHP (Fig. 6). As shown in Fig. 6 (a) to (c), the transplanted decellularized blood vessel maintained a caliber equal to the recipient's blood vessel, which meant that dilatation was not observed at 4, 12, or 24 weeks after implantation. Fig. 6 (d) to (f) shows that no thrombus formation was observed for any of the samples. The inner surfaces of the transplanted blood vessels were luminous, implying that the inner surface was fully covered with recipient endothelial cells. The infiltration of the recipient cells into the transplanted blood vessel is shown in Fig. 6 (g) to (i). The cells infiltrated into the transplanted blood vessel in a time-dependent manner, which indicates that remodeling of the transplanted blood vessel occurred normally.

It has been reported that the HHP treatment could destroy the lipid bilayer membranes of bacteria, fungi, and viruses with lipid membranes as well as animal cells, which means that HHP treatment also has a sterilizing effect. As the inactivation of viruses and extinction of bacilli have been reported when the applied pressure was higher than 600 MPa [26], the pressure of 980 MPa in our HHP condition was high enough to ensure a high sterilization effect.

4. Conclusion

By controlling the temperature during pressurization, decellularized tissue without structural damage can be obtained. The mechanical properties of the decellularized tissue were not altered at all under appropriate conditions. The amount of cell debris remaining inside the blood vessel was too small to be detected. The allogenic transplantation study indicated that decellularized blood vessels endured the arterial blood pressure and that there was no clot formation on the luminal surface. In addition, cellular infiltration into the vessel wall was observed 4 weeks after implantation. Because the isostatic pressurization can treat the samples set in the chamber homogeneously, it is thought that HHP treatment is an effective method for the decellularization of a wide variety of tissue sizes.

Acknowledgements

This work was supported in part by Research on Human genome, Tissue Engineering from the Ministry of Health, Labor and Welfare, and by the Core Research of Evolutional Science and Technology from Japan Science and Technology Agency (JST-CREST).

Appendix

Figures with essential colour discrimination. Figs. 2,3,5,6 in this article may be difficult to interpret in black and white. The full colour images can be found in the on-line version, at doi:10.1016/j.biomaterials.2010.01.073.

References

[1] Conconi MT, De Coppi P, Bellini S, Zara G, Sabatti M, Marzaro M, et al. Homologous muscle acellular matrix seeded with autologous myoblasts as a tissue-engineering approach to abdominal wall-defect repair. Biomaterials 2005;26:2567–74.
[2] Liang HC, Chang Y, Hsu CK, Lee MH, Sung HW. Effects of crosslinking degree of an acellular biological tissue on its tissue regeneration pattern. Biomaterials 2004;25:3541–52.
[3] Uchimura E, Sawa Y, Taketani S, Yamanaka Y, Hara M, Matsuda H. Novel method of preparing acellular cardiovascular grafts by decellularization with poly(ethylene glycol). J Biomed Mater Res A 2003;67A:834–7.
[4] Bolland F, Korossis S, Wilshaw SP, Ingham E, Fisher J, Kearney JN, et al. Development and characterisation of a full-thickness acellular porcine bladder matrix for tissue engineering. Biomaterials 2007;28:1061–70.
[5] Chen RN, Ho HO, Tsai YT, Sheu MT. Process development of an acellular dermal matrix (ADM) for biomedical applications. Biomaterials 2004;25:2679–86.
[6] Badylak SF, Freytes DO, Gilbert TW. Extracellular matrix as a biological scaffold material: structure and function. Acta Biomaterialia 2009;5:1–13.
[7] Freytes DO, Tullius RS, Valentin RS, Stewart-Akers AM, Badylak SF. Hydrate versus lyophilized forms of porcine extracellular matrix derived from the urinary bladder. J Biomed Mater Res A 2008;4:862–72.
[8] Badylak SF. Xenogeneic extracellular matrix as a scaffold for tissue reconstruction. Transpl Immunol 2004;12:367–77.
[9] McFetridge PS, Daniel JW, Bodamyali T, Horrocks M, Chaudhuri JB. Preparation of porcine carotid arteries for vascular tissue engineering applications. J Biomed Mater Res A 2004;70A:224–34.
[10] Ketchedjian A, Jones AL, Krueger P, Robinson E, Crouch K, Wolfinbarger L, et al. Recellularization of decellularized allograft scaffolds in ovine great vessel reconstructions. Ann Thorac Surg 2005;79:888–96.
[11] Rieder E, Kasimir MT, Silberhumer G. Decellularization protocols of porcine heart valves differ importantly in efficiency of cell removal and susceptibility of the matrix to recellularization with human vascular cells. J Thorac Cardiovasc Surg 2004;127:399–405.
[12] Sawada K, Terada D, Yamaoka T, Kitamura S, Fujisato T. Cell removal with supercritical carbon dioxide for acellular artificial tissue. J Chem Tech Biotechnol 2008;83:943–9.
[13] Gilbert TW, Sellaro TL, Badylak SF. Decellularization of tissue and organs. Biomaterials 2006;27:3675–83.
[14] Fujisato T, Minatoya K, Yamazaki S, Meng Y, Niwaya K, Kishida A, et al. Preparation and recellularization of tissue-engineering bioscaffold for heart valve replacement. In: Mori H, Matsuda H, editors. Cardiovascular regeneration therapies using tissue engineering approaches. Tokyo: Springer; 2005. p. 83–94.
[15] Sasaki S, Funamoto S, Hashimoto Y, Kimura T, Honda T, Hattori S, et al. In vivo evaluation of a novel scaffold for artificial corneas prepared by using ultra high hydrostatic pressure to decellularize porcine corneas. Mol Vis 2009;15:2022–8.
[16] Bader A, Schilling T, Teebken OE, Brandes G, Herden T, Steinhoff G. Tissue engineering of heart valves – human endothelial cell seeding of detergent acellularized porcine valves. Eur J Cardiothorac Surg 1998;14:279–84.
[17] Booth C, Korosis SA, Wilcox HE, Watterson KG, Kearney JN, Fisher J. Tissue engineering of cardiac valve prostheses I: development and histological characterization of an acellular porcine scaffold. J Heart Valve Dis 2002;11:457–62.
[18] Leyh RG, Wilhelmi M, Rebe P, Ciboutari S, Haverich A, Mertsching H. Tissue engineering of viable pulmonary arteries for surgical correction of congenital heart defects. Ann Thorac Surg 2006;81:1466–71.
[19] Korossis SA, Booth C, Wilcox HE, Watterson KG, Kearney JN, Fisher J. Tissue engineering of cardiac valve prostheses II: biomechanical characterization of decellularized porcine aortic heart valves. J Heart Valve Dis 2002;11:463–71.
[20] Kingsley DH, Hoover DG, Papafragkou E, Richards GP. Inactivation of hepatitis A virus and a calicivirus by high hydrostatic pressure. J Food Protect 2002;65:1605–9.
[21] Ichimori H, Hata T, Matsuki H, Kaneshina S. Barotropic phase transitions and pressure-induced interdigitation on bilayer membranes of phospholipids with varying acyl chain lengths. Biochim Biophys Acta 1998;1414:165–74.
[22] LeBail A, Chevalier D, Mussa DM, Ghoul M. High pressure freezing and thawing of foods: a review. Int J Refrig 2002;25:504–13.
[23] Douzou P. In: Franks F, editor. Biophysics and biochemistry at low temperatures. Nature, vol. 318; 1985. p. 416.
[24] Borges EN, Silva RC, Futino DO, Rocha-Junior CMC, Amorim CA, Bao SN, et al. Cryopreservation of swine ovarian tissue: effect of different cryoprotectants on the structural preservation of preantral follicle oocytes. Cryobiology 2009;59:195–200.
[25] Dahl SLM, Chen ZZ, Solan AK, Brockbank KGM, Niklason LE, Song YC. Feasibility of vitrification as a storage method for tissue-engineered blood vessels. Tissue Eng 2006;12:291–300.
[26] Moerman F. High hydrostatic pressure inactivation of vegetative microorganisms, aerobic and anaerobic spores in pork Marengo, a low acidic particulate food product. Meat Sci 2005;69:225–32.

Residual Vessel Length on Magnetic Resonance Angiography Identifies Poor Responders to Alteplase in Acute Middle Cerebral Artery Occlusion Patients

Exploratory Analysis of the Japan Alteplase Clinical Trial II

Teruyuki Hirano, MD; Makoto Sasaki, MD; Etsuro Mori, MD; Kazuo Minematsu, MD; Jyoji Nakagawara, MD; Takenori Yamaguchi, MD; for the Japan Alteplase Clinical Trial II Group

Background and Purpose—It remains unknown whether the effects of 0.6 mg/kg alteplase differ with occlusion site of the middle cerebral artery (MCA). We therefore evaluated the effects of 0.6 mg/kg intravenous alteplase in patients with different sites of MCA occlusion.

Methods—An exploratory analysis was made of 57 patients enrolled in the Japan Alteplase Clinical Trial II (J-ACT II), originally designed to evaluate 0.6 mg/kg alteplase in Japanese patients with unilateral occlusion of the MCA (M1 or M2 portion). The residual vessel length (in mm), determined by pretreatment magnetic resonance angiography, was used to reflect the occluded site. The proportions of patients with valid recanalization (modified Mori grade 2 to 3) at 6 and 24 hours and a modified Rankin Scale (mRS) score of 0 to 1 and of 0 to 2 at 3 months were compared between the groups dichotomized according to length of the residual vessel. Multiple logistic-regression models were generated to elucidate the predictors of valid recanalization, mRS 0 to 1, and mRS 0 to 2.

Results—Receiver operating characteristics analysis revealed that 5 mm was the practical cutoff length for dichotomization. In patients with an M1 length <5 mm (n=12), the frequencies of valid recanalization at 6 and 24 hours (16.7% and 25.0%) were significantly lower compared with those (62.1% and 82.8%, respectively) of the 45 patients with a residual M1 length ≥5 mm and an M2 occlusion (P=0.008 for 6 hours, P<0.001 for 24 hours). The proportions of patients who achieved an mRS of 0 to 1 and an mRS of 0 to 2 were also lower for those with an M1 length <5 mm (8.3% and 16.7%, respectively) compared with the other group (57.8% and 68.9%, respectively; P=0.003 for mRS 0 to 1, P=0.002 for mRS 0 to 2). In logistic-regression models, the site of MCA occlusion (<5 mm) was a significant predictor of valid recanalization at 6 and 24 hours and of an mRS of 0 to 1 and of mRS of 0 to 2.

Conclusions—In patients with acute MCA occlusion, a residual vessel length <5 mm on magnetic resonance angiography can identify poor responders to 0.6 mg/kg alteplase.

Clinical Trial Registration—URL: http://www.clinicaltrials.gov. Unique identifier: NCT00412867.

(*Stroke*. 2010;41:2828-2833.)

Key Words: acute ischemic stroke ■ middle cerebral artery occlusion ■ tissue plasminogen activator ■ recanalization ■ magnetic resonance angiography

Intravenous thrombolysis with recombinant tissue plasminogen activator is effective in carefully selected patients with acute ischemic stroke.[1,2] Among patients treated with intravenous alteplase, stroke severity, systolic hypertension, early ischemic changes on computed tomography, persistent arterial occlusion, stroke subtype, and time to thrombolytic treatment have been repeatedly demonstrated as independent predictors of poor outcome.[3–10] Furthermore, the Japan Alteplase Clinical Trial II (J-ACT II) clearly demonstrated that recanalization of the occluded artery represented the most powerful predictor of a favorable outcome at 3 months in selected patients with magnetic resonance angiography (MRA)–documented middle cerebral artery (MCA) occlusions.[11] Information concerning early predictors of recanalization resistance may thus be useful for selecting patients to receive more aggressive reperfusion strategies.

Previous angiographic,[12–14] transcranial Doppler,[15] and MRA[16–18] studies have demonstrated that more proximal

Received June 22, 2010; accepted September 7, 2010.

From the Department of Neurology (T.H.), Faculty of Life Sciences, Kumamoto University, Kumamoto; Advanced Medical Center (M.S.), Iwate Medical University, Morioka; Department of Behavioral Neurology and Cognitive Neuroscience (E.M.), Tohoku University Graduate School of Medicine, Sendai; Department of Stroke and Cerebrovascular Diseases (K.M.), National Cerebral and Cardiovascular Center, Suita, Osaka; Department of Neurosurgery and Stroke Center (J.N.), Nakamura Memorial Hospital, Sapporo; and National Cardiovascular Center (T.Y.), Suita, Osaka, Japan.

Correspondence to Teruyuki Hirano, Department of Neurology, Faculty of Life Sciences, Kumamoto University, 1-1-1 Honjo, Kumamoto 860-0811, Japan. E-mail terry07@kumamoto-u.ac.jp

Stroke is available at http://stroke.ahajournals.org

DOI: 10.1161/STROKEAHA.110.594333

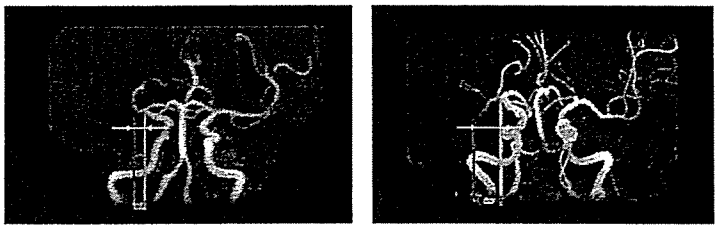

Figure 1. Measurement of residual vessel length in patients with M1 occlusions. Examples are shown of the residual vessel length measured by 3-dimensional time-of-flight MRA. The site of M1 occlusion was determined in an anteroposterior view as the horizontal distance from the ICA bifurcation to the distal end of the flow signal.

occlusions, such as those of the internal carotid artery (ICA)[14,17–20] or tandem ICA/MCA,[21] carry a greater thrombus burden, whereas distal MCA occlusions are more likely to recanalize with systemic alteplase therapy. A meta-analysis revealed that recanalization, either spontaneous or related to thrombolytic or interventional therapies, is less likely with ICA occlusions.[22] ICA occlusion has been shown to predict a poorer clinical outcome compared with MCA occlusion.[14,17,19,20] However, little is yet known about the differences in recanalization rates and response to alteplase among patients with various sites of MCA occlusion. We therefore performed an exploratory analysis of patients with MCA occlusion enrolled in J-ACT II, giving special attention to the residual vessel length as documented on pretreatment MRA.

Methods

J-ACT II is a prospective, single-dose, open-label, multicenter, phase IV trial, originally designed to evaluate 0.6 mg/kg alteplase in Japanese patients with unilateral occlusion of the MCA. Details of the trial have been published previously.[11] In brief, 58 patients with ischemic stroke within 3 hours of onset whose arterial occlusion was identified in the M1 or M2 segment on standardized MRA were enrolled. The results showed that the rates of early and delayed recanalization and a favorable outcome elicited by 0.6 mg/kg alteplase were comparable to the previously reported findings for the regular dose of 0.9 mg/kg.

Site of MCA Occlusion

All baseline MRA data were re-evaluated centrally by 2 reviewers, 1 expert neurologist, and 1 expert neuroradiologist (the image-reading panel), all of whom were blinded to all clinical information except the affected side. For patients with M1 occlusions, the site of occlusion was determined in an anteroposterior view on 3-dimensional time-of-flight MRA as the horizontal distance from the ICA bifurcation to the distal end of the flow signal. The residual vessel length (in mm) was used to reflect the occluded site in the patients with M1 occlusions (Figure 1).

Evaluation of Recanalization

MRA was repeated at baseline, 6 hours, and 24 hours after symptom onset. The time allowance for the 6-hour MRA was between the end of alteplase infusion and 8 hours from symptom onset, and that for the 24-hour MRA was between 24 and 36 hours after symptom onset.

Recanalization was evaluated centrally by the image-reading panel according to the modified Mori grade: grade 0, no reperfusion; grade 1, movement of thrombus not associated with any flow improvement; grade 2, partial (branch) recanalization in <50% of the branches in the occluded arterial territory; and grade 3, nearly complete recanalization with reperfusion in ≥50% of the branches in the occluded arterial territory.[11] The recanalization rate was estimated by regarding grades 2 and 3 as valid recanalization, corresponding to Thrombolysis in Myocardial Infarction grades 2 and 3.

Clinical Evaluation

Functional outcome after 3 months was assessed by the modified Rankin Scale (mRS) score. Patients with an mRS of 0 to 1 at 3 months were regarded as having a favorable outcome. In addition, an mRS of 0 to 2 was judged to be indicative of functional independence, that is, avoiding death or dependency.

Statistical Analysis

The proportions of patients with valid recanalization at 6 and 24 hours after symptom onset, a favorable outcome (mRS 0 to 1), and functional independence (mRS 0 to 2) at 3 months were compared between the groups dichotomized according to length of residual vessel on MRA. Receiver operating characteristics curves were constructed for the patients with M1 occlusions to make comparisons between vessel length and clinical outcome.

The predictors of valid recanalization at 6 and 24 hours, mRS 0 to 1, and mRS 0 to 2 were assessed by multiple logistic-regression analysis. Knowledge of disease-related factors before alteplase administration, such as time from onset, presence of hypertension, diabetes mellitus, baseline National Institutes of Health Stroke Scale score, and Alberta Stroke Program Early Computed Tomography Score (ASPECTS),[6] as well as MCA occlusion site, was included in a stepwise regression analysis, for which age and sex were forcibly entered into the model to adjust for their possible confounding effects.

Table 1. Comparison of Demographic and Baseline Characteristics of the Patients (N=57) According to Site of MCA Occlusion

	Total (N=57)	M1 <5 mm (n=12)	M1 ≥5 mm (n=29)	M2 (n=16)
Mean±SD age, y	70.7±11.2	74.6±9.8	66.4±11.7	75.5±8.2
Female, n	23 (40.4%)	8 (66.7%)	12 (41.4%)	3 (18.8%)
Baseline NIHSS score (range)	12 (5–22)	17 (5–22)	12 (6–22)	11 (5–21)
Stroke subtype, n				
Cardioembolic	49 (86.0%)	10 (83.3%)	25 (86.2%)	14 (87.5%)
Atherothrombotic	5 (8.8%)	2 (16.7%)	2 (6.9%)	1 (6.3%)
Other/not differentiated	3 (5.3%)	0 (0%)	2 (6.9%)	1 (6.3%)
Concomitant diseases				
Hypertension, n	36 (63.2%)	9 (75.0%)	13 (44.8%)	14 (87.5%)
Diabetes	10 (17.5%)	2 (16.7%)	3 (10.3%)	5 (31.3%)
Dyslipidemia	18 (31.6%)	3 (25.0%)	10 (34.5%)	5 (31.3%)
Atrial fibrillation	34 (59.6%)	9 (75.0%)	15 (51.7%)	10 (62.5%)
Previous stroke/TIA	12 (21.1%)	1 (8.3%)	7 (24.1%)	4 (25.0%)
ASPECTS value (range)	9 (3–10)	8 (3–10)	9 (5–10)	9 (7–10)

NIHSS indicates National Institutes of Health Stroke Scale; TIA, transient ischemic attack. Data show the mean (SD), median (interquartile range), or No. (%).

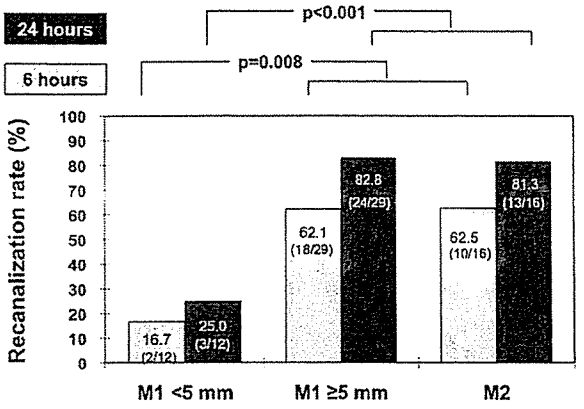

Figure 2. Rate of valid recanalization at 6 and 24 hours by site of vessel occlusion. The rate of valid recanalization was significantly lower in patients with a residual M1 length <5 mm at both 6 and at 24 hours.

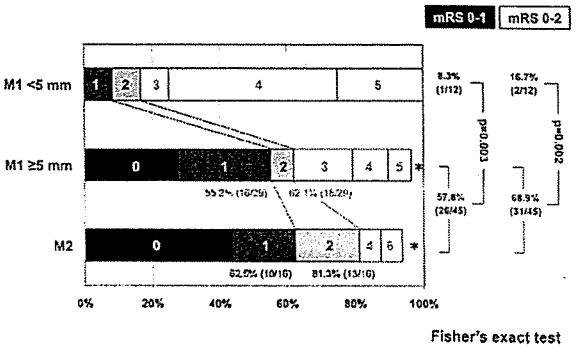

Figure 3. Distribution of scores at 3 months on the mRS scale by site of vessel occlusion. The proportion of patients with a favorable outcome, ie, an mRS score of 0 to 1, was significantly lower in patients with a residual M1 length <5 mm. Similar results were obtained when the frequency of functional independence, ie, an mRS of 0 to 2, was investigated. *Data were not obtained in 1 patient each with a residual M1 length ≥5 mm and M2. These patients were assigned an mRS ≥3.

To examine the possible interaction of MCA occlusion site with recanalization for the 3-month outcome, the following recanalization patterns were evaluated with the logistic model in addition to the disease-related factors: (1) model 1, in which recanalization on 6-hour MRA was entered; (2) model 2, in which recanalization on 24-hour MRA was entered; and (3) model 3, in which recanalization within 6 hours and delayed recanalization (that is, arterial occlusion unchanged on 6-hour MRA but recanalized on 24-hour MRA) were entered. Significance was set at $P<0.05$ in all models. The odds ratio (OR) and 95% CIs were also determined. SAS 9.1.3 was used for statistical analyses.

Results

Of the 58 patients enrolled in the trial, 41 (70.7%) were evaluated as having an M1 occlusion. Their residual M1 length ranged from 0.0 (origin) to 17.7 mm (distal end), whereas the contralateral M1 length ranged from 19.5 to 32.1 mm (mean±SD, 26.1±3.1 mm). One patient was judged to have no occluded artery on baseline MRA by the image-reading panel and was therefore excluded from the present analysis. The remaining 16 patients (27.6%) were evaluated as having an M2 occlusion. Further analyses were therefore performed on 57 patients with MCA occlusion. Table 1 summarizes these patients' characteristics.

The cumulative frequency of valid recanalization at 6 and 24 hours increased as the residual M1 length increased. No patient had recanalization on 6-hour MRA that subsequently disappeared on 24-hour MRA. Receiver operating characteristics analysis revealed that valid recanalization differed between the groups dichotomized by residual vessel length at both 6 (Az 0.701, $P=0.027$) and 24 (Az 0.817, $P=0.001$) hours. The optimal cutoff residual M1 lengths for predicting valid recanalization at 6 and 24 hours were the same, 5.3 mm. When the patients with M1 occlusions were divided into 2 groups (residual vessel length <5 mm or ≥5 mm), the frequency of valid recanalization was significantly lower in the patients with a residual M1 length <5 mm (n=12) compared with the combined group with an M1 length ≥5 mm (n=29) and those with M2 occlusions (n=16) ($P=0.008$ for 6 hours, $P<0.001$ for 24 hours; Fisher's exact test; Figure 2). In logistic-regression models, the site of MCA occlusion (<5 mm) was the only significant predictor of valid recanalization at both 6 (OR=0.076; 95% CI, 0.010 to 0.573) and 24 (OR=0.023; 95% CI, 0.002 to 0.245) hours.

Similarly, receiver operating characteristics analysis demonstrated that the proportions of patients with a favorable outcome (mRS 0 to 1) and functional independence (mRS 0 to 2) were also different among patients with M1 occlusions, with an optimal cutoff length of 5.3 mm. The distribution of scores on the 3-month mRS was different among patients with M1 lengths <5 mm compared with those with an M1 length ≥5 mm and M2 occlusions (Figure 3). On logistic-

Table 2. Predictors of Favorable Outcome and Functional Independence by Multiple Logistic Regression Analysis

	OR	95% CI	*P* Value
mRS 0–1			
Sex (female vs male)	1.011	0.274–3.726	0.9871
Age (by 1 year)	0.989	0.932–1.050	0.7155
Time from onset to treatment (by min)	0.998	0.971–1.027	0.9112
Diabetes	0.891	0.146–5.428	0.9006
Hypertension	1.872	0.465–7.528	0.3773
Baseline NIHSS (by 1 point)	0.878	0.737–1.046	0.1466
Occluded site (<5 mm vs others)	**0.082**	**0.008–0.812**	**0.0325**
ASPECTS value (by 1 point)	1.429	0.788–2.592	0.2392
mRS 0–2			
Sex (female vs male)	0.639	0.152–2.689	0.5416
Age (by 1 year)	1.016	0.952–1.085	0.6290
Time from onset to treatment (by min)	0.978	0.948–1.008	0.1508
Diabetes	0.607	0.080–4.632	0.6302
Hypertension	1.025	0.235–4.473	0.9743
Baseline NIHSS (by 1 point)	0.890	0.746–1.061	0.1925
Occluded site (<5 mm vs others)	**0.125**	**0.020–0.793**	**0.0274**
ASPECTS value (by 1 point)	**2.121**	**1.082–4.158**	**0.0285**

NIHSS indicates National Institutes of Health Stroke Scale. Table entries in bold-faced type are statistically significant.

Table 3. Predictors of Favorable Outcome and Functional Independence by Multiple-Logistic Regression Analysis in 3 Different Models of Posttreatment Recanalization

	Model 1: 6-Hour Recanalization Model			Model 2: 24-Hour Recanalization Model			Model 3: 6-Hour and Delayed Recanalization Model		
	OR	95% CI	*P* Value	OR	95% CI	*P* Value	OR	95% CI	*P* Value
mRS 0–1									
Sex (female vs male)	0.846	0.198–3.619	0.8212	0.814	0.168–3.933	0.7974	0.668	0.137–3.245	0.6167
Age (by 1 year)	0.986	0.924–1.052	0.6689	0.989	0.921–1.062	0.7555	0.973	0.905–1.046	0.4632
Time from onset to treatment (by min)	1.006	0.976–1.037	0.7024	0.997	0.967–1.027	0.8273	1.003	0.972–1.034	0.8721
Diabetes	0.341	0.042–2.783	0.3152	0.456	0.053–3.893	0.4728	0.281	0.028–2.783	0.2779
Hypertension	1.847	0.419–8.147	0.4177	2.919	0.544–15.671	0.2115	2.556	0.449–13.087	0.2602
Baseline NIHSS (by 1 point)	0.903	0.748–1.091	0.2915	**0.797**	**0.643–0.989**	**0.0391**	0.859	0.701–1.054	0.1456
Occluded site (<5 mm vs others)	0.173	0.016–1.901	0.1515	0.544	0.041–7.290	0.6453	0.568	0.040–8.068	0.6759
ASPECTS value (by 1 point)	1.755	0.881–3.497	0.1096	2.111	0.981–4.541	0.0560	2.007	0.940–4.287	0.0718
Recanalization within 6 h	**6.772**	**1.346–34.080**	**0.0203**	...	...	...	**38.972**	**3.222–471.318**	**0.0040**
Recanalization within 24 h	...	...	...	**32.762**	**3.572–300.514**	**0.0020**	...	...	...
Delayed recanalization	...	...	...	...	...	...	**18.607**	**1.357–255.149**	**0.0286**
mRS 0–2									
Sex (female vs male)	0.546	0.113–2.646	0.4521	0.525	0.100–2.763	0.4471	0.522	0.104–2.636	0.4317
Age (by 1 year)	1.007	0.938–1.081	0.8476	1.017	0.947–1.092	0.6420	1.004	0.935–1.079	0.9029
Time from onset to treatment (by min)	0.987	0.955–1.020	0.4274	0.978	0.946–1.010	0.1784	0.986	0.955–1.018	0.3942
Diabetes	0.233	0.021–2.586	0.2357	0.362	0.035–3.713	0.3926	0.228	0.019–2.730	0.2434
Hypertension	1.115	0.236–5.277	0.8906	1.524	0.298–7.802	0.6129	1.288	0.264–6.281	0.7543
Baseline NIHSS (by 1 point)	0.925	0.759–1.127	0.4382	0.850	0.699–1.035	0.1056	0.911	0.746–1.112	0.3594
Occluded site (<5 mm vs others)	0.250	0.035–1.798	0.1684	0.447	0.052–3.821	0.4618	0.363	0.043–3.073	0.3522
ASPECTS value (by 1 point)	**2.683**	**1.217–5.918**	**0.0145**	**2.949**	**1.279–6.798**	**0.0111**	**2.791**	**1.231–6.331**	**0.0140**
Recanalization within 6 h	**7.362**	**1.250–43.371**	**0.0274**	...	...	...	**13.179**	**1.478–117.510**	**0.0209**
Recanalization within 24 h	...	...	...	**15.502**	**1.953–123.034**	**0.0095**	...	...	...
Delayed recanalization	...	...	...	...	...	...	3.132	0.322–30.427	0.3250

NIHSS indicates National Institutes of Health Stroke Scale. Table entries in bold-faced type are statistically significant.

regression analysis including the disease-related factors present before alteplase administration, a residual M1 length <5 mm was the only significant predictor of a favorable outcome (OR=0.082; 95% CI, 0.008 to 0.812; Table 2). A residual M1 length <5 mm (OR=0.125; 95% CI, 0.020 to 0.793), together with a high ASPECTS value (OR=2.121; 95% CI, 1.082 to 4.158), was significantly related to functional independence at 3 months (Table 2).

Possible interactions between the pretreatment residual vessel length and patterns of recanalization were evaluated by multiple logistic-regression analysis (Table 3). Among the models for favorable outcome, recanalization in model 1, recanalization and baseline National Institutes of Health Stroke Scale score in model 2, and 6-hour and delayed recanalization in model 3 were significant predictors. Among the models for functional independence, recanalization and ASPECTS score in model 1, recanalization and ASPECTS score in model 2, and 6-hour recanalization and ASPECTS score in model 3 were significant predictors.

Discussion

In the present exploratory analysis of the J-ACT II cohort, we found that a residual M1 length <5 mm on MRA was a negative predictor of early and delayed recanalizations as well as for a favorable outcome and functional independence at 3 months. Patients with residual M1 lengths <5 mm are poor responders to 0.6 mg/kg alteplase. The site of vessel occlusion was a strong predictor of outcome before systemic alteplase administration.

In a previous magnetic resonance imaging–based, open-label, nonrandomized study, the German Stroke Excellence Network Initiative,[16] the reported recanalization rate of proximal MCA occlusions was comparable with distal MCA and M2 occlusions (76.7% for the proximal MCA, 60.0% for the distal MCA, and 87.5% for M2) in the 76 patients treated with thrombolysis. On the other hand, the difference in recanalization rate was significant between an MCA origin and other sites of MCA occlusion in our study. In addition to the different alteplase doses between Europe and Japan, the lack of a clear definition of "proximal" and "distal" MCA might have led to this discrepancy. In our study, cumulative analysis followed by receiver operating characteristics analysis demonstrated that <5 mm was the practical cutoff length between proximal and distal sites within the M1 portion.

Our results paralleled those of Saqqur et al,[15] who examined the effects of alteplase by transcranial Doppler. They showed that patients with distal MCA occlusions were more likely to recanalize and were twice as likely to achieve an

mRS of 0 to 1 than were those with proximal MCA occlusions. Their transcranial Doppler–based definitions of the occluded site in the MCA and of complete recanalization differed from ours, however. The proportions of patients achieving an mRS of 0 to 1 decreased with more proximal occlusions: distal MCA, 52%; proximal MCA, 25%; tandem ICA/MCA, 21%; and terminal ICA, 18%.

What are the potential reasons for different outcomes between patients with residual M1 lengths <5 mm and others? In terms of thrombus size and the association of thrombi with atherosclerosis, clot size is bigger in patients with a residual M1 length <5 mm, and there may be differences in clot composition between proximal and distal M1 occlusions.[23] Fibrin-rich clots have been shown to display a greater propensity for lysis by alteplase compared with platelet-rich clots.[10] Relative to other stroke subtypes, the rate of complete recanalization has been reported to be higher in patients with cardioembolic stroke.[10] Although there was no statistical difference, atherosclerotic occlusion was found more frequently in patients with proximal M1 occlusions (16.7% in M1 <5 mm; 6.7% in M1 ≥5 mm and M2, P=0.281).

Another possible explanation concerns the number of perforating arteries originating from the M1 portion. Patients with a residual M1 length <5 mm seldom spare perforators that allow a continuous blood stream. Effective delivery and distribution of alteplase into the clot may thus become severely disturbed. Experimental studies have demonstrated that the fibrinolytic rate is dependent on the pressure gradient to which the clot is exposed.[24]

In our first logistic-regression model including only pretreatment factors, the site of vessel occlusion (M1 <5 mm or other) was a strong predictor of 3-month outcome. Once important posttreatment factors, like early and/or delayed recanalization, were included in the second of the 3 different models, the site of vessel occlusion no longer remained as significant. This is reasonable, because the site of vessel occlusion before treatment with alteplase was strongly correlated to posttreatment recanalization. To achieve an mRS of 0 to 1, the key is recanalization immediately after thrombolysis, as repeatedly reported.[25–29] Using the Safe Implementation of Treatment in Stroke-International Stroke Thrombolysis Register database, Kharitonova et al[30] also noted that disappearance of a hyperdense MCA signs, an indirect marker of recanalization on computed tomography, was significantly related to functional independence and survival.

On the other hand, an mRS of 0 to 2 might be achieved independently of recanalization if the patient has good collateral flow, indicated by a high ASPECTS value.[31] Regarding the influence of pretreatment ASPECTS, the Pro-Urokinase for Acute Cerebral Thromboembolism II trial demonstrated that patients with ASPECTS scores >7 were 3 times more likely to achieve an mRS of 0 to 2.[32]

It might be reasonable to modify our treatment strategy according to the MRA information concerning the site of pretreatment vessel occlusion. We speculate that patients with M1-origin occlusions (residual vessel length <5 mm) as well as those with ICA occlusions may be potential candidates for rescue interventional therapies, such as intra-arterial thrombolysis and mechanical thrombectomy, should intravenous thrombolysis fail to achieve recanalization and reperfusion.

The present study has several limitations. First, the number of patients was relatively small because the target population was strictly limited to MRA-documented M1 or M2 occlusions. Second, we could not evaluate collateral status because MRA was the only required modality for imaging. Good collateral flow up to the distal end of the clot might have accelerated recanalization.[33] Third, the alteplase dose was 0.6 mg/kg, which is the specified dose in the Japanese license.[34] The recanalization rate in patients with a residual M1 length <5 mm could have been improved with the 0.9 mg/kg dose of alteplase, although J-ACT II demonstrated efficacy in terms of vascular and clinical outcomes.[11]

In conclusion, the effect of 0.6 mg/kg intravenous alteplase differs according to the MRA-documented site of MCA occlusion. In patients with acute MCA occlusions, a residual M1 length <5 mm on MRA can identify poor responders to 0.6 mg/kg alteplase.

Sources of Funding

This clinical trial was supported by Kyowa Hakko Kirin Co, Ltd, and Mitsubishi Tanabe Pharma Corporation.

Disclosures

Teruyuki Hirano has received honoraria from Mitsubishi Tanabe Pharma and Kyowa Hakko Kirin. Makoto Sasaki has received honoraria from Mitsubishi Tanabe Pharma, Kyowa Hakko Kirin, and Lundbeck. Etsuro Mori has received a research grant, honoraria, and consulting fees from Mitsubishi Tanabe Pharma; honoraria and consulting fees from Kyowa Hakko Kirin; and consulting fees from Lundbeck. Kazuo Minematsu has received a research grant and honoraria from Mitsubishi Tanabe Pharma and honoraria from Kyowa Hakko Kirin and Lundbeck. Jyoji Nakagawara has received honoraria from Mitsubishi Tanabe Pharma, Kyowa Hakko Kirin, and Lundbeck. Takenori Yamaguchi has received consulting fees from Mitsubishi Tanabe Pharma and research grants from Kyowa Hakko Kirin and Lundbeck.

References

1. The National Institute of Neurological Disorders and Stroke rt-PA Stroke Study Group. Tissue plasminogen activator for acute ischemic stroke. *N Engl J Med.* 1995;333:1581–1587.
2. Hacke W, Kaste M, Bluhmki E, Brozman M, Dávalos A, Guidetti D, Larrue V, Lees KR, Medeghri Z, Machnig T, Schneider D, von Kummer R, Wahlgren N, Toni D; ECASS Investigators. Thrombolysis with alteplase 3 to 4.5 hours after acute ischemic stroke. *N Engl J Med.* 2008;359:1317–1329.
3. Dávalos A, Toni D, Iweins F, Lesaffre F, Bastianello S, Castillo J. Neurological deterioration in acute ischemic stroke: potential predictors and associated factors in the European Cooperative Acute Stroke Study (ECASS) I. *Stroke.* 1999;30:2631–2636.
4. Albers GW, Bates VE, Clark WM, Bell R, Verro P, Hamilton SA. Intravenous tissue-type plasminogen activator for treatment of acute stroke: the Standard Treatment with Alteplase to Reverse Stroke (STARS) study. *J Am Med Assoc.* 2000;283:1145–1150.
5. Marler JR, Tilley BC, Lu M, Brott TG, Lyden PC, Grotta JC, Broderick JP, Levine SR, Frankel MP, Horowitz SH, Haley DC, Lewandowski CA, Kwiatkowski TP, for the NINDS rt-PA Stroke Study Group. Early stroke treatment associated with better outcome: the NINDS rt-PA stroke study. *Neurology.* 2000;55:1649–1655.
6. Barber PA, Demchuk AM, Zhang J, Buchan AM. Validity and reliability of a quantitative computed tomography score in predicting outcome of hyperacute stroke before thrombolytic therapy. *Lancet.* 2000;355:1670–1674.

7. Demchuk AM, Tanne D, Hill MD, Kasner SE, Hanson S, Grond M, Levine SR; The Multicentre tPA Stroke Survey Group. Predictors of good outcome after intravenous tPA for acute ischemic stroke. *Neurology*. 2001;57:474–480.
8. Labiche LA, Al-Senani F, Wojner AW, Grotta JC, Malkoff M, Alexandrov AV. Is the benefit of early recanalization sustained at 3 months? a prospective cohort study. *Stroke*. 2003;34:695–698.
9. Hacke W, Donnan GA, Fieschi C, Kaste M, von Kummer R, Broderick JP, Brott T, Frankel M, Grotta JC, Haley EC Jr, Kwiatkowski T, Levine SR, Lewandowski C, Lu M, Lyden P, Marler JR, Patel S, Tilley BC, Albers G, Bluhmki E, Wilhelm M, Hamilton S; ATLANTIS Trials Investigators; ECASS Trials Investigators; NINDS rt-PA Study Group Investigators. Association of outcome with early stroke treatment: pooled analysis of ATLANTIS, ECASS, and NINDS rt-PA stroke trials. *Lancet*. 2004;363:768–774.
10. Molina CA, Montanar J, Arenillas JF, Ribo M, Rubiera M, Alvarez-Sabin J. Differential pattern of tissue plasminogen activator–induced proximal middle cerebral artery recanalization among stroke subtypes. *Stroke*. 2004;35:486–490.
11. Mori E, Minamatsu K, Nakagawara J, Yamaguchi T, Sasaki M, Hirano T; for the J-ACT II Group. Effects of 0.6 mg/kg intravenous alteplase on vascular and clinical outcomes in middle cerebral artery occlusion: Japan Alteplase Clinical Trial II (J-ACT II). *Stroke*. 2010;41:461–465.
12. del Zoppo GJ, Poeck K, Pessin MS, Wolpert SM, Furlan AJ, Ferbert A, Alberts MJ, Zivin JA, Wechsler L, Busse O, Greenlee R, Brass L, Mohr JP, Feldmann E, Hacke W, Kase CS, Biller J, Gress D, Otis SM. Recombinant tissue plasminogen activator in acute thrombotic and embolic stroke. *Ann Neurol*. 1992;32:78–86.
13. Lewandowski CA, Frankel M, Tomsick TA, Broderick J, Frey J, Clark W, Starkman S, Grotta J, Spilker J, Khoury J, Brott T. Combined intravenous and intra-arterial rt-PA versus intra-arterial therapy of acute ischemic stroke: Emergency Management of Stroke (EMS) Bridging Trial. *Stroke*. 1999;30:2598–2605.
14. Linfante I, Llinas RH, Selim M, Chaves C, Kumar S, Parker RA, Caplan LR, Schlaug G. Clinical and vascular outcome in internal carotid artery vs middle cerebral artery occlusions after intravenous tissue plasminogen activator. *Stroke*. 2002;33:2066–2071.
15. Saqqur M, Uchino K, Demchuk AM, Molina CA, Garami Z, Calleja S, Akhtar N, Orouk FO, Salam A, Shuaib A, Alexandrov AV; for CLOTBUST Investigators. Site of arterial occlusion identified by transcranial Doppler predicts the response to intravenous thrombolysis for stroke. *Stroke*. 2007;38:948–954.
16. Röther J, Schellinger PD, Gass A, Siebler M, Villringer A, Fiebach JB, Fiehler J, Jansen O, Kucinski T, Schoder V, Szabo K, Junge-Hülsing GJ, Hennerici M, Zeumer H, Sartor K, Weiller C, Hacke W; for the Kompetenznetzwerk Schlaganfall Study Group. Effect of intravenous thrombolysis on MRI parameters and functional outcome in acute stroke <6 hours. *Stroke*. 2002;33:2438–2445.
17. Nakashima T, Toyoda K, Koga M, Matsuoka H, Nagatsuka K, Takada T, Naritomi H, Minematsu K. Arterial occlusion sites on magnetic resonance angiography influence the efficacy of intravenous low-dose (0.6 mg/kg) alteplase therapy for ischaemic stroke. *Int J Stroke*. 2009;4:425–431.
18. De Silva DA, Brekenfeld C, Ebinger M, Christensen S, Barber PA, Butcher KS, Levi CR, Parsons MW, Bladin CF, Donnan GA, Davis SM; for the Echoplanar Imaging Thrombolytic Evaluation Trial (EPITHET) Investigators. The benefits of intravenous thrombolysis relate to the site of baseline arterial occlusion in the Echoplanar Imaging Thrombolytic Evaluation Trial (EPITHET). *Stroke*. 2010;41:295–299.
19. Kim YS, Garami Z, Mikulik R, Molina CA, Alexandrov AV. Early recanalization rates and clinical outcomes in patients with tandem internal carotid artery/middle cerebral artery occlusion and isolated middle cerebral artery occlusion. *Stroke*. 2005;36:869–871.
20. Marks MP, Olivot JM, Kemp S, Lansberg MG, Bammer R, Wechsler LR, Albers GW, Thijs V. Patients with acute stroke treated with intravenous tPA 3–6 hours after stroke onset: correlations between MR angiography findings and perfusion- and diffusion-weighted imaging in the DEFUSE study. *Radiology*. 2008;249:614–623.
21. Rubiera M, Ribo M, Delgado-Mederos R, Santamarina E, Delgado P, Montaner J, Alvarez-Sabín J, Molina CA. Tandem internal carotid artery/middle cerebral artery occlusion: an independent predictor of poor outcome after systemic thrombolysis. *Stroke*. 2006;37:2301–2305.
22. Rha JH, Saver JL. The impact of recanalization on ischemic stroke outcome: a meta-analysis. *Stroke*. 2007;38:2438–2445.
23. Marder VJ, Chute DJ, Starkman S, Abolian AM, Kidwell C, Liebeskind D, Ovbiagele B, Vinuela F, Duckwiler G, Jahan R, Vespa PM, Selco S, Rajajee V, Kim D, Sanossian N, Saver JL. Analysis of thrombi retrieved from cerebral arteries of patients with acute ischemic stroke. *Stroke*. 2006;37:2086–2093.
24. Blinc A, Francis CW. Transport processes in fibrinolysis and fibrinolytic therapy. *Thromb Haemost*. 1996;76:481–491.
25. Mori E, Yoneda Y, Tabuchi M, Yoshida T, Ohkawa S, Ohsumi Y, Kitano K, Tsutsumi A, Yamadori A. Intravenous recombinant tissue plasminogen activator in acute carotid artery territory stroke. *Neurology*. 1992;42:976–982.
26. von Kummer R, Hacke W. Safety and efficacy of intravenous tissue plasminogen activator and heparin in acute middle cerebral artery stroke. *Stroke*. 1992;23:646–652.
27. Yamaguchi T, Hayakawa T, Kiuchi H. Intravenous tissue plasminogen activator ameliorates the outcome of hyperacute embolic stroke. *Cerebrovasc Dis*. 1993;3:269–272.
28. Yamaguchi T, Kikuchi H, Hayakawa T. Clinical efficacy and safety of intravenous tissue plasminogen activator in acute embolic stroke: a randomized, double-blind, dose-comparison study of duteplase. In: Yamaguchi T, Mori E, Minematsu K, del Zoppo GJ, eds. *Thrombolytic Therapy in Acute Ischemic Stroke III*. Tokyo: Springer-Verlag; 1995:223–229.
29. Chalela JA, Kang DW, Luby M, Ezzeddine M, Latour LL, Todd JW, Dunn B, Warach S. Early MRI findings in patients receiving tissue plasminogen activator predict outcome: insights into the pathophysiology of acute stroke in the thrombolysis era. *Ann Neurol*. 2004;55:105–112.
30. Kharitonova T, Thorén M, Ahmed N, Wardlaw JM, von Kummer R, Thomassen L, Wahlgren N, for the SITS investigators. Disappearing hyperdense middle cerebral artery sign in ischaemic stroke patients treated with intravenous thrombolysis: clinical course and prognostic significance. *J Neurol Neurosurg Psychiatry*. 2009;80:273–278.
31. Hirano T, Yonehara T, Inatomi Y, Hashimoto Y, Uchino M. Presence of early ischemic changes on computed tomography depends on severity and the duration of hypoperfusion: a single photon emission-computed tomographic study. *Stroke*. 2005;36:2601–2608.
32. Hill MD, Rawley HA, Adler F, Eliasziw M, Furlan A, Higashida RT, Wechsler LR, Roberts HC, Dillon WP, Fischbein NJ, Fieszt CM, Schulz GA, Buchan AM. Selection of acute ischemic stroke patients for intra-arterial thrombolysis with pro-urokinase by using ASPECTS. *Stroke*. 2003;34:1925–1931.
33. Miteff F, Levi CR, Bateman GA, Spratt N, McElduff P, Parsons MW. The independent predictive utility of computed tomography angiographic collateral status in acute ischaemic stroke. *Brain*. 2009;132:2231–2238.
34. Yamaguchi T, Mori E, Minematsu K, Nakagawara J, Hashi K, Saito I, Shinohara Y. Alteplase at 0.6 mg/kg for acute ischemic stroke within 3 hours of onset: Japan Alteplase Clinical Trial (J-ACT). *Stroke*. 2006;37:1810–1815.

7-12

Thrombolysis With 0.6 mg/kg Intravenous Alteplase for Acute Ischemic Stroke in Routine Clinical Practice

The Japan post-Marketing Alteplase Registration Study (J-MARS)

Jyoji Nakagawara, MD; Kazuo Minematsu, MD; Yasushi Okada, MD; Norio Tanahashi, MD; Shinji Nagahiro, MD; Etsuro Mori, MD; Yukito Shinohara, MD; Takenori Yamaguchi, MD; for J-MARS Investigators

Background and Purpose—In Japan, alteplase at 0.6 mg/kg was approved in October 2005 for use within 3 hours of stroke onset by the Ministry of Health, Labor and Welfare (MHLW). The aim of the Japan post-Marketing Alteplase Registration Study (J-MARS), which was requested by MHLW at the time of approval, was to assess the safety and efficacy of 0.6 mg/kg alteplase in routine clinical practice for the Japanese.

Methods—A total of 7492 patients from 942 centers were enrolled in the J-MARS, an open-label, nonrandomized, observational study, from October 2005 to October 2007. Primary outcome measures were symptomatic intracranial hemorrhage (a deterioration in NIHSS score ≥4 from baseline) and favorable outcome (modified Rankin Scale score, 0–1) at 3 months after stroke onset.

Results—The proportion of patients with symptomatic intracranial hemorrhage in 7492 patients (safety analysis) was 3.5% (95% confidence interval [CI], 3.1%–3.9%) within 36 hours and 4.4% (95% CI, 3.9%–4.9%) at 3 months. The overall mortality rate was 13.1% (95% CI, 12.4%–13.9%) and the proportion of patients with fatal symptomatic intracranial hemorrhage was 0.9% (95% CI, 0.7%–1.2%). The outcomes at 3 months were available for 4944 patients and the proportion of favorable outcome (efficacy analysis) was 33.1% (95% CI, 31.8%–34.4%). The subgroup analysis in patients between 18 and 80 years with a baseline NIHSS score <25 demonstrated that favorable outcome at 3 months was 39.0% (95% CI, 37.4%–40.6%).

Conclusions—These data suggest that 0.6 mg/kg intravenous alteplase within 3 hours of stroke onset could be safe and effective in routine clinical practice for the Japanese. (***Stroke.* 2010;41:1984-1989.**)

Key Words: acute ischemic stroke ■ alteplase ■ postmarketing registration ■ thrombolysis ■ tissue plasminogen activator

Since the recombinant tissue plasminogen activator stroke study organized by the National Institute of Neurological Disorders and Stroke (NINDS)[1] demonstrated that intravenous alteplase treatment within 3 hours of stroke onset improved functional outcome in 1995, this treatment has been an approved medical therapy for patients with acute ischemic stroke and is recommended as the first-line treatment by most national and international guidelines.[2,3] Intravenous alteplase treatment of ischemic stroke within the 3-hour time window has been shown to be safe and effective in previous randomized controlled trials.[4–8] However, the safety and efficacy of thrombolysis with alteplase in routine clinical practice should be investigated in each country.

Alteplase was licensed for the treatment of acute ischemic stroke in the United States in 1996 and in the European Union in 2002 for selected patients treated within the 3-hour time window. In Japan, a prospective, single-arm, open-label study called the Japan Alteplase Clinical Trial (J-ACT)[9] was conducted from April 2002 to September 2003. Although the internationally recommended dosage of intravenous alteplase was adjusted to 0.9 mg/kg, the challenging dose of 0.6 mg/kg was selected in J-ACT based on previous recombinant tissue plasminogen activator studies for Japanese patients. Randomized controlled trials of duteplase, a recombinant tissue plasminogen activator similar to alteplase, have been conducted for acute stroke patients within 6 hours of onset in

Received May 10, 2010; accepted June 1, 2010.

From Nakamura Memorial Hospital (J.N.), Hokkaido, Japan; National Cerebral and Cardiovascular Center (K.M.), Osaka, Japan; National Hospital Organization Kyushu Medical Center (Y.O.), Fukuoka, Japan; Saitama Medical University International Medical Center (N.T.), Saitama, Japan; University of Tokushima Graduate School (S.N.), Tokushima, Japan; Tohoku University Graduate School of Medicine (E.M.), Miyagi, Japan; Federation of National Public Service Personnel Mutual Aid Associations Tachikawa Hospital (Y.S.), Tokyo, Japan; National Cardiovascular Center (T.Y.), Osaka, Japan.

Correspondence to Jyoji Nakagawara, Departments of Neurosurgery and Stroke Center, Nakamura Memorial Hospital, South-1, West-14, Chuo-ku, Sapporo, Hokkaido, 060-8570, Japan. E-mail george@med.nmh.or.jp

Stroke is available at http://stroke.ahajournals.org

DOI: 10.1161/STROKEAHA.110.589606

157

Japan.[10–12] After a pilot study,[10] 20 million international units (MIU) of duteplase proved to be superior to placebo based on the angiographic recanalization rate.[11] In a randomized, double-blind, dose-comparison study, partial recanalization and complete recanalization in 18 of 54 (33.3%) patients administered 20 MIU and in 25 of 59 (42.4%) patients administered 30 MIU, respectively, were not found to be statistically different.[12] However, massive brain hematoma/hemorrhagic transformation occurred in 2 of 56 (3.6%) patients administered 20 MIU and 9 of 65 (13.8%) patients administered 30 MIU.[12] Therefore, it was considered that the optimal dose of alteplase for J-ACT was 0.6 mg/kg, which was equivalent to 20 MIU per person or 0.33 MIU/kg at a mean body weight of 60 kg. The underlying rationale has been published on the Stroke web site (http://stroke.ahajournals.org/cgi/content/full/37/7/1810).[9] In J-ACT, 103 patients were treated with 0.6 mg/kg intravenous alteplase, and the proportion of modified Rankin Scale (mRS) score of 0 to 1 at 3 months was 36.9% (38/103; 90% confidence interval [CI], 29.1%–44.7%), and the incidence of symptomatic intracranial hemorrhage (sICH) within 36 hours was 5.8% (6/103; 90% CI, 2.0% to 9.6%).[9] Consequently, alteplase at 0.6 mg/kg was approved and a license was granted in October 2005 by the Ministry of Health, Labor and Welfare (MHLW), Japan. At the time of approval, the MHLW required the sponsors (Mitsubishi Tanabe Pharma Corporation and Kyowa Hakko Kirin Co, Ltd) to perform a large-scale postmarketing registry study to assess the safety profile of 0.6 mg/kg intravenous alteplase and a clinical study for documentation of the dosage efficacy (Japan Alteplase Clinical Trial II [J-ACT II]).[13] The sponsors asked the centers practicing thrombolysis with alteplase for participation in the postmarketing registry. The results of both studies will contribute to a standard for the reassessment of the benefit-to-risk profile of intravenous alteplase treatment.

The aim of Japan post-Marketing Alteplase Registration Study (J-MARS) was to investigate whether thrombolysis with 0.6 mg/kg intravenous alteplase could be safe and effective in routine clinical practice for the Japanese. Here, we compared the results of J-MARS with those of the Safe Implementation of Thrombolysis in Stroke-Monitoring Study (SITS-MOST) performed as a postmarketing study in the European Union.[14]

Patients and Methods

J-MARS was an open-label, multicenter, nonrandomized, observational study including clinical centers practicing thrombolysis for acute stroke in Japan. Participation in this study was possible for any medical centers that committed to register all patients treated with alteplase for 2 years after its approval and to collaborate in the elucidation of causes of any treatment complications. Joining this registry was not compulsory. The primary outcome measures in the protocol were sICH within 36 hours and at 3 months and favorable outcome (mRS score, 0–1) at 3 months after stroke onset. The MHLW approved the protocol of this study and the sponsors instructed the investigators to perform the study according to Good Postmarketing Study Practice, which is the authorized standard for a postmarketing registration study. The ethics approval was obtained from institutional ethics committee when required. Thrombolysis with 0.6 mg/kg intravenous alteplase was applied for the patients in accordance with the existing labeling and guidelines for intravenous alteplase treatment in Japan.[15,16] Informed consent was obtained from the patient (or a relative if the patient could not understand the treatment). Recruitment of patients in J-MARS started in October 2005 and ended in October 2007.

Baseline and demographic characteristics, stroke severity, time intervals, risk factors, and medication history were collected. NIHSS score at 24 hours and mRS score at 3 months were requested as the outcome measures. The proportion of each mRS score at 3 months was also calculated. Any adverse events for patients in this study were reported via their case report forms (CRF) to the sponsors, who reported serious drug-related adverse reactions to MHLW.

All patients who were enrolled in this study underwent CT or MRI before and within 36 hours after treatment as a general rule. Further follow-up brain scans after that were optional; however, patients who presented neurological deterioration underwent additional scan. These scans were not reviewed centrally. sICH was defined as any intracranial hemorrhage with a neurological deterioration of NIHSS score ≥4 points from baseline, or from the lowest NIHSS score after baseline to 24 hours, or the intracranial hemorrhage leading to death. In addition, number of patients with sICH was stratified according to number of enrolled patients per center. Functional independence (mRS score, 0–1) was assessed at 3 months after stroke onset by face-to-face or telephone interview with the patient or the patient's caregiver, or by letter reply form. Intracranial hemorrhage rates were calculated from any CT or MRI within 36 hours after alteplase treatment, and also from any additional scans.

Statistical Analysis

The proportion and 95% CI of patients with sICH, favorable outcome, and mortality rate were calculated. We used the statistical approach to calculate the upper and lower limits of the CI. Bar charts of proportions of patients were made to compare with the corresponding proportions of the NINDS study,[1] the J-ACT,[9] the SITS-MOST,[14] the Standard Treatment with Alteplase to Reverse Stroke study (STARS),[17] and the Canadian Alteplase for Stroke Effectiveness Study (CASES).[18] All analyses were performed with SAS version 9.1.3.

Results

According to the logistics research, 8313 patients with acute ischemic stroke at 1100 centers were treated with intravenous alteplase from October 2005 to October 2007 all over Japan, and a total of 7692 patients from 959 centers were registered in J-MARS. However, 200 patients from 83 centers (2.6%; 200/7692) whose CRF were not collected because of nonfulfillment by the investigators were excluded. Finally, 7492 patients (90%; 7492/8313) with CRF from 942 centers (86%; 942/1100) were enrolled in the safety analysis (Figure 1). The proportion of patients with sICH, prestroke independence (mRS score, 0–1), and functional outcomes at 3 months were obtained from the CRF. The overall mortality rate was estimated from the fatal records in the CRF. The median participated time in the registry for these 942 centers was 17.9 months. Table 1 shows baseline characteristics in 7492 patients, including risk factors, presence of concomitant disease, degree of neurological severity, and blood pressure in J-MARS in comparison with SITS-MOST. Table 1 also shows stroke subtypes of the subjects and median time from stroke onset to alteplase treatment in both studies.

Table 2 demonstrates the rates of adverse events, drug-related adverse reactions, intracranial hemorrhages confirmed by brain scans, and overall mortality in 7492 patients. The proportion of patients with sICH was 3.5% (259/7492; 95% CI, 3.1%–3.9%) within 36 hours and 4.4% (329/7492; 3.9%–4.9%) at 3 months. The overall mortality rate within 3 months was 13.1% (985/7492; 12.4%–13.9%) and the proportion of patients with fatal sICH was 0.9% (70/7492; 0.7%–1.2%).

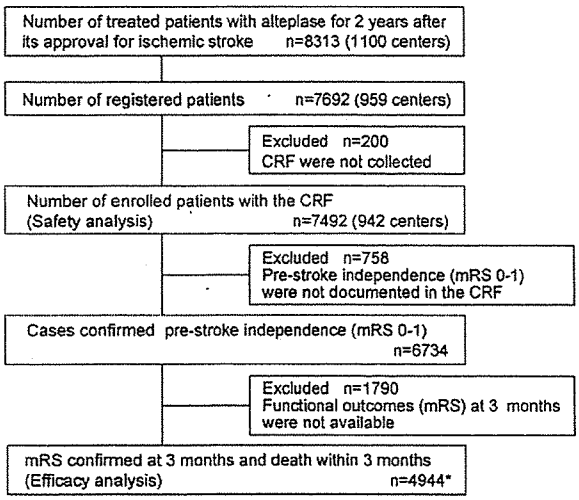

Figure 1. Flow chart showing the disposition of patients. *Of 4944 patients, modified Rankin Scale (mRS) scores at 3 months for 4060 patients were documented in their case report forms, and those of 884 patients were confirmed by attending physicians and records at hospital discharge.

Regarding neurological outcome in J-MARS, the median NIHSS score was 15 (interquartile range, 9–20) at baseline and 10 (interquartile range, 4–18) at 24 hours from starting therapy. Of the total 7492 patients, 758 patients had no documentation for prestroke independence (mRS score, 0–1) in the CRF (Figure 1). In these 758 patients, prestroke disability states of 741 patients were reported as mRS score 2 to 5, and those of remaining 17 patients were not mentioned. They were included in the safety analysis but not in the efficacy analysis, because favorable outcome was defined as mRS score 0 to 1 in this study. Number of patients who confirmed prestroke independence (mRS score, 0–1) was 6734. Follow-up data at 3 months were available for 4944 of 6734 patients whose prestroke independence was confirmed (Figure 1); 1790 of 6734 patients were excluded from the efficacy analysis because their mRS scores at 3 months were not available. Functional outcomes at 3 months (90±14 days) were obtained in 4060 of 4944 patients (including virtually all deceased cases within 3 months). For the other 884 patients who were surviving at 3 months, their functional outcomes were unavailable in the CRF, but their mRS score were confirmed by attending physicians and records at hospital discharge. The proportion of favorable outcome at 3 months in J-MARS was 33.1% (1637/4944; 31.8%–34.4%). The functional outcome estimated by mRS score at 3 months was compared with data from relevant published studies in Figure 2.

Table 1. Baseline Characteristics of Patients Analyzed in J-MARS and SITS-MOST

	J-MARS (n=7492)	SITS-MOST (n=6483)
Age, y	72 (65–79)	68 (59–75)
Gender, female	2836 (37.9%)	2581 (39.8%)
Prestroke independence, mRS score 0–1	6734 (89.9%)	5899/6337 (93.1%)
Concomitant disease		
Hypertension	3852 (51.4%)	3710/6318 (58.7%)
Diabetes mellitus	1272 (17.0%)	1020/6374 (16.0%)
Atrial fibrillation	3331 (44.5%)	1507/6306 (23.9%)
Heart failure	679 (9.1%)	467/6339 (7.5%)
Previous stroke	1373 (18.3%)	643/6395 (10.1%)
NIHSS score	15 (9–20)	12 (8–17)
Systolic blood pressure, mm Hg	150 (136–164)	150 (137–166)
Diastolic blood pressure, mm Hg	81 (71–90)	81 (74–90)
Stroke subtype		
Cardioembolic	4509 (60.2%)	2270 (35%)
Atherothrombotic	1838 (24.5%)	2279 (35.2%)*
Lacunar	316 (4.2%)	535 (8.3%)
Other/not differentiated	811 (10.8%)	1171 (18.1%)
Unknown	18 (0.2%)	228 (3.5%)
Stroke onset to treatment time, min	133 (110–160)	140 (115–165)

Data are median (interquartile range) or n (%).
*Large vessel disease with or other than substantial carotid stenosis.
J-MARS indicates Japan post-Marketing Alteplase Registration Study; mRS, modified Rankin scale; SITS-MOST, Safe Implementation of Thrombolysis in Stroke-Monitoring Study.

Table 2. N (%) of Patients With All Adverse Events, Drug-Related Adverse Reactions, Intracranial Hemorrhage, and Overall Mortality

Total N of Patients	7492
Adverse events	2412 (32.2%)
Drug-related adverse reactions	1627 (21.7%)
Intracranial hemorrhages	1217 (16.2%)
sICH	
Within 36 hr	259 (3.5%)
At 3 mo	329 (4.4%)
Fatal sICH	70 (0.9%)
Overall mortality	985 (13.1%)

sICH, symptomatic intracranial hemorrhages.

The median NIHSS score at baseline was 15 for J-MARS (n=3576) and 12 for SITS-MOST (Figure 2). The proportion of patients with NIHSS score ≥25 at baseline was 9.4% (463/4944) in J-MARS. The proportion of patients with alteplase treatment initiated later than 3 hours after symptom onset was 1.8% (91/4944).

In SITS-MOST, the subjects were restricted to those between ages 18 and 80 years with an NIHSS score <25.[14] The subgroup analysis with selected conditions such as those of SITS-MOST showed that the proportion of favorable outcome at 3 months was 39.0% (37.4%–40.6%) in J-MARS (n=3576) in comparison with 38.9% (37.7%–40.1%) in SITS-MOST (Figure 3).

We stratified number of patients with sICH according to number of enrolled patients per center (Figure 4). The percentage of sICH for centers with a small enrolled number (≤4) was 6.0% (4.7%–7.7%), and those for centers with a relatively larger enrolled number (20–29 and ≥30) were 3.2% (2.3%–4.4%) and 3.2% (2.4%–4.2%), respectively.

Discussion

The results from J-MARS suggested that 0.6 mg/kg intravenous alteplase could be an effective treatment with satisfac-

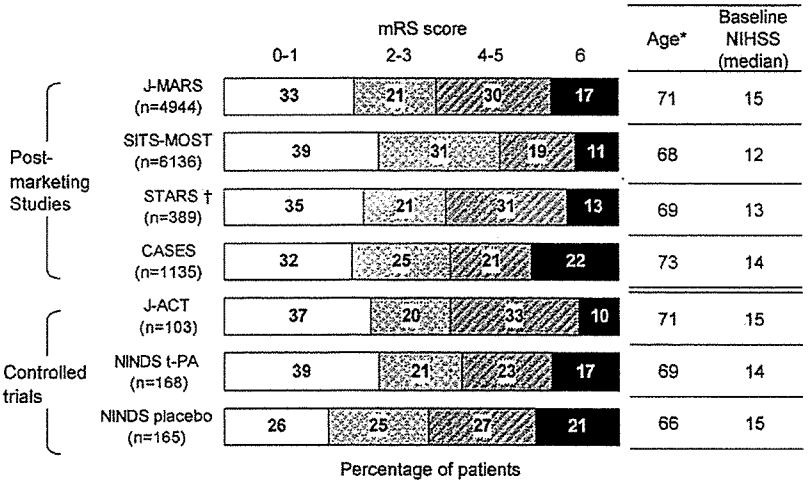

Figure 2. modified Rankin Scale (mRS) score at 3 months in J-MARS, other postmarketing studies, and controlled trials. *Data of J-MARS, SITS-MOST, and CASES are medians. The other data are means. †The mRS score at 30 days in STARS.

tory safety profile when used in a 3-hour time window in routine clinical practice for the Japanese. For the first 2 years after the approval of intravenous alteplase treatment in Japan, most patients who received this treatment were registered in J-MARS. The main aim of J-MARS was to confirm whether the levels of safety recognized in published clinical studies could be reproduced in routine clinical practice, especially with regard to sICH.

In J-MARS, the proportion of patients with sICH was 4.4% (3.9%–4.9%) at 3 months. The definitions of sICH have been slightly different among published studies.[1,9,14,17,18] These differences could restrict any direct comparison of the results from those studies. In SITS-MOST, the proportion of patients with sICH was 7.3% (6.7%–7.9%) according to the National Institute of Neurological Disorders and Stroke and Cochrane review definition[19,20] (defined as any hemorrhage plus any neurological deterioration [NIHSS score ≥1] or that leads to death within 7 days) and 4.6% (4.1%–5.1%) according to the European Cooperative Acute Stroke Study (ECASS) definition[21] (defined as any hemorrhage plus a neurological deterioration of NIHSS score ≥4 points from baseline, or from the lowest NIHSS score after baseline to 7 days or leading to death).[14] Our results showed that the proportions of patients who had sICH in J-MARS and SITS-MOST were comparable when the ECASS definition was applied to those in SITS-MOST (4.4% vs 4.6%).

In J-MARS, we stratified number of patients with sICH according to number of enrolled patients from each participating center to investigate the correlation between the experience and the safety with stroke thrombolysis. The number of enrolled patients per center in J-MARS was small compared to that of SITS-MOST, but the percentage of sICH in centers with a relatively large number (≥20 cases) of enrollment was lower than that in centers with relatively small number (≤19 cases) of enrollment (Figure 4). This finding suggested that the experience of stroke thrombolysis was one important factor for safe clinical practice.

The proportion of favorable outcome at 3 months in J-MARS remained at 33.1%, which is nearly the same rate as that seen in CASES, in which favorable outcome was 32%.[18] The modest data collection rate of functional outcome evaluations at 3 months (4944/7492) seems to be an inevitable limitation of this observational study and could be a possible source of detection and exclusion biases. Although mRS scores for surviving patients at 3 months were not always reported in the CRF, virtually all fatal cases within 3 months were identified in the fatal records in the CRF. Accordingly, the proportion of mRS score 6 at 3 months (17% in Figure 2)

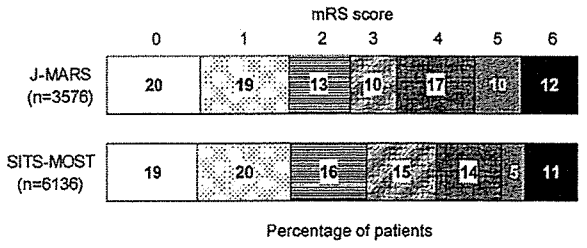

Figure 3. modified Rankin Scale (mRS) score at 3 months in subgroup restricted to patients between ages 18 and 80 years with NIHSS score <25 in J-MARS in comparison with SITS-MOST. The actual numbers of patients in each category for J-MARS (n=3576): mRS score 0, 704; mRS score 1, 690; mRS score 2, 466; mRS score 3, 344; mRS score 4, 598; mRS score 5, 363; mRS score 6, 411. Median ages: J-MARS, 69 years; SITS-MOST, 68 years. Median of baseline NIHSS score: J-MARS, 13; SITS-MOST, 12.

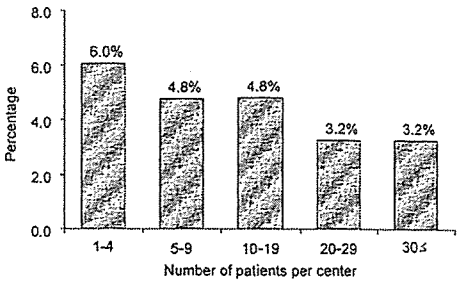

Figure 4. Percentage of symptomatic intracranial hemorrhage according to enrolled number of patients per center.

was seemingly higher than the overall mortality rate (13.1% in Table 2). Certainly, mortality at 3 months in J-MARS was higher than that in J-ACT (10% in Figure 2).[9] The median NIHSS score at baseline was 15 in J-MARS, which is the same value as in J-ACT (Figure 2). In J-ACT, patients with a comatose state at baseline were excluded, and the highest NIHSS score at baseline was actually 30. However, a considerable number of patients with the severe baseline condition of NIHSS score >30 or with a comatose state were included in J-MARS, and their outcomes were almost always unfavorable.

In SITS-MOST, the proportion of favorable outcome at 3 months was 39%.[14] Concerning the relatively higher favorable outcome in SITS-MOST, it could be a contributing factor that study recruitment was restricted to patients between ages 18 and 80 years with NIHSS score <25. In SITS-MOST, the median age was 68 years (vs 72 years in J-MARS), and the median NIHSS score was 12 (vs 15 in J-MARS).[14] Thus, clinical severity could be less severe in SITS-MOST. Consequently, we tried the subgroup analysis of J-MARS in patients between ages 18 and 80 years with an NIHSS score <25, which demonstrated that the favorable outcome at 3 months was 39%, which is much the same as that in SITS-MOST (39%; Figure 3).

Recently, the Stroke Acute Management with Urgent Risk-factor Assessment and Improvement (SAMURAI) study was conducted in 10 Japanese stroke centers with much experience in alteplase treatment from October 2005 to July 2008.[22] Six hundred patients treated with 0.6 mg/kg intravenous alteplase were enrolled in SAMURAI study and they were partially overlapped with those in J-MARS. In SAMURAI study, the proportion of favorable outcome at 3 months was 33.2% (29.5%–37.0%) of the total 600 patients and 37.2% (33.2%–41.4%) when 65 patients with a prestroke mRS score 2 to 5 were excluded from the analysis. Analysis of 399 patients with a prestroke mRS score 0 to 1 who met the criteria of SITS-MOST showed that the proportion of favorable outcome at 3 months was 40.6% (35.9%–45.5%). Although SAMURAI study group was composed of stroke centers with much experience in alteplase treatment, the proportion of favorable outcome in SAMURAI study was not so superior to that of the present study. The results of J-MARS, the national postmarketing study in Japan, could be positively ranked with those of SITS-MOST.

Conclusion

In conclusion, the result of J-MARS demonstrated that 0.6 mg/kg intravenous alteplase achieved low rates of sICH and sufficient favorable outcome in clinical practice in Japan. In addition, the results from J-ACT II showed that early recanalization of an occluded middle cerebral artery was generated by 0.6 mg/kg intravenous alteplase and directly associated with favorable clinical outcome.[13] The results of these Japanese studies suggest that thrombolysis with 0.6 mg/kg intravenous alteplase could be comparable to those with 0.9 mg/kg alteplase used in North America and the European Union. Hereafter, the safety and efficacy of thrombolysis with 0.6 mg/kg intravenous alteplase could contribute not only to routine clinical practice but also to occasional combined approach with thrombolysis and endovascular devises for patients with acute ischemic stroke.

Acknowledgments

The authors thank the investigators involved in this postmarketing registration study.

Sources of Funding

This study was supported by Mitsubishi Tanabe Pharma Corporation and Kyowa Hakko Kirin Co, Ltd.

Disclosure

Jyoji Nakagawara received honoraria from Mitsubishi Tanabe Pharma, Kyowa Hakko Kirin, and Lundbeck, received a consulting fee from Lundbeck. Kazuo Minematsu received research grants from Mitsubishi Tanabe Pharma, Kyowa Hakko Kirin, and Lundbeck, and received honoraria from Mitsubishi Tanabe Pharma and Kyowa Hakko Kirin. Yasushi Okada received an honorarium from Mitsubishi Tanabe Pharma and a consulting fee from Lundbeck, Norio Tanahashi received an honorarium from Mitsubishi Tanabe Pharma. Shinji Nagahiro received a research grant and honorarium from Mitsubishi Tanabe Pharma. Etsuro Mori received a research grant from Mitsubishi Tanabe Pharma, honorarium from Mitsubishi Tanabe Pharma and Kyowa Hakko Kirin, and consulting fees from Mitsubishi Tanabe Pharma, Kyowa Hakko Kirin, and Lundbeck. Yukito Shinohara received an honorarium from Mitsubishi Tanabe Pharma. Takenori Yamaguchi received honoraria from Mitsubishi Tanabe Pharma, Kyowa Hakko Kirin, and Lundbeck, and received consulting fees from Mitsubishi Tanabe Pharma and Lundbeck. All authors have disclosed the financial relationships with the companies relevant to alteplase and desmoteplase.

References

1. Tissue plasminogen activator for acute ischemic stroke. The National Institute of Neurological Disorders and Stroke rt-PA Stroke Study Group. *N Engl J Med.* 1995;333:1581–1587.
2. Adams HP Jr, del Zoppo G, Alberts MJ, Bhatt DL, Brass L, Furlan A, Grubb RL, Higashida RT, Jauch EC, Kidwell C, Lyden PD, Morgenstern LB, Qureshi AI, Rosenwasser RH, Scott PA, Wijdicks EF. Guidelines for the early management of adults with ischemic stroke: a guideline from the American Heart Association/American Stroke Association Stroke Council, Clinical Cardiology Council, Cardiovascular Radiology and Intervention Council, and the Atherosclerotic Peripheral Vascular Disease and Quality of Care Outcomes in Research Interdisciplinary Working Groups: the American Academy of Neurology affirms the value of this guideline as an educational tool for neurologists. *Stroke.* 2007;38:1655–1711.
3. The European Stroke Initiative Executive Committee and European Stroke Initiative Writing Group. European stroke initiative recommendations for stroke management—update 2003. *Cerebrovasc Dis.* 2003;16:311–337.
4. Hacke W, Donnan G, Fieschi C, Kaste M, von Kummer R, Broderick J, Brott T, Frankel M, Grotta J, Haley EJ, Kwiatkowski T, Levine S, Lewandowski C, Lu M, Lyden P, Marler J, Patel S, Tilley B, Albers G, Bluhmki E, Wilhelm M, Hamilton S. ATLANTIS Trials Investigators, ECASS Trials Investigators, NINDS rt-PA Study Group Investigators. Association of outcome with early stroke treatment: pooled analysis of ATLANTIS, ECASS, and NINDS rt-PA stroke trials. *Lancet.* 2004;363:768–774.
5. Hacke W, Kaste M, Fieshchi C, Toni D, Lesaffre E, von Kummer R, Boysen G, Bluhmki E, Hoxter G, Mahagne MH, Hennerici M. (for the ECASS Study Group). Intravenous thrombolysis with recombinant tissue plasminogen activator for acute hemispheric stroke. *JAMA.* 1995;274:1017–1025.
6. Hacke W, Kaste M, Fieshchi C, von Kummer R, Davalos A, Meier D, Larrue V, Bluhmki E, Davis S, Donnon G, Schneider D, Diez-Tejedor E, Trouillas P. (Second European-Australasian Acute Stroke Study Investigators). Randomised double-blind placebo-controlled trial of thrombolytic therapy with intravenous alteplase in acute ischaemic stroke (ECASS II). *Lancet.* 1998;352:1245–1251.

7. Clark WM, Wissman S, Albers GW, Jhamandas JH, Madden KP, Hamilton S. Recombinant tissue-type plasminogen activator (alteplase) for ischemic stroke 3 to 5 hours after symptom onset. The ATLANTIS Study: a randomized controlled trial. Alteplase Thrombolysis for Acute Noninterventional Therapy in Ischemic Stroke. *JAMA*. 1999;282: 2019–2026.
8. Clark WM, Albers GW, Madden KP, Hamilton S. The rtPA (alteplase) 0- to 6-hour acute stroke trial, part A (A0276g): results of a doubleblind, placebo-controlled, multicenter study. Thrombolytic therapy in acute ischemic stroke study investigators. *Stroke*. 2000;31:811–816.
9. Yamaguchi T, Mori E, Minematsu K, Nakagawara J, Hashi K, Saito I, Shinohara Y, the Japan Alteplase Clinical Trial (J-ACT) Group. Alteplase at 0.6 mg/kg for acute ischemic stroke within 3 hours of onset: Japan Alteplase Clinical Trial (J-ACT). *Stroke*. 2006;37:1810–1815.
10. Mori E, Yoneda Y, Tabuchi M, Yoshida T, Ohkawa S, Ohsumi Y, Kitano K, Tsutsumi A, Yamadori A. Intravenous recombinant tissue plasminogen activator in acute carotid artery territory stroke. *Neurology*. 1992;42: 976–982.
11. Yamaguchi T, Hayakawa T, Kiuchi H, for the Japanese Thrombolysis Study Group. Intravenous tissue plasminogen activator ameliorates the outcome of hyperacute embolic stroke. *Cerebrovasc Dis*. 1993;3: 269–272.
12. Yamaguchi T, Kikuchi H, Hayakawa T, for the Japanese Thrombolysis Study Group. Clinical efficacy and safety of intravenous tissue plasminogen activator in acute embolic stroke: a randomized, double-blind, dose-comparison study of duteplase. In: Yamaguchi T, Mori E, Minematsu K, del Zoppo GJ, eds. *Thrombolytic Therapy in Acute Ischemic Stroke III*. Tokyo, Japan: Springer-Verlag; 1995:223–229.
13. Mori E, Minematsu K, Nakagawara J, Yamaguchi T, Sasaki M, Hirano T. Effect of 0.6 mg/kg intravenous alteplase on vascular and clinical outcomes in middle cerebral artery occlusion—Japan Alteplase Clinical Trial II. *Stroke*. 2010:41:461–465.
14. Wahlgren N, Ahmed N, Davalos A, Ford GA, Grond M, Hacke W, Hennerici MG, Kaste M, Kuelkens S, Larrue V, Lees KR, Roine RO, Soinne L, Toni D, Vanhooren G. Thrombolysis with alteplase for acute ischaemic stroke in the Safe Implementation of Thrombolysis in Stroke-Monitoring Study (SITS-MOST): an observational study. *Lancet*. 2007; 369:275–282.
15. Guideline Committee for intravenous rt-PA (alteplase) in acute ischemic stroke: guidelines for intravenous application of rt-PA (alteplase). *Jpn J Stroke*. 2005;26:327–354.
16. Shinohara Y, Yamaguchi T. Outline of the Japanese Guidelines for the Management of Stroke 2004 and subsequent revision. *Int J Stroke*. 2008: 3:55–62.
17. Albers GW, Bates VE, Clark WM, Bell R, Verro P, Hamilton SA. Intravenous tissue-type plasminogen activator for treatment of acute stroke: the Standard Treatment with Alteplase to Reverse Stroke (STARS) study. *JAMA*. 2000;283:1145–1150.
18. Hill MD, Buchan AM. Thrombolysis for acute ischemic stroke: results of the Canadian Alteplase for Stroke Effectiveness Study. *CMAJ*. 2005:172: 1307–1312.
19. Wardlaw JM, del Zoppo G, Yamaguchi T. Thrombolysis for acute ischaemic stroke. *Cochrane Database Syst Rev*. 2000:2:CD000213.
20. Wardlaw JM, Zoppo G, Yamaguchi T, Berge E. Thrombolysis for acute ischaemic stroke. *Cochrane Database Syst Rev*. 2003;3:CD000213.
21. Larrue V, von Kummer RR, Muller A, Bluhmki E. Risk factors for severe hemorrhagic transformation in ischemic stroke patients treated with recombinant tissue plasminogen activator: a secondary analysis of the European-Australasian Acute Stroke Study (ECASS II). *Stroke*. 2001;32: 438–441.
22. Toyoda K, Koga M, Naganuma M, Shiokawa Y, Nakagawara J, Furui E, Kimura K, Yamagami H, Okada Y, Hasegawa Y, Kario K, Okuda S, Nishiyama K, Minematsu K, for the Stroke Acute Management with Urgent Risk-factor Assessment and Improvement (SAMURAI) Study Investigators. Routine use of intravenous low-dose recombinant tissue plasminogen activator in Japanese patients. General outcomes and prognostic factors from the SAMURAI Register. *Stroke*. 2009:40:3591–3595.